Regulation of interferon inducible Ser/Thr RNA-dependent protein kinase (PKR) by short imperfectly base-paired viral dsRNAs

by

Edis Dzananovic

A thesis submitted to Faculty of Graduate Studies of

The University of Manitoba

in partial fulfillment of the requirements of the degree of

DOCTOR OF PHILOSOPHY

Department of Chemistry

University of Manitoba

Winnipeg

ABSTRACT

In response to viral infection cells produce the interferon inducible Ser/Thr RNA-dependent protein kinase (PKR) that binds viral dsRNAs. After initial binding, PKR self-associates and then becomes autophosphorylated. PKR then phosphorylates its substrate, eukaryotic initiation factor 2α, which slows viral protein translation, thus helping the host cell response. PKR consists of tandem double stranded RNA binding motifs (dsRBMs) connected via a flexible linker to a kinase domain. A number of studies involving individual dsRBMs from proteins other than PKR have highlighted the key features required for interaction with perfectly duplexed RNA. However, viral dsRNA molecules are highly structured and often contain deviations from perfect RNA helices. HIV-1 TAR and adenovirus VA_I RNAs are well-characterized PKR binding partners. HIV-1 is an activator of PKR that adopts a mostly double-stranded structure with distortions including a trinucleotide bulge and hexaloop. Adenovirus VA_I RNA has double-stranded secondary structural elements including a dsRNA-binding (apical stem), an inhibitory stem-loop (central stem) that inhibits PKR from performing its enzymatic reaction, and the terminal stem. A truncated version of VA_I lacking the terminal stem called $VA_I\Delta TS$ (often used as wild type RNA in this study), binds to PKR and prevent its self-association. The interaction and binding affinities of PKR with all RNAs was determined using electrophoretic mobility shift assays. To investigate the role of the central stem-loop in the mechanism of inhibition of PKR by the $VA_I\Delta TS$ RNA, truncated versions of $VA_I\Delta TS$ with mutations in the central stem were transcribed. *In vitro* studies that include well-established enzymatic assays test activation and inhibition of PKR in presence of the

mutant versions of $VA_I\Delta TS$. The solution conformations of the dsRBMs of PKR in complex with TAR and $VA_I\Delta TS$ determined using small-angle X-ray scattering studies show dsRBMs of PKR interact with both stem and loop regions of the RNAs. SAXS modeling of $VA_I\Delta TS$, mutant RNAs together with activation assays show that loop and bulge regions are crucial for the tertiary structural integrity and function of central stem. Taken together this data provides framework for the recognition of imperfectly base-paired viral dsRNA by PKR and PKR's regulation through RNA tertiary structure.

TABLE OF CONTENTS

LIST OF TABLES

LIST OF FIGURES

LIST OF COPYRIGHT MATERIAL

Licensed content publisher: RNA Society.org

Licensed content publication: RNA journal

Licensed content title: Recognition of viral RNA stem-loops by the tandem double-stranded RNA binding domains of PKR.

Published: March 19, 2013 DOI: 10.1261/rna.035931.112

Sections where the licensed materials can be found: 3.1, 3.2, 3.3, 3.4, 3.5, 3.6, 3.7

Licensed content publisher: Elsevier

Licensed content publication: Journal of Structural Biology

Licensed content title: Solution conformation of adenovirus virus associated RNA-I and its interaction with PKR

Published: 2014 Jan;185(1):48-57. doi: 10.1016/j.jsb.2013.11.007. Epub 2013 Nov 28.

Sections where the licensed materials can be found: 4.1, 4.2, 4.3, 4.4, 4.5, 4.6, 4.7, 4.8, 4.9, 4.10

CONTRIBUTION OF AUTHORS

Chapter 3 of the thesis was adapted from:

Dzananovic, E., Patel, T. R., Deo, S., McEleney, K., Stetefeld, J. and McKenna, S. A. (2013) Recognition of viral RNA stem-loops by the tandem double-stranded RNA binding domains of PKR. RNA. **19**, 333-344. E.Dz primarily carried out the preparation and writing of manuscript. In addition, E.Dz. was responsible for designing and performing the experiments as well as analyzing experimental data. T.P. gave assistance with carrying out *ab initio* modeling of macromolecules. S.D. contributed to preparation of protein, RNAs, and buffers. K.M. was responsible for operating the Small angle X-ray instrument. S.M. and J.S. are principal investigators.

The writing of Chapter 4 was adopted from:

Dzananovic, E., Patel, T. R., Chojnowski, G., Boniecki, M. J., Deo, S., McEleney, K., Harding, S. E., Bujnicki, J. M. and McKenna, S. A. (2014) Solution conformation of adenovirus virus associated RNA-I and its interaction with PKR. J Struct Biol. **185**, 48-57.

E.Dz. was responsible for writing the manuscript, and designing and carrying out experiments including analysis of experimental data. T.P. contribution involved assistance with AUC experiments as well helping with *ab initio* modeling. Members of J.B. group, G.C. and M.B. contributed to in silico modeling of RNAs, proteins, and their complexes. S.D. contributed to preparation of protein, RNAs, and buffers. K.M. was responsible for operating the Small angle X-ray instrument. S.H. provided the access and assistance with operating the AUC instrument. S.M. is a principal investigator.

Chapter 5 is an adaptation of a manuscript titled "*The structural integrity of the central stem-loop of adenovirus VA_I RNA is essential for PKR inhibition*" that is in the process of being submitted for publication. Co-authors on this manuscript include Edis Dzananovic, Trushar R. Patel, Soumya Deo, Grzegorz Chojnowski, Astha, Evan P. Booy, Kevin McEleney, Janusz M. Bujnicki, Sean A. McKenna. E.Dz was primarily involved in carrying out the preparation and writing of manuscript. In addition, E.Dz. was responsible for designing and performing the experiments including analysis of experimental data. T.P. assisted with *ab initio* modeling of macromolecules. S.D. contributed to preparation of protein, RNAs, and buffers. High-resolution modeling is to be performed by members of J.B. group, G.C. and Astha (data not included in thesis). E. B. contributed by providing technical assistance with western blotting. K.M. was responsible for operating the Small angle X-ray instrument. S.M. is a principal investigator.

LIST OF ABREVATIONS

A	adenosine
ADAR	adenosine deaminases acting on RNA
AS	apical stem-loop
ATP	adenosine tri-phosphate
AUC	analytical ultracentrifugation
bp	base-pair
C	cysteine
C	cytosine
CARD	Caspase activation and recruitment domain
CD	central domain
CDK9	cyclin-dependent kinase 9
CS	central stem-loop
CTD	C-terminal regulatory domain
CycT1	cycline T1
DLS	dynamic light scattering
D_{max}	maximum particle dimension
DNA	deoxyribonucleic acid
DSIF	DRB Sensitivity Inducing Factor
dsRBD	double stranded RNA binding domain
dsRBM	double stranded RNA binding motif
dsRNA	double stranded RNA
EBNA	Epstein–Barr nuclear antigen
EBV	Epstein–Barr virus
E. coli	*Escherichia coli*
EDTA	Ethylenediaminetetraacetic acid
eIF-2α	eukaryotic initiation factor 2α
EMSA	electrophoretic mobility shift assay
F	phenylalanine

G	guanosine
GCN2	control non-derepressible 2 kinase
GDP	guanosine di-phosphate
GTP	guanosine tri-phosphate
HCV	hepatitis C virus
HRI	hemin-regulated inhibitor
HRP	horseradish peroxidase
HIV	human immunodeficiency virus
I	inosine
IFN	interferon
IFNAR	interferon α/ β receptor
IKK	inhibitor of nuclear factor kappa-B kinase
IκB	inhibitor of κB
IL	interleukin
IPTG	isopropyl β-d-thiogalactopyranoside
IRES	internal ribosome entry site
IRF	interferon regulatory factor
ISG	interferon-stimulated gene
ISGF	interferon stimulatory gene factor
ISRE	interferon stimulated response elements
ITC	isothermal titration calorimetry
JAK/STAT	Janus Kinase/signal transducers and activators of transcription
K	lysine
LB	Luria-Bertani
LMP	latent membrane protein
MDA5	melanoma differentiation associated gene 1
MEF	mouse embryo fibroblast
Met	methionine
mRNA	messenger RNA
MyD88	myeloid differentiation primary response 88
NELF	negative elongation factor

NFkB	nuclear factor kappa-light-chain-enhancer of activated B cells
ng	nanogram
NMR	nuclear magnetic resonance
NSD	normalized spatial discrepancy
NTP	nucleotide triphosphate
OAS	2' 5' -oligoadenylate synthetase
OASL	OAS Like
PACT	PKR-associated activator
PAMP	pathogen associated molecular patterns
PERK	PKR-like endoplasmic reticulum kinase
PKR	RNA-dependent protein kinase
Poly I:C	polyinosinic-polycytidylic acid
P-TEFb	positive transcription elongation factor b
PRR	pattern recognition receptor
PVDF	polyvinyl difluoride
Rb	retinoblastoma
RD	repressor domain
rG	radius of gyration
rH	hydrodynamic radius
RIG-I	retinoic acid-inducible gene I
RISC	RNA-induced silencing complex
RLR	RIG-I Like Receptor
RNA	ribonucleic acid
RNAi	RNA interference
RNase L	ribonuclease L
SAXS	small angle X-ray scattering
SDS-PAGE	sodium dodecyl sulfate polyacrylamide gel electrophoresis
SEC	size exclusion chromatography
Ser	serine
SOB	super optimal broth
ssRNA	single stranded RNA

ssDNA	single stranded DNA
SV	sedimentation velocity
TAR	transactivation response element
Tat	transactivator of transcription
TBE	Tris/Borate/EDTA
Thr	threonine
TIA-1	cytotoxic granule-associated RNA binding protein
TLR	Toll-like receptor
TNF	tumor necrosis factor
TRBP	TAR RNA binding protein
tRNA	transfer RNA
Tris	trisaminomethane
TRIF	TIR-domain containing adaptor inducing interferon (IFN)-β
TS	terminal stem
U	uridine
UTR	untranslated region
TYK	tyrosine kinase
VA	viral associated
wt	wild type

CHAPTER 1: INTRODUCTION

One of the most important abilities for an organism to survive is to respond quickly and effectively to a state of infection. The ability of an organism to recognize and respond to the presence of an antigen is called immunity [1]. The human body is frequently invaded by a variety of pathogens such as bacteria, viruses, protozoa, and parasitic worms. In addition, these pathogens constantly evolve to be able to evade the immune system and propagate. For these reasons the human immune system is comprised of overlapping intricate pathways to ensure that pathogens are removed from the body and in the case of reoccurrence, our immune system can react faster and more efficiently. The human immune system consists of two subsystems: the innate immune system and the adaptive immune system [1, 2].

The innate immune system is the first line defense against pathogens and it fights the infection in a cell-mediated manner as well as through the humoral immune response. Cell-mediated immunity includes the immune response to antigens through activation of various cytokines, phagocytes, and cytotoxic T-lymphocytes, and does not involve the production of antibodies, while the humoral response is mediated through involvement of antibodies [3]. The adaptive, or acquired, immune system is a very complex system that involves application of specialized cells and processes to eliminate specific pathogens from the body. In addition to preventing the spread of the infection, adaptive immunity is responsible for establishing a long-term protection against the pathogen in the case of future encounter. This effect is mediated through production of B memory cells, which are a special type of lymphocyte that can store the antibodies that were previously used to

clear out the specific antigen [4]. Innate immunity is also involved in activating the adaptive immune response though a process called antigen presentation [5, 6]. Unlike the adaptive immune system, the innate immune system does not give long-lasting or protective immunity to the host, however, it does recruit immune cells to the site of the inflammation through the production of cytokines. These immune cells, in turn, can clear out the antigens from the infected organs and tissues. Additionally, the innate immune system can activate the complement system [5]. The complement system evolved as a part of innate immune system and it involves a large number of proteins that are found in blood known as zymogens [5]. Zymogens are precursor proteins that are usually self-cleaved into active enzyme at the site of infection. Activated zymogen can also cleave and activate a subsequent downstream zymogen; this process results in amplification of the pathway. Activated complement pathway proteins covalently attach to the pathogens and prepare them for phagocytosis. Some proteins of complement system can damage bacterial pathogens by creating pores in their membranes [5]. The innate immune system mounts a rapid response mediated by phagocytes including macrophages and dendritic cells (DCs) in order to either clear the infection or prevent the spread of the infection until an adaptive response is mounted.

The focus of my thesis is on the interaction of the host interferon-induced double stranded RNA-activated protein kinase (**PKR**) with an adenovirus small non-coding RNA called adenovirus virus-associated RNA (**VA_I**). The introduction section begins with an overview on innate immunity and recognition of nucleic acids by the innate immune system, focusing on host pattern recognition receptors that are known to be activated by viral RNAs. Next, I will explain the role of interferons in the innate

immunity. Following this, I will highlight several specific proteins that are related to PKR in terms of their function in innate immunity. In the final section of the introduction I will give an extensive overview on PKR and VA_I, their structures, mechanisms of action, and the different pathways that they intertwine with. The introduction will be followed by Chapter 2 outlining the Materials and Methods used to acquire data. The experimental work will be presented in Chapters 3-5, each representing a distinct series of experiments. The thesis concludes with a Summary and discussion of Future Directions (Chapter 6).

1.1 INNATE IMMUNE SYSTEM

Initially it was thought that innate immunity was very simple and not as significant as the adaptive immunity in protection against pathogens [7]. Today, it is widely recognized that innate immunity employs complex cellular pathways to mount a rapid response to an infection. It utilizes a range of pattern recognition receptors (PRRs); proteins responsible for detecting molecules unique to a pathogen (virus, bacteria, fungi) called pathogen associated molecular patterns (PAMPS) [8]. PRRs are germline-encoded proteins expressed in variety of cells [9]. PRRs consist of several different families of proteins that can be distinguished by ligand specificity, cellular localization, and activation of specific signaling pathways that lead to distinct antipathogen responses.

PAMPS are conserved molecular motifs that are essential for pathogens survival [2, 10]. PAMPS can be found as a part of glycoproteins, lipopolysaccharides, proteoglycans, and nucleic acids essential to bacteria, fungi, and viruses [1, 11]. PAMPs can be detected at the cell surface by receptors such as Toll-like receptors (TLRs), via TLRs in the endosome, or RIG-I-like receptors (RLRs) in the cytoplasm [9, 12, 13].

Specific PAMPs are recognized by different groups of PRRs [8, 14, 15]. Glycoproteins, lipopolysaccharides, and proteoglycans are readily detected at the cell surface by the Toll-like receptors (TLRs) [2, 9, 12]. Hemagglutinin protein, found on the envelope of the measles virus, can be detected by the Toll-like receptor 2 (TLR2) [16]. Once a virus enters the cell, viral nucleic acids can be detected by RLR helicases such as retinoic acid-inducible gene 1 (RIG-I) and Melanoma Differentiation-Associated protein 5 (MDA5) [17-19]. In the endosome, TLR3 and TLR7/8 can detect viral single-stranded or double-stranded RNA respectively, which will trigger downstream signal transduction pathways [19, 20]. Regardless of whether the viral infection is detected at the surface by TLRs or by the cytoplasmic PRRs, the initial binding of PAMPS leads to expression of Interferon α/β through the activation of transcription factors, including interferon regulatory factor 3 (IRF3) and interferon regulatory factor 7 (IRF7) [21-24]. Activated interferons first link innate immunity with the adaptive immunity by initiating the differentiation of Interferon α/β-producing cells into dendritic cells [25, 26]. Second, interferon induces the expression of interferon-stimulated genes (ISGs) [2, 27, 28]. ISGs are a group of genes that express proteins that establish an antiviral response in target cells and collectively work to inhibit viral proliferation [2, 8, 27, 28]. PKR, the focus of this thesis, is the product of an ISG.

1.1.1 RIG-I-like receptors (RLRs)

RIG-I-like receptors, abbreviated **RLRs**, are a type of PRR's involved in the recognition of viruses by the innate immune system. RLRs act as sensors of viral replication within the cytoplasm through direct interaction with viral dsRNA, which could be a part of viral genome or a direct product of the genome [29]. RLRs are a family

of proteins that include RIG-I, MDA5 and probably ATP-dependent RNA helicase DHX58 (LGP2) [30-32].

RIG-I is a cytosolic sensor that gets activated upon interaction with viral RNA [31, 33, 34]. Activated RIG-I phosphorylates several target proteins, which leads to activation of transcription factors NFκB and IRF3/7 that are responsible for the production of type I interferons (INFs) and other cytokines **(Figure 1.1)** [35-37].

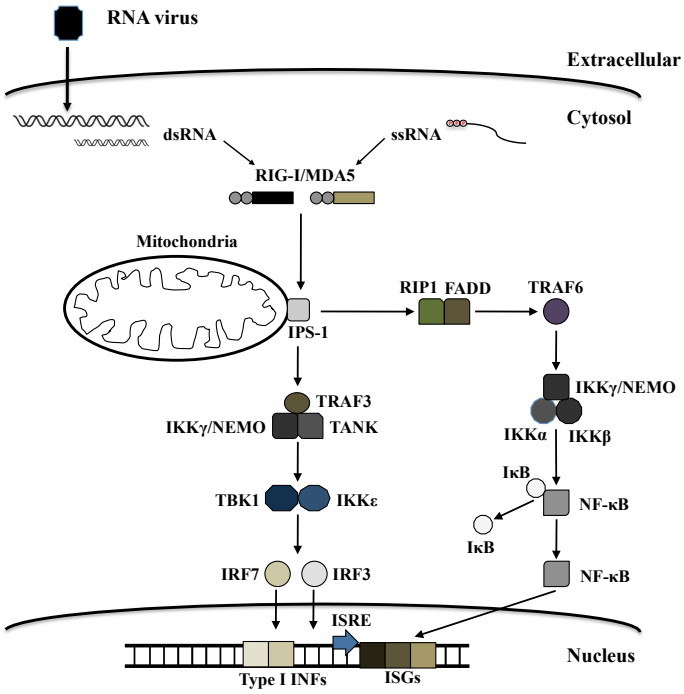

Figure 1.1: RLRs signaling in response to recognition of viral PAMPs which leads to activation of NFκB and IRF3/7 responsible for the production of type I INFs and other cytokines

RIG-I plays a role in initial viral detection and it establishes the antiviral state by inducing the expression of type I interferons, proinflammatory cytokines and ISGs [38-41]. RIG-I is a DExD/H box helicase that contains a N-terminal tandem CARD (Caspase activation and recruitment domain) domain [32, 42]. CARDs mediate the interaction of RIG-I with downstream signaling proteins that leads to activation of INF α and β. In

addition, it contains a repressor domain (RD) in its C-terminal regulatory domain (CTD) [43]. The RD domain prevents RIG-I from initiating its signaling cascade in the absence of its activator. RIG-I can interact with single-stranded and double-stranded RNAs [44, 45]. RIG-I binds to the exposed 5' triphosphate on either single-stranded RNA or the blunt-end of the duplex [45-48]. The interaction is sequence independent, thus enabling the protein to bind to wide range of RNAs. The interaction between RIG-I and the target RNAs is mediated by the CTD, the ATPase core, and the insertion domain [42]. The insertion domain, a RecA-like fold, is a part of the ATPase core that binds to the dsRNA, while the CTD can interact with a broad range of RNAs, as well as mediating the interaction between the RNA-bound RIG-I and its downstream protein partners [49-52].

MDA5 activation is mediated by high molecular weight long dsRNAs from a wide range of viruses [53]. Like RIG-I, MDA5 contains two CARD domains and the helicase domain, but it does not have a RD [31, 32, 54]. MDA5 activation is accomplished through ATP hydrolysis in the helicase domain [55, 56]. This allows the tandem CARD domains of MDA5 to interact with the downstream components of the signaling pathway that will eventually lead to the activation of type I INFs through NFκB and IRF3/7 [31]. Therefore MDA5 activates INFs through the same signaling pathway as RIG-I **(Figure 1.1)**.

1.1.2 Toll-like receptors (TLRs)

TLRs are membrane bound PRRs that can bind to distinctive types of nucleic acids [13, 16]. They are a large family of proteins that are primarily localized in the cell membrane as well as a small subset of endosomal TLRs linked to antiviral immunity including TLR3 and TLR7/8 [19, 20, 57].

TLR3 is endosomal with a horseshoe-shaped structure that binds dsRNA [38]. The interaction between TLR3 and the dsRNA is not sequence dependant and usually RNA of 90 base pairs (bp) or longer can activate TLR3 [58]. Activation of TLR3 will lead to production of type I INFs through the TIR-domain containing adaptor inducing interferon (IFN)-β (TRIF) dependent pathway **(Figure 1.2)** [38, 59, 60].

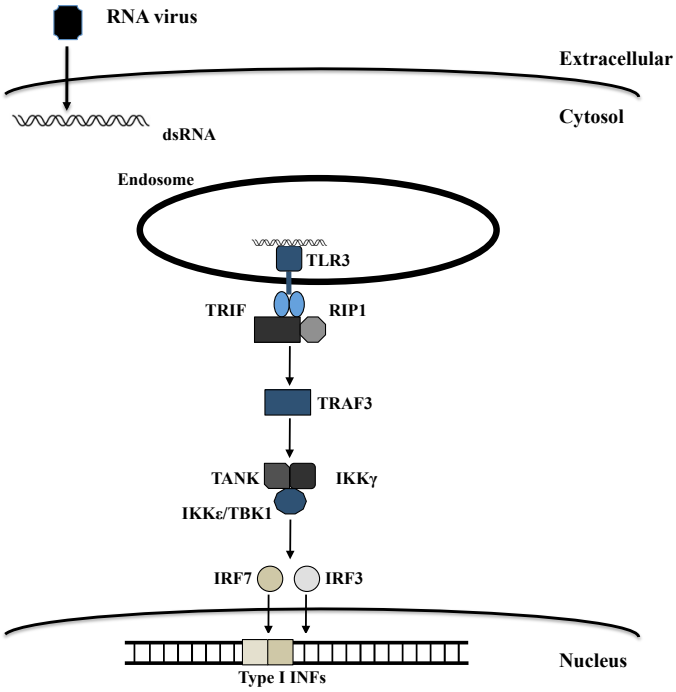

Figure 1.2: Recognition of viral PAMPs by TLR3 in endosome leading to production of type I INFs through the TRIF-dependent pathway

TRIF is a membrane-associated protein that mediates the activation of interferon β pathways through IRF3/IRF7 activation by non-canonical IKK kinases signaling (Figure 1.2) [61-63].

TLR7 and 8 are endosomal membrane-bound proteins that are phylogenetically closely related [64, 65]. TLR 7/8 bind to ssRNAs with high GU and AU content [64, 66, 67]. Once the virus is enclosed by the endosome, TLR7/8 interact with viral ssRNA

leading to the activation of interferon cascade through the Myeloid differentiation primary response gene 88 (MyD88)-dependent pathway **(Figure 1.3)** [64, 66, 68-71]. TLR7/8 activate type I INFs and other pro-inflammatory cytokines through the IRF7 and NFκB activation **(Figure 1.3)** [69-71].

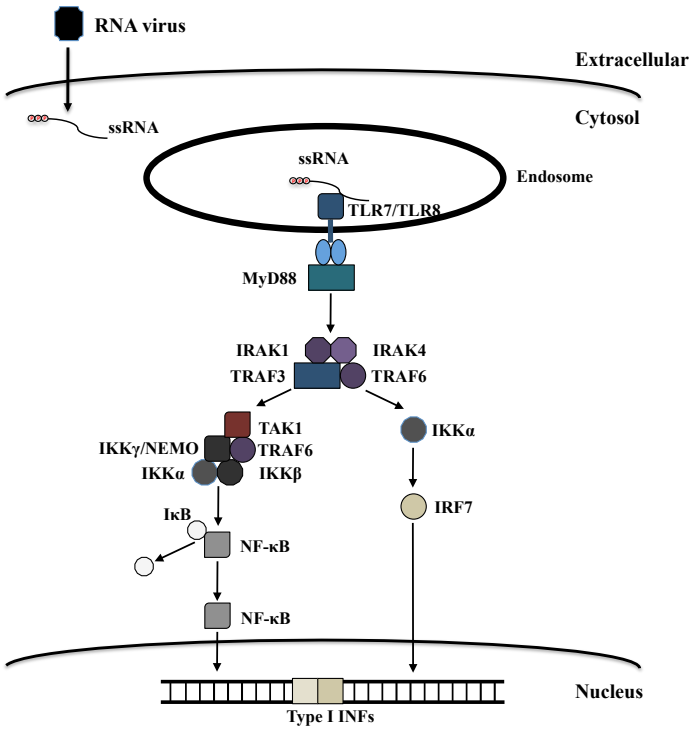

Figure 1.3: Recognition of viral PAMPs by TLR7 and TLR8 in endosome leading to production of type I INFs through the MyD88-dependent pathway

Even though both TLR7 and TLR8 bind to ssRNA, there is a functional difference between the two, mainly based on which pathways they initiate, and which cytokines they induce in different cell types [65, 72]. For example, it has been shown in monocyte-derived DC (pDC) cells that the presence of ssRNA oligonucleotide can stimulate type I INFs production through IRF7 signaling [72]. Additionally TLR7 is expressed in other immune cells, such as B cells and monocytes/macrophages [73, 74]. TLR8 is known to

be expressed in monocytes/macrophages; however, its signaling is mediated through the NF-κ B activation followed by inflammatory cytokine expression [73, 75, 76].

1.2 INTERFERON RESPONSE TO VIRAL INFECTION

One of the main roles of many PRRs including the aforementioned ones, is to enhance the production of type I interferons in response to viral infection. Expression of type I interferons leads to activation of a signal-transduction pathway that triggers the transcription of a diverse set of ISGs that establish an antiviral response in target cells and act as effector proteins with direct antiviral activity [7, 24, 77, 78]. Type I INFs are part of a large group of glycoproteins that are activated during the host's infection. Type I INFs include IFN-α (alpha), IFN-β (beta), and IFN-κ (kappa) among others. Interferon α and β are usually expressed in the innate immune response to viruses [28, 79]. More then ten different genes encode for IFN-α isoforms whereas a single gene encodes for expression of IFN-β [80-82]. Most cell types produce IFN-β, while IFN-α is prevalently expressed in plasmacytoid dendritic cells [81, 83]. Type I INFs initially bind to a heterodimeric receptor complex known as the IFN-α receptor (IFNAR) that consists of IFNAR1 and IFNAR2 subunits [84]. Binding of the INF-α/β enables autophosphorylation of the cytoplasmic domain of the receptor followed by the activation of proteins that are associated with the receptors, Janus kinase 1 (JAK1) and tyrosine kinase 2 (TYK2)[85]. The IFNAR1 subunit is associated with TYK2, whereas IFNAR2 is associated with JAK1 [85-88]. JAK1 and TYK2 in turn phosphorylate and activate signal transducer and activator of transcription 1 and 2 (STAT 1/2) at tyrosine residues; this leads to the formation of STAT1–STAT2–IRF9 (IFN-regulatory factor 9) transcription factor complexes, which are known as IFN-stimulated gene (ISG) factor 3 (ISGF3) complexes.

These complexes translocate to the nucleus and activate the transcription of ISGs [89-92].

INFs themselves do not posses antiviral properties but instead signals that the body is in state of the infection, and helps to recruit innate and adaptive immune cells to the site of infection [21]. INFs act in both autocrine (cell secretes chemical messengers that bind to the receptors on the surface of the secreting cell resulting in signaling that will bring on changes within the cell) and paracrine (cell secretes chemical messengers that bind to the receptors on the surface of nearby cells thus causing signaling that will bring on changes in those cells) manner through the JAK/STAT pathway bringing about the transcription of a group of IFN stimulated genes (ISGs) **(Figure 1.4)** [77]. Transcription of these genes brings about the production of proteins with a broad range of antiviral activities that will sequester/prevent further viral propagation.

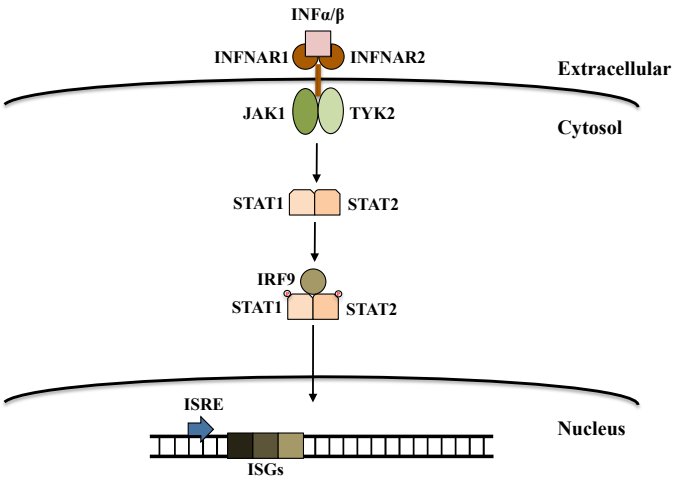

Figure 1.4: Activation of ISGs through Type I INF

1.3 IFN-STIMULATED GENES (ISGs)

One of the most important roles of the INFs is bringing about the transcription of ISGs. As stated previously, transcription of IFN-stimulated genes is activated through the JAK/STAT signaling pathway. Expressed INF α/β binds to IFNAR that leads to

phosphorylation of transcription factors STAT 1 and STAT2. STAT 1 and STAT 2 dimerize and move to nucleus where they form a trimeric complex with the IFN-regulatory factor 9 (IRF9) which are known as IFN-stimulated gene (ISG) factor 3 (ISGF3) complexes [83, 93-95]. ISGF3 binds to the consensus sequence TTTCNNTTTC known as IFN-stimulated response elements (ISREs) thereby activating the transcription of hundreds of ISGs, which establish a cellular antiviral state [83, 96-98]. ISGs code for proteins that detect PAMPs on viral molecules, and these proteins can induce apoptosis, catalyze cytoskeletal remodeling, regulate post-transcriptional events including splicing, mRNA editing, RNA degradation and the multiple steps of protein translation, as well as subsequent post-translational modification [77, 90]. ISGs express proteins that individually can block viral transcription, degrade viral RNA, inhibit translation, and modify protein function. Some of the better-studied ISGs that recognize viral RNAs as PAMPs are Adenosine deaminase acting on RNA 1 (ADAR1), 2',5'-oligoadenylate synthetases/Ribonuclease L, and the focus of this thesis, the double stranded RNA-activated protein kinase.

1.3.1 Adenosine deaminase acting on RNA 1 (ADAR1)

ADAR1, encoded by an ISG, is an RNA-binding protein that is involved in RNA-editing through post-translational modification of mRNA by changing its nucleotide content. ADAR1 can edit viral genomic and mRNA [99]. RNA processing by ADAR1 introduces a mismatch mutation into the viral genomic RNA or mRNA which results in change of the sequence that can affect viral replication, propagation, or altering the code for a viral protein thereby affecting the protein function [100-102]. ADAR1 catalyzes the deamination at C6 position of the adenosine (A) bases of dsRNA substrates [103-106].

The modification leads to the substitution of adenosine with inosine (I). In the case of coding RNA, the substituted inosine will be read by the translation machinery as a guanosine instead of adenosine, which can lead to introduction of incorrect amino acid. In addition, the same substitutions are created during RNA-dependent RNA replication used by many viruses [107, 108]. On the structural level, the resulting inosine:uridine (I:U) base pairs are less stable than A:U base pairs thus impacting the overall stability of the RNA structure [109-111]. Editing of dsRNA by ADAR1 can be site specific, as seen in the case of glutamate and serotonin pre-mRNA, as well as in the hepatitis delta virus antigenome RNA [104, 105, 112-114]. Editing can be also performed on multiple subsequent adenosines found on the RNA duplex as well as on synthetic dsRNA [103, 104].

ADAR1 contains N-terminal nucleic acids binding domains. It has two Z-DNA binding domains and three dsRNA binding motifs (dsRBMs) [103, 115]. The dsRNA-binding motifs interact with dsRNA in mostly sequence independent fashion [116]. The C-terminus of ADAR1 contains the deaminase domain that performs the A to I editing. Deaminase and RNA binding domains cooperatively work together to bring about the catalytic activity of the enzyme [117]. A single gene codes for ADAR1 that transcribes two different molecular weight proteins [103, 104, 118]. The smaller protein (p110) is constitutively expressed in the cells, while the larger version (p150) is induced by INF signaling [104, 119, 120]. ADAR1 plays a very important role in bone marrow development, apoptosis, and antiviral innate immunity. Knockout of the ADAR1 gene in mice is lethal [100], and the absence of ADAR1 (p110 and p150) has a positive influence on INF production and apoptosis in ADAR1 deficient mice cell lines [101]. From this it

can be seen that ADAR1 plays very important function in the survival of the organism as a major protein of the innate immune response to viruses.

1.3.2 2',5'-Oligoadenylate synthetases (OAS)

OAS are a family of proteins initially identified as IFN-induced proteins that are distinguished by their ability to synthesize unique 2′,5′-linked phosphodiester bonds to polymerize ATP into oligomers of adenosine (2′,5′-A) [121, 122]. Synthesized 2′,5′-A specifically activate RNaseL leading to cellular and viral RNA degradation [123, 124]. OAS in humans include OAS1, OAS2, OAS3 and OASL (OAS-like) [123]. As the OAS proteins are constitutively expressed at low levels they act as PRRs for the detection of viral dsRNA in the cytosol. OAS1 has two splice isoforms in humans that produce two isoforms that differ at their C-termini by 18 and 54 amino acids, respectively. OAS2 produces four alternatively spliced transcripts that encode two proteins as well. OAS3 encodes a single transcript that produces a single protein [122]. These proteins have considerable homology to each other, with OAS1, OAS2 and OAS3 encoding one, two and three "OAS" domains, respectively [123]. An OAS domain adopts a palm fold that contains five antiparallel β strands separated by two α helices (α β β α β β β) [125]. The most distinctive of the OAS proteins is OASL. Two OASL transcripts are expressed producing two proteins. The OASL protein also has an OAS domain, however, it is catalytically inactive.

OAS1 and OAS2 contain a tripeptide motif (CFK) within their OAS domains that is not conserved in the OAS domains of OAS3 and OASL [126]. The tripeptide motif enables OAS1 and OAS2 to form tetramer and dimer respectively, which are the active forms of enzymes that are capable of synthesizing trimeric and tetrameric 2′,5′-linked

adenylate oligomers [127, 128]. It has been shown that the oligomerization of OAS1 and subsequent synthesis of the oligoadenylate chains can be initiated by OAS1 binding viral dsRNAs [129-131]. Trimeric and tetrameric 2′,5′-linked adenylates synthesized by OAS1 or OAS2 can bind to and activate RNaseL [122, 132, 133]. Since OAS3 does not contain tripeptide motif, its active form is a monomer that synthesizes dimeric 2′,5′-linked adenylates [128]. The dimeric 2′,5′-linked adenylates are not efficient activators of RNaseL, and consequently, are thought to regulate alternative processes, with one report suggesting a role in gene expression by regulating DNA topoisomerase I [134].

RNaseL is constitutively expressed as an inactive monomer. Auto-inhibition of the RNaseL is relieved upon binding of 2′,5′-oligoadenylates followed by subsequent homodimerization [135, 136]. The active dimeric enzyme then degrades ssRNA [137, 138]. RNA degraded by RNaseL is able to activate additional cytoplasmic PRRs (RIG-I and MDA5) resulting in type I IFN gene induction and production of other ISGs [139]. This has been shown in RNaseL deficient cells, where a decrease in IFNβ production has been observed due to reduced signaling via these PRRs [140]. Due to their perceived common antiviral action via RNaseL, the antiviral function of the OAS proteins has been investigated using RNaseL-deficient mice. These mice show increased susceptibility to RNA viruses from the *Picornaviridae*, *Reoviridae*, *Retroviridae*, *Myxoviridae*, and *Flaviviridae* families [141]. However, ensuing activation of RNaseL is less commonly observed, presumably because of virally encoded inhibitory factors.

1.4 REGULATION OF INNATE IMMUNITY THROUGH THE RNA-DEPENDENT PROTEIN KINASE (PKR)

The focus of my thesis is an ISG protein product, PKR and its interaction with

small non-coding viral dsRNAs. PKR is a Ser/Thr kinase involved in the first line defense in the innate immune response against viral infections [142]. (PKR) is a double-stranded RNA-activated protein kinase also known as eukaryotic translation initiation factor 2-alpha kinase 2, P1 kinase, p68 kinase, encoded by the *EIF2AK2* gene in humans [143]. The human PKR gene is located on chromosome 2p21-22 [144-146]. The PKR gene consists of 17 exons [145, 147]. PKR belongs to the family of kinases that phosphorylate the alpha subunit of eIF2 that include general control non-derepressible 2 kinase (GCN2), PKR-like endoplasmic reticulum kinase (PERK), and the hemin-regulated inhibitor (HRI) [148, 149].

Expression of PKR varies throughout tissues and developmental stages. During human fetal development, levels of PKR are hardly detectable in blastema and immature mesenchymal cells, but found to be high in a variety of differentiated tissues including epithelial cells [150]. In adult tissues, PKR is expressed at a lower level in the proliferating immature zone of squamous mucosa, while non-proliferating mature keratinocytes shows higher expression of PKR [151]. It has been suggested that the overexpression of human PKR plays a potential role in cell growth regulation by inhibiting cell proliferation in mammalian cells [152]. Conversely, expression of catalytically inactive mutants of PKR (K296R) in NIH 3T3 cells results in tumorigenicity in nude mice [152, 153]. Overexpression of PKR in HeLa cells leads to apoptosis [154]. Recent studies with mouse embryonic fibroblasts derived from the PKR knockout mice have demonstrated its function in apoptosis, induced by both dsRNA and lipopolysaccharide [155].

PKR is a 551 amino acid protein, and consists of tandem copies of a conserved

double stranded RNA binding motif (dsRBMs) in the N-terminal domain of the protein, with a C-terminal Ser/Thr kinase domain [156]. The dsRNA-binding region of PKR spans residues 1-169, and the two dsRBMs are connected by a 23 amino acid long flexible linker [157]. The kinase domain is 299 amino acids long and it includes residues 252 to 551. The dsRNA-binding domain of PKR is connected to the kinase domain by a third region, a long flexible inter-domain linker (80-residue), implicated in PKR self-association **(Figure 1.5A)** [158, 159].

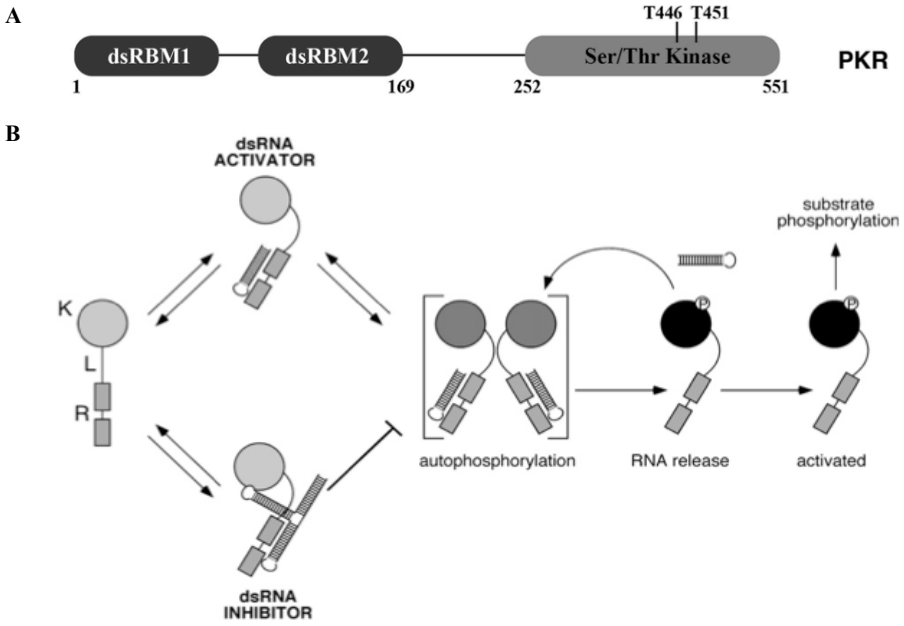

Figure 1.5: A) Schematic representation of PKR. B) Activation and inhibition of PKR by dsRNA

Upon viral infection and subsequent production of viral dsRNAs, PKR binds viral dsRNA that leads to its activation and autophosphorylation of residues on a crucial loop overhanging the kinase active site of the PKR [160]. PKR's binding to dsRNA leads to a conformational change in protein that enables activation and autophosphorylation [161, 162]. Thr446 and Thr451 residues in the activation loop of kinase domain are required to

be phosphorylated for the full PKR activation [162]. PKR can be rendered catalytically inactive by mutating the lysine residue in ATP-binding site Lys296 to Arg (K296R) [163]. Phosphorylated PKR in turn phosphorylates its target substrate, the eukaryotic initiation factor 2α (eIF2α) at Ser51 **(Figure 1.5B)**. eIF2 is a heterotrimeric G protein (α, β, and γ subunits), that is responsible for delivering of Met-$tRNA_i^{Met}$ to the P site of 40S subunit of ribosome and thus initiating translation [164]. eIF2 cycles between its active (GTP-bound) and inactive (GDP-bound) state. The cycling between the GTP and GDP-bound states is regulated by eIF2B. Phosphorylation at Ser51 of α subunit by PKR results in formation of a high-affinity complex between eIF2 and eIF2B. This inhibits the guanidine nucleotide exchange activity of the eIF2 heterotrimeric complex, thereby preventing translation initiation and consequently slowing down the translation of viral proteins [164, 165]. Inhibition of viral protein translation attenuates viral propagation, thereby providing time to the host cell to mount an optimal adaptive immune response [166-168].

1.4.1 The double-stranded RNA-binding motif, a adaptable RNA recognition motif

The double-stranded RNA-binding motif (dsRBM) adopts a canonical αββββα fold that binds to the dsRNAs [169-171]. The fold contains a 3-stranded antiparallel β-sheet flanked by 2 α-helices (Figure 1.5) [169, 170]. Besides its ability to bind dsRNA, the dsRBM can serve as a protein-protein recognition domain [172, 173]. The motif was first discovered by comparing the protein sequence of Staufen and *Xenopus laevis* RNA-binding protein A against the protein database [174]. The domain is found in animals, bacteria, and viruses [175]. Proteins containing the dsRBM(s) possess a myriad of functions including RNA editing and processing, translational control, and protein

modulation amongst the others [176-179]. Proteins can have multiple copies of dsRBMs. ADAR contain 3 copies of the motif, while *Drosophila* Staufen protein contains 5 copies [169, 180]. Human PKR contains a tandem repeat of dsRBMs. NMR studies of PKR_{1-169} in isolation revealed that each dsRBM from PKR adopts a canonical fold containing a 3-stranded antiparallel β-sheet flanked by 2 α-helices with tandem dsRBMs joined by a 23 amino acid linker forming a dsRNA-binding domain of PKR (dsRBDs) that encompass residues 1-169 of full length protein (PKR_{1-169}) [157]. Structures of a single dsRBM from proteins other than PKR in complex with perfectly duplexed dsRNA indicate that approximately 1.5 turns (~15 bp) of the A-form RNA helix (comprising consecutive minor-major-minor grooves) are recognized, and that the contacts are mediated primarily through the 2'-hydroxyl groups of the ribose sugar, explaining the observed selectivity for the RNA [169, 170, 180-183]. The residues in the loop 2 and loop 4 of the dsRBMs mediate the interaction between the dsRBM and the RNA A-form helix with the minor and the major grooves of the RNA [181]. In addition, helix 1 of the motif is interacting directly with the bases from the second minor grove involved in binding. dsRBM1 contains conserved residues throughout the motif, while in the case of the dsRBM2 the conserved residues are found in the C-terminal region of the motif [174]. Both dsRBMs of PKR are required for the high affinity interaction with dsRNA [160]. The affinity of dsRBMs of PKR for dsRNA ranges from 10 to 100 nM [160, 184]. RNA longer then 30 bp is required for optimal activation [151]. *In vitro* experiments show individual domains can bind the dsRNA, with dsRBM1 showing higher affinity compared to dsRBM2 [160, 185].

1.4.2 Kinase domain of PKR is required for dimerization and autophosphorylation

The C-terminal region of PKR encompasses a Ser/Thr kinase domain responsible for target substrate recognition and phosphorylation. Structural studies on the kinase domain in complex with eIF2a detailed the overall Ser/Thr kinase fold as well as the features required for target substrate interaction [165]. The catalytic domain of the protein has a typical protein kinase fold consisting of an N-terminal lobe that is mostly β-sheet and a C-terminal lobe that is predominantly helical. The N-terminal lobe of the kinase domain (residues 258–369) consists of a five-stranded antiparallel β sheet, a canonical helix αC, and a noncanonical helix α0 (residues 258–266), which assimilates into the top groove of the β sheet. The C-terminal lobe (residues 370–551) is comprised of two paired antiparallel β strands and eight α helices [165]. Dimerization and substrate recognition occurs on physically remote ends of the kinase domain. PKR dimerization takes place between the two N-lobes of kinase domain. It also includes a large portion of helix αC, helix α0, the β2-β3 connecting segment and strands β4 and β5 [165]. The recognition of Ser51 on eIF2α is mediated by αG helix of PKR in the surface of the C lobe of kinase domain [165]. Autophosphorylation of PKR at Thr446 and Thr451 promotes substrate recognition and subsequent phosphorylation. Thr446 and Thr451 are found in the activation segment of the kinase domain. This segment is stabilized by the interaction of Thr446 with two Arg residues (Arg307 from the N lobe and Arg413 from C lobe) and Lys304 from the N lobe helix αC. The phosphorylation of eIF2α by kinase domain of PKR requires initial recognition of Ser51 of eIF2α by the αG helix of PKR. This will lead to partial unfolding of segment of eIF2α, which makes the Ser51 accessible for the ATP binding active site of PKR [165, 186, 187]. This mechanism suggests that the

PKR kinase domain has a very specific way of interacting with protein partners thus limiting the number of interacting partners through its kinase domain. This distinguishes PKR from most kinases that recognize a specific and short target peptide sequence.

EIF2α is a trimeric protein complex involved in delivery of Met-tRNA to the ribosomal 40S subunit, thus initiating protein translation [188, 189]. The protein cycles between its active GTP bound and inactive GDP bound states. The cycling between the active and inactive state is performed by eIF2B [164]. The pool of eIF2B in cytoplasm is very low which makes it a crucial regulatory step in protein translation [165]. Once eIF2α is phosphorylated at the residue Ser51, the affinity of eIF2 for eIF2B increases. This makes the eIF2B unavailable for removing of the GDP from the inactive eIF2 complex resulting in the inhibition of translation initiation [168].

The mechanism of PKR activation is still not fully understood, but it is well established that dimerization of the PKR is a key step in PKR activation [160, 165, 190-195]. Additionally, the flexible region found between the dsRBMs as well as the linker connecting the dsRBMs to kinase domain seem to play a crucial role in PKR dimerization and activation [158, 159]. Previous studies have suggested significant flexibility in the two linkers (one between the dsRBMs, the other between the dsRBMs and kinase domains, see **Figure 1.5A**) allowing for two distinct conformations to be observed; an extended "open" conformation where dsRBMs and kinase domains are not in contact, and a collapsed "closed" conformation [158, 161, 196-198]. The data suggest a direct communication between domains that allows propagation of the activation signal initiated by dsRNA binding to the dsRBD, to the kinase domain, via the interdomain linker. The

reverse is also possible, as kinase domain phosphorylation results in reduced affinity for dsRNA ligand [197].

1.5 PKR INVOLVMENT IN SIGNALLING PATHWAYS

PKR is expressed constitutively at low levels in mammalian cells. PKR can bind to dsRNA, dextran sulfate, heparin, chondroitin sulfate, poly-L-glutamine, and several other proteins of human and pathogen origin. The interaction is mostly mediated by the dsRBMs of PKR. These interacting partners behave as either PKR activators or inhibitors. The activators facilitate the dimerization of PKR, while the inhibitors prevent this event. PKR is involved in myriad of pathways including translation regulation, cell stress, signal transduction, tumor suppression, and apoptosis.

1.5.1 Regulation of PKR by cellular proteins

The presence of stress-inducing molecules, such as hydrogen peroxide, ceramide, arsenite, thapsigargin, and cytokines (including IFNγ, IL-3 and TNF) can lead to PKR activation through interaction with **PKR-associated activator (PACT)** [199, 200]. PACT is expressed ubiquitously at a very low level in many tissues [200]. Overexpression of PACT due to cell stress leads to PKR activation, which in turn phosphorylates eIF2α [200, 201]. Phosphorylation of PACT at Ser18 and Ser287 leads to its binding and activation of PKR [202]. Phosphorylated PACT binds to PKR through its own dsRBMs creating a heterodimer. PACT contains three copies of the dsRBM domain [173]. The first two dsRBMs interact with the dsRBMs from PKR, while the third plays a crucial role interacting with the kinase domain of PKR [173, 203].

The trans-activation response (TAR) RNA binding protein (TRBP) is a dsRNA-binding protein first recognized and named by its ability to bind human

immunodeficiency virus type 1 (HIV-1) TAR RNA [204, 205]. TRBP binding to TAR RNA relieves translational block caused by the TAR RNA structure, as a result HIV-1 level of gene expression increases [206]. TRBP is also found to be an inhibitor of PKR [207]. In virally infected cells, TRBP inhibits PKR by directly binding to it and blocking PKR's kinase activity, or by sequestering the dsRNA from the PKR as seen in case of HIV-1 TAR RNA [172, 207]. TRBP's ability to inhibit PKR was first observed in cells infected with vaccinia virus lacking E3L protein where TRBP facilitated viral growth that was attributed to dsRNA sequestering by TRBP [207]. TRBP can inhibit PKR by direct interaction through their dsRBDs [172]

TRBP can interact with both the PACT and PKR [207, 208]. TRBP has ~40% similarity to PACT at the amino acid sequence level [200]. It also contains three copies of the dsRBMs, and just like PACT the first two dsRBMs of TRBP are used for dsRNA binding [209]. TRBP interacts with PACT through all three dsRBMs [208]. In an uninfected state TRBP is found in the complex with PACT [210]. This prevents the PACT mediated PKR activation. When the cell is found in state of stress, phosphorylation of PACT at Ser287 enables PACT to dissociate from the TRBP that leads to stress-mediated activation of PKR. PKR then go on to phosphorylate eIF2α and eventual cell apoptosis [201, 211, 212].

1.5.2 PKR's involvement in signal transduction

PKR is involved in several pathways implicated in gene transcription cell growth and apoptosis. Tumor suppressor **p53** is a transcription factor involved in cell response to genotoxic stress. Activation of p53 in response to cellular stress leads to cell cycle arrest or apoptosis. It has been shown that PKR can induce apoptosis in U937 cells in response

to TNF-α signaling [213]. Simultaneously, this was correlated with PKR's ability to activate/promote activation of p53. An additional study showed that PKR can directly interact with the C-terminus of p53 and phosphorylate it at Ser392 residue [214]. Mouse embryo fibroblasts (MEF) with fully knockout PKR gene also point to PKR's role in changing p53 function in response to adriamycin or gamma irradiation [214].

PKR plays a role in apoptosis by activating **Nuclear factor kappa B (NF-κB)**. In resting cells, NF-κB is associated in complex with Inhibitor of kappa B (IκB). Phosphorylation of IκB releases the NF-κB from the complex, and allows the NF-κB to move into nucleus where it regulates transcription [215]. IκB is phosphorylated by a trimeric IKK complex at two serine residues (Ser32 and 36). IKK is composed of the catalytic IKKα and IKKβ subunits and a regulatory protein IKK gamma, also called NEMO (NF-κB essential modulator) [216]. The phosphorylation of IκB will result in its ubiqutination and eventual proteolytic degradation [217, 218]. PKR's role in NF-κB signaling was first observed in response to dsRNA treatment. It was shown that PKR down-regulation negatively correlates with NF-κB activation [219]. Furthermore MEF cells with PKR knockout upon being treated with a synthetic dsRNA polyInosine:polyCytosine (polyI:polyC or polyIC) resulted in a much lower level of expression of type I IFN mRNA then cells with wt PKR [220]. PKR activated in dsRNA-dependent manner physically interacts with IKK complex that leads to activation of NF-κB [217, 221, 222]. However, it is not clear whether PKR interaction with IKK, or PKR's kinase activity, is required for the activation of IKK complex by PKR. It has been demonstrated that with PKR with mutation (K296R) can still be co-immunoprecipitated with IKK, although this catalytically inactive PKR mutant behaves as a poor activator of

IKK [223, 224]. On the other hand, in the same research carried out this time in PKR knockout cells but transfected with either wild type PKR or catalytically inactive PKR show that only wild type PKR is capable of initiating the NF-κB signaling.

1.5.3 PKR interaction with dsRNA

In the presence of the viral dsRNA in the host cell, PKR expression is induced by TLR3 signaling that stimulates the INF cascade [78, 142, 225]. As previously stated, PKR binds to long stretches of dsRNA, but it can also tolerate loops, bulges, junctions, and pseudoknots [226-231]. PKR can interact with genomic RNA, mRNAs, non-coding RNAs, and synthetic RNAs [232]. Both dsRBMs are required for full binding affinity, and while dsRNAs 30 bp or longer are optimal for PKR dimerization and activation, shorter RNAs that contain small dsRNA stretches are shown to activate PKR as well [157, 194, 230]. There are several well-characterized viral dsRNAs that interact with PKR including adenovirus VA (viral associated) RNAs (VA_I and VA_{II}), HIV-1 transactivation response (TAR) element, Epstein–Barr virus-encoded small RNAs (EBER-1 and EBER-2), Hepatitis C virus internal ribosome entry site (HVC IRES), and 5' untranslated region of IFN-γ mRNA [233-238]. These RNAs act as either activators or inhibitors of PKR. In addition to working with VA_I, I have also performed studies on characterizing the interaction between PKR and TAR. In this section I will give an overview on several viral PKR dsRNA substrates including those used in experiments in this thesis.

HIV-1 transactivation response (TAR) element is a well-characterized viral dsRNA activator of PKR. TAR is an RNA stem-loop structure spanning nucleotides +1 to +59 of the newly synthesized viral mRNA **(Fig. 1.6)** [233].

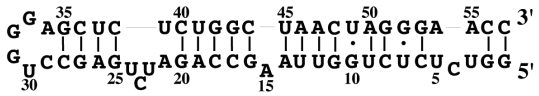

Figure 1.6: Schematic of HIV TAR secondary structure

TAR adopts an A-form RNA helix with distortions including a trinucleotide bulge and hexaloop [239, 240]. Transcription of HIV-1 genes is intiated at TAR element [204, 241]. The translational block formed by the TAR RNA structure can be relieved by several proteins including HIV Trans-Activator of Transcription (Tat) protein [202, 204, 242-244]. Tat binds to the highly conserved stem-loop region of TAR and it additionally recruits the human positive transcription elongation factor b (P-TEFb) to the site [245-247]. P-TEFb is crucial for the Tat transactivation. P-TEFb is a complex of proteins that consists of the cyclin-dependent kinase 9 (CDK9) and its regulatory partner cyclin T1 (CycT1) [245, 247]. Recruited P-TEFb phosphorylates the C-terminal domain (CTD) of RNA Polymerase II along with elongation factors DRB Sensitivity Inducing Factor (DSIF) and negative elongation factor (NELF) [248]. Phosphorylated polymerase that was previously stalled at the TAR site can now start transcribing viral mRNA resulting in production of viral proteins [248].

HIV-infected cells treated with interferon demonstrate a decreased production of HIV proteins as well as HIV particles [249]. The interferon-mediated response is ascribed to the activity of PKR in lymphocytes as transduction of PKR into T-cell progeny protects cells from HIV-1 infection and severely inhibits HIV-1 replication rates in infected cells [250]. PKR binds directly to TAR which leads to its dimerization and autophosphorylation [226, 251, 252]. Phosphorylation of eIF2α by PKR leads to translational arrest in the cell [248]. Interestingly, PKR can also phosphorylate Tat, which

leads to increased affinity of Tat for TAR and enhances the transcription of viral genes [253]. A recent study has suggested that defects (*i.e.* bulge or hexaloop) serve as anti determinants to PKR binding and activation, and that TAR unwinding and dimerization represents the activating species [254]. However, the biological basis for TAR dimerization remains unresolved at present.

Viruses produce small dsRNAs that contain well-structured conserved regions that upon interaction with PKR obstructs PKR's self-association [236, 255-258]. During a latent state of infection, Epstein-Barr virus (EBV) constitutively expresses several gene products, including the **Epstein–Barr virus-encoded small RNAs**, **EBER-1 and EBER-2 RNAs** [257, 259]. EBER1 inhibits PKR by preventing its self-association [160, 258]. EBV is a γ herpesvirus with a double-stranded DNA genome [260]. The virus is widespread in human populations and is usually present in the dormant state throughout the host's life. EBV was first characterized as a causative agent of Burkitt's lymphoma [260], and later it has been associated with several other human tumors; however, in most cases the infection by EBV does not result in formation of cancer [261-263].

After initial infection of B-lymphocytes, EBV genome circularizes and the virus progresses through the lytic life cycle [264]. During the lytic phase, EBV causes B-lymphocytes to undergo apoptosis [265]. A small portion of EBV enters memory B cells and goes into the latent phase, thus maintaining the pool of EBV within the host [265, 266]. During the latent phase, the virus is not replicated and only a small subset of genes are being expressed: Epstein–Barr nuclear antigen (EBNAs), latent membrane proteins (LMPs), and EBERs which are transcribed in high copies [267]. Epstein–Barr nuclear antigen (EBNA-1 and EBNA-2) are transcription factors responsible for regulation of

viral transcription, and are implicated in cell apoptosis by destabilizing p53 transcription factor thus accounting for anti-apoptotic functions of EBV [268]. LMPs are integral membrane proteins that also possess anti-apoptotic properties [269]. LMPs exert their anti-apoptotic effects through activation of NF-κB, MAP kinase and PI3k pathways [269, 270]. EBER-1 and EBER-2 are small non-coding dsRNAs (167- and 172-nucleotide-long respectively) that have three major stem-loops with several internal bulges, loops, junctions, and non-canonical base pairs [271]. The double-stranded stem loop regions of EBER1 stem IV contain a highly conserved region GGGU that is involved in binding specifically to the PKR dsRBM1 domain [272]. Expression of EBER-1 in EBV-negative cells prevents INF-induced apoptosis by inhibiting PKR's pro-apoptotic activity [273]. It is believed that EBER-1 inhibits PKR by preventing PKR's self-association and sequestering PKR from viral dsRNA activators [257, 274].

Hepatitis C virus (HCV) **internal ribosome entry site (IRES)** is a segment of the HCV RNA based genome required for initiation of translation [275, 276]. HCV is a member of the *Flaviviridae* family, and its genome is made up of positive-sense single-stranded RNA. The virus causes several diseases in humans including chronic hepatitis, cirrhosis, and hepatocellular carcinoma [277]. HCV IRES is located at the 5' end of the HCV genome [275, 276]. The IRES binds to the 40S subunit of ribosome and it positions its start codon next to the peptidyl-tRNA site. The initiation of translation through IRES requires recruitment of only few initiation factors including initiator Met-tRNA, the trimeric GTPase eIF2, as well as the IF2 orthologous eIF5B, another GTPase, and the large multiprotein assembly eIF3 [278-280].

The HCV IRES element has a very complex structure with several stretches of

double-stranded regions [281-284]. The structure is comprised of four domains (I-IV) with defined functions: domain I is not required for IRES function, domain II is located near the ribosomal P-site codon, and recruits and modulates initiation factor binding and function, domain III mediates the interaction with a protein-rich ribosomal surface near the tRNA exit site, whereas the domain IIIabc junction, stem loop IIIe, and the RNA pseudoknot are essential for ribosomal interaction [279, 285-288]. *In vitro* activations studies have shown that HCV IRES is a potent activator of PKR with maximum activation rates achieved at equimolar ratio of RNA and protein [237]. The high affinity interaction with PKR is mediated by domains III and IV of HCV IRES, which coincides with the highest activation. In addition, *in vitro* activation of PKR by IRES leads to PKR mediated phosphorylation of eIF2α. However, it has been shown that IRES directed translational initiation does not require presence of eIF2 but instead uses eIF5B for GTP hydrolysis [289]. Initiation of translation through eIF5B allows HCV to circumvent PKR-mediated inhibition of protein synthesis.

1.6 VA_I AS A PKR INHIBITOR

One of the most studied PKR inhibitors is adenovirus **VA (viral associated) RNA I (VA_I)** [160, 234, 235, 290-292]. Adenovirus first isolated from adenoids is non-enveloped that belongs to the family of Adenoviridae [293, 294]. Adenovirus is best know for causing the common cold and other illnesses of respiratory system, but it is also known to be implicated in wide range of diseases including gastroenteritis, conjunctivitis, and cystitis [295-297]. In addition, in recent years adenovirus has been used as vector for gene therapy [298-300].

Adenovirus has a linear double-stranded genome contained inside an icosahedral

capsid [294]. Initially the virus is engulfed into the cell, and upon un-coating the adenovirus genome migrates into the nucleus [301]. The adenovirus life cycle consist of both early and late phases which coincides with production of early and late genes [302]. Expression of the early genes results in production of proteins that are mostly involved in blocking the host immune system, preventing apoptosis, and ultimately initiating production of the late genes [302, 303]. One of the earliest and most important proteins expressed are from the E1a genes. E1a codes for two proteins (different splice variants of the same gene), which are involved in activation of viral gene expression, evasion of host immune system, and viral replication [301, 303-305]. The two proteins encoded by E1a gene are 289 and 243 amino acids long, respectively. The longer splice variant of E1a gene is an activator of transcription protein, while the shorter one is a repressor of transcription [306-308]. Even though it not being a DNA-binding protein itself, E1a protein regulates transcription by recruiting itself to chromatin via help of transcription factors [306, 309-311]. Once localized to chromatin, E1a recruits chromatin-remodeling factors and other transcription regulators that enable change in gene expression. As stated previously, E1a (289) does not bind to DNA but instead activate E2F that leads to transcription of viral genome [311]. E2F is a transcription factor involved in control of gene expression as an activator of transcription [312-315]. E2F is found in an inhibitory complex with a member of retinoblastoma (Rb) family proteins, a key regulator of exit from the G_1 phase of the cell cycle [316]. E1a binding to Rb releases the E2F out of inhibitory complex [317]. E2F replaces the repressors from the E2F-regulated genes which forces the cell to enter cell cycle [318]. Activation of E2F leads to expression of E2 early viral genes, required for replication [319]. Expression of the late genes will lead

to the production of capsid and other proteins required for viral packaging and release [301, 304].

Adenovirus can also express two small non-coding VA RNAs (VA_I and VA_{II}) depending on the serotype, with a considerable difference in sequence despite similar lengths (157-160 nucleotides for VA_I and 158-163 nucleotides for VA_{II}). VA_I and VA_{II} are required for efficient translation of viral and cellular mRNAs late in infection [320]. Most of the experiments carried out concerning VA RNA structure and function have used human adenovirus serotypes 2 and 5 as a model [302]. VA_I and VA_{II} are made at the same time as E1a proteins and they are continuously produced throughout the late phase of viral replication. VA RNAs are transcribed by the host RNA Polymerase III, and their expression is independent of E1A-mediated transactivation, therefore VA RNAs are always transcribed from the adenovirus genome in adenovirus-infected cells [305]. Deletion of VA_I RNA causes a 10-20-fold decrease in viral growth, while deletion in both VA RNAs results in 60-fold decrease in viral growth [321]. However, deletion of the VA_{II} alone has little impact on viral replication [322]. During the late phase VA_I expression reaches 10^8 copies per cell [302].

In addition to its role in viral growth, another important function of VA_I is in the mediation of innate immunity and RNAi pathways. PKR has been identified as one of the key enzymes responsible for an overall decrease in protein synthesis in host cells in the absence of VA_I RNA [234, 290]. Upon binding to PKR, VA_I RNA acts as an inhibitor of PKR and prevents its self-association [160, 234, 235, 290-292]. Based on functional studies, mutagenesis, comparative sequence analysis, and structure probing studies, the secondary structure of VA_I RNA has been determined to consist mainly of a double-

stranded RNA (dsRNA) with three major domains; an apical stem-loop (AS), a central stem-loop (CS), and a terminal stem (TS) **(Figure 1.7)** [321, 323, 324].

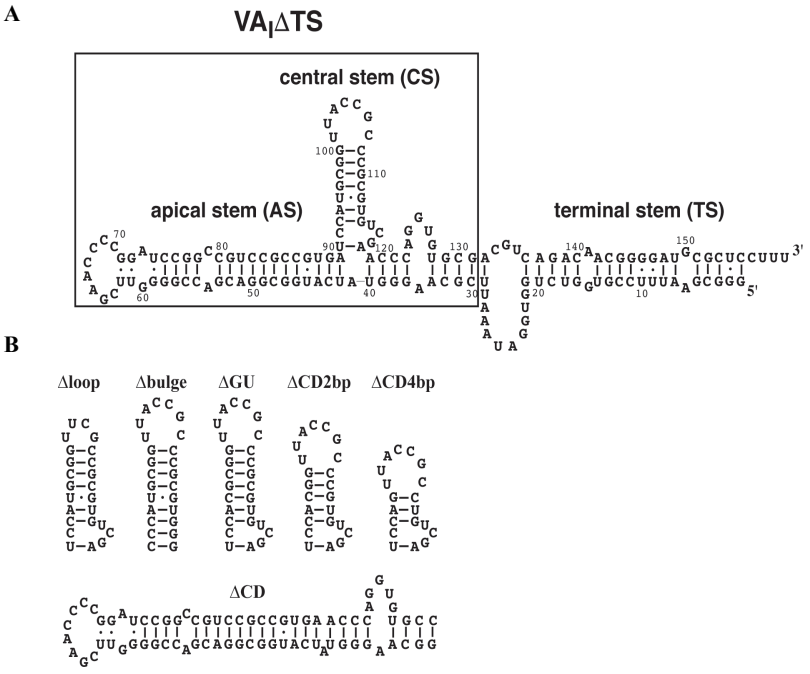

Figure 1.7: A) Secondary structure of VA$_I$ RNA presenting the apical stem (AS), central stem (CS), terminal stem (TS) and VA$_I$ΔTS (boxed). B) Schematic representation of mutations in the central stem-loop of VA$_I$ΔTS

The apical stem-loop serves to bind to dsRBMs of PKR. Recent studies have shown that apical stem exists in two different conformations in the infected cell with different functional activities [292]. The CS of VA$_I$ is responsible for the PKR inhibition by preventing self-association of PKR and subsequent autophosphorylation [160, 274, 291, 292]. Surprisingly, PKR autophosphorylation assays, isothermal calorimetry, NMR studies and RNA footprinting have demonstrated that the central stem does not make a high affinity interaction with any region of PKR [160, 274, 291, 292]. The most straightforward interpretation based on the literature is that the central stem serves as a steric block to self-association of two PKR proteins required for PKR autophosphorylation. The VA$_I$ terminal stem (nucleotides 1-29 and 132-159) is not

required for PKR inhibition *in vitro* [291]. The terminal stem is required for binding of Exportin 5, which transports VA_I from the nucleus to the cytoplasm [325].

Interestingly, VA_I can bind to Dicer (an endoribonuclease that cleaves dsRNA as part of the RNAi) [326, 327], and a small percentage of VA_I RNA is cleaved by the Dicer at the terminal stem [328]. The cleaved terminal stem (called mivaRNA) can be incorporated into an RNA-induced silencing complex (RISC), and also acts as a non-competitive inhibitor of Argonaute 2, a catalytic component of RISC that performs cleavage of dsRNA [328, 329]. Dicer cleavage of VA_I can yield two different mivaRNAs: mivaRI-137 and mivaRI-138 [330]. Bioinformatic analysis of the Adenovirus genome shows no potential sequence targets for the mivaRNAs [331]. Microarray experiments together with bioinformatic analysis were carried out to identify potential host cellular targets of mivaRNAs, and the target genes whose expression could potentially be controlled by mivaRNAs were classified into five groups: genes involved in cell signaling, cell growth and apoptosis, DNA transcription or DNA repair, and RNA metabolism [330]. The same study demonstrated that mivaRI-138 binds to the 3′UTR of TIA-1 (cytotoxic granule-associated RNA binding protein) and decreases TIA-1 mRNA and protein expression. Dicer-processed VA_I lacking its terminal stem ($VA_I\Delta TS$) is the shortest version that binds to PKR with identical affinity to full length RNA, and is sufficient to mediate inhibition of PKR *in vitro* [184, 274, 291, 332]. In this thesis, $VA_I\Delta TS$ is often used as the wild type (wt) RNA to study its mechanism of PKR inhibition.

1.7 RATIONALE FOR THE THESIS

PKR was discovered from the observation that cell extracts prepared from IFN-treated vaccinia virus-infected cells were susceptible to a translational block after addition to a cell-free system of the exogenous mRNA [333]. Later, it was shown that PKR's interaction with dsRNA leads to its enzymatic activation via autophosphorylation. Activated PKR subsequently phosphorylates eIF2α, thus attenuating the translation of cellular proteins. PKR is a Ser/Thr kinase that has tandem dsRNA-binding motifs (dsRBMs) and kinase domain that is connected to the dsRBMs by the flexible linker [157-159, 165]. It has been shown that PKR requires approximately 15 bp of RNA per dsRNA binding motif and that RNAs longer then 30 bp are good activators of PKR [151, 169, 170, 180-183]. In addition, specific structural features such as bulges, loops, *etc*., and nucleotide modifications (*i.e.* 5'-phosphorylation state) have been observed to be accommodated by PKR, and in some cases significantly affect both the affinity for and activation of PKR [226-231].

HIV-1 TAR RNA and Adenovirus VA RNA (VA_I) are viral dsRNAs that form high-affinity interaction with PKR [160, 226, 234, 235, 251, 252, 290-292]. HIV-1 TAR is a well-characterized activator of PKR [226, 251, 252]. TAR adopts mostly dsRNA helix with distortions including a trinucleotide bulge and hexaloop [239, 240]. HIV-infected cells treated with interferon demonstrate a decreased production of HIV proteins as well as HIV particles that is ascribed to the activity of PKR in lymphocytes as transduction of PKR into T-cell progeny protects cells from HIV-1 infection and severely inhibits HIV-1 replication rates in infected cells [249, 250]. Adenovirus VA RNA (VA_I) is a small non-coding mostly dsRNA that binds to PKR and prevents it from exerting its

antiviral effect [160, 234, 235, 290-292]. Cells infected with adenovirus lacking VA_I show a global decrease in protein translation due to the PKR's antiviral activities [234, 290]. VA_I dsRNA consists of three major stem-loop regions with different functions; an apical stem-loop which binds to the PKR dsRBM region; the central stem-loop domain that is responsible for PKR inhibition; and a terminal (Dicer-processed) stem structure that is entirely dispensable or the PKR kinase inhibition activity of VA_I [160, 274, 291, 292]. In addition to its capability to bind to and inhibit PKR, VA_I is a substrate of Dicer [328]. Cleavage of VA_I by Dicer leads to the formation of VA_I-derived microRNA that can bind to and saturate RISC complex and therefore effectively inhibit RNAi system. The remaining Dicer processed truncated version of VA_I ($VA_I\Delta TS$) inhibits PKR to the same extent as the wt RNA [184, 274, 291, 332].

Given that each individual dsRBM requires approximately 15 bp for interaction, it is unclear how the tandem dsRBM domains of PKR are interacting with TAR RNA and the apical stem of VA_I. High-resolution information on tandem dsRBM-dsRNA complexes has been difficult to obtain, likely due to the flexibility of both the interdomain linker between dsRBM1 and 2 and the inherent flexibility of stem-loop RNA structures. Chapters 3 and 4 (Results) investigate how each dsRBM of PKR orients and interacts with TAR and $VA_I\Delta TS$ RNAs to provide a plausible framework for the recognition of imperfectly base-paired RNA ligands by the tandem dsRBMs of PKR.

The mechanism of inhibition of PKR by VA_I also remains unclear. Identification of specific sequence(s) or structure(s) in the central domain of VA_I that could form direct contacts with PKR that are potentially required to prevent PKR's self-association and activity has remained elusive. Despite this, I originally hypothesized that the central

inhibitory stem-loop domain of VA_I has a complex tertiary structure that is critical for inhibition of PKR by preventing self-association. Chapter 5 (Results) of the thesis investigates the mechanisms of interaction and inhibition of PKR by the adenovirus VA_I RNA and its truncated version ($VA_I\Delta TS$). The working hypothesis is that specific structural features of the central stem will correlate with the ability to inhibit PKR. To test my hypothesis, I have designed mutations to the central stem of $VA_I\Delta TS$ that do not affect the structural integrity of the RNA but will have an impact on function *in vitro*.

I used electrophoresis mobility shift assays (EMSA), and isothermal calorimetry (ITC) to measure binding affinities between PKR and dsRNA ligands. Biophysical techniques including dynamic light scattering (DLS), analytical ultracentrifugation (AUC), and small angle X-ray scattering (SAXS) were used to investigate the structural features of individual RNAs, proteins, and complexes. *In vitro* studies included well-established enzymatic assays that test activation and inhibition of purified recombinant PKR in presence of the mutant versions of $VA_I\Delta TS$. The minimum requirement for PKR activation is autophosphorylation at the residue Thr446. After incubation of PKR with RNA in presence of ATP, commercially available antibodies for Thr446 were used to detect for the presence of phosphorylated (activated) PKR by performing Western blotting.

Following the results chapters, in the final chapter (Chapter 6: Summary and Future Directions) an attempt is made to link and rationalize the result chapters. Also I try to establish the link between the specific features of tertiary structure of RNA and extent of its role on PKR autophosphorylation that allow PKR to perform its function in response to viral infections. Overall, this work give insight into regulation of PKR's

activity by imperfectly base-paired viral dsRNAs.

CHAPTER 2: MATERIAL AND METHODS

2.1 PROTEIN SAMPLE PURIFICATION

PKR is a 551 amino acid long protein that consists of two major domains: dsRNA-binding domain, which is a tandem repeat of dsRNA-binding motif, and a kinase domain, which is catalytic part of the protein. Interestingly, individual domains can be expressed as recombinant proteins. The dsRNA-binding domain encompasses residues 1 to 169 (PKR_{1-169}), and it can bind to dsRNA with similar affinities to full length PKR [160, 274, 334]. The protein fragments were cloned into pET29b plasmid (kanamycin resistance) within the NdeI/KpnI restriction sites. Transformation into *Escherichia coli* (*E. coli*) strain BL21(DE_3)-Rosetta (Novagene) includes initially mixing ~50 ng of plasmid with 50 μL of cells and incubating on ice for 15 min for plasmid uptake. Following this, cells were heat-shocked at 42 °C for 30s, followed by incubation on ice for additional 2 min. Cells were then allowed to recover in super optimal broth (SOB) in shaking incubator at 37 °C for an hour followed by plating on Luria-Bertani (LB) agar plate containing appropriate antibiotic (100 μg/mL) for the selectivity and overnight incubation at 37 °C.

Recombinant human PKR_{1-169} as well as full length PKR were expressed and purified as C-terminal His_6 fusion proteins in the E. coli BL21(DE_3) strain. Full length PKR was co-expressed with λ phosphatase to obtain a dephosphorylated (inactive) protein for further characterization. In the case of PKR_{1-169} bacterial cell cultures were grown to A_{600}=0.4 in LB Broth medium supplemented with the appropriate antibiotics, followed by induction with 1 mM isopropyl β-d-thiogalactopyranoside (IPTG) for 3 h at 37 °C. For full length PKR expression, prior to addition of IPTG cells were cooled on ice

for 15 min and then protein was expressed overnight at 20 °C. All subsequent steps were performed at 4 °C and the procedure is identical for the purification of both full length PKR and PKR_{1-169}. First the cell culture was spun down to pellet the cells at 5000 x g for 10 min in an centrifuge (Thermofisher Scientific, USA). The pelleted cells were resuspended in 20 mL of ice-cold lysis buffer (50 mM Tris–HCl (pH 8.0), 1 M NaCl, 5% (v/v) glycerol, 5 mM β-mercaptoethanol) and lysed by sonication (Fisher Scientific, USA). The lysed cells were then centrifuged at 32000 x g for 25 min. Following centrifugation the supernatant was applied to a 5 mL Ni-NTA column (Qiagen) pre-equilibrated with lysis buffer. The column was washed with 10 column volumes of His-A buffer (50 mM Tris–HCl (pH 8.0), 1 M NaCl, 5 mM β-mercaptoethanol, 1 mM imidazole), followed by ten column volumes of His-B buffer (50 mM Tris–HCl (pH 8.0), 300 mM NaCl, 5 mM β-mercaptoethanol, 10 mM imidazole), followed by 5 column volumes of His-C buffer (50 mM Tris–HCl (pH 8.0), 300 mM NaCl, 5 mM β-mercaptoethanol, 25 mM imidazole) before elution in 20 ml of His-elution buffer (50 mM Tris–HCl (pH 8.0), 300 mM NaCl, 100 mM imidazole, 10% glycerol, and 5 mM β-mercaptoethanol). Affinity purified PKR_{1-169} was subjected to size exclusion chromatography (SEC) using a HiLoad 26/60 Superdex 75 gel filtration column (2.6 x 60 cm, GE Healthcare Life Sciences, USA) in 50 mM Tris (pH 7.50), 100 mM NaCl, and 5 mM 2-mercaptoethanol, while final purification of full length PKR was performed on HiLoad 26/60 Superdex 200 size exclusion column. The eluted fractions were monitored by means of absorbance at 280 nm and fractions containing purified protein were combined and concentrated using Millipore concentrator filters (Millipore, USA). Protein purity was confirmed by SDS-PAGE and concentration was determined using the known

extinction coefficient (ε_{PKR}=41070 $cm^{-1}M^{-1}$, and $\varepsilon_{PKR1-169}$=9200 $cm^{-1}M^{-1}$) as measured by UV-Vis spectrophotometry (NanoDrop2000c, Thermo Scientific, USA).

2.2 RNA PREPARATIONS AND PURIFICATION

All plasmids were transformed into either *E. coli* MAX Efficiency® DH5α™ Competent Cells (Life Technologies, Invitrogen). RNA sequences were cloned into pUC119 vector (ampicillin resistance) within the HindIII/EcoRI sites, and plasmids were linearized by either BstZ17I or BsaI restriction enzyme (**Figure 2.1**).

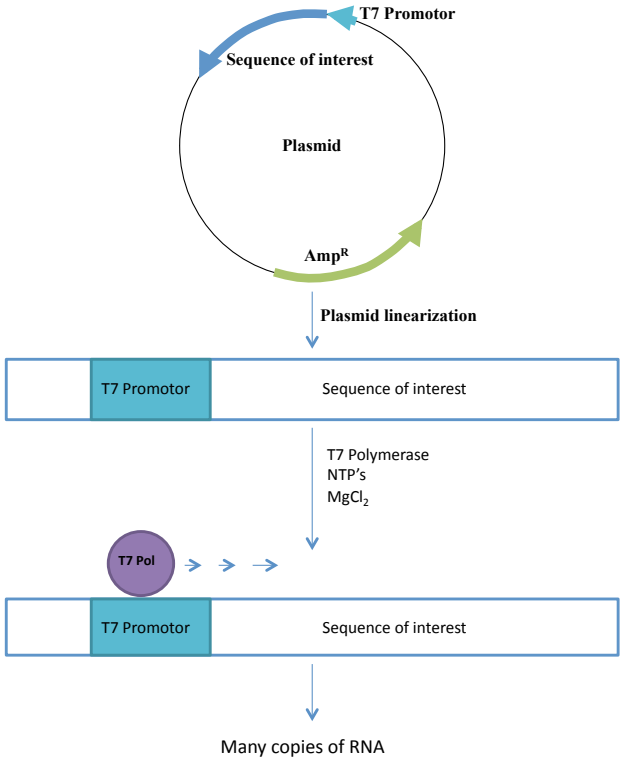

Figure 2.1: *In vitro* RNA transcription. Plasmid is linearized with restriction enzyme and extracted using phenol/chloroform/isoamyl alcohol. RNAs were transcribed by *in vitro* transcription from a linearized plasmid using T7 polymerase. Final purification of RNAs is performed by SEC.

Sequences corresponding to each produced RNA are as follows:

HIV-1 TAR:
5’−GGUCUCUCUGGUUAAGCCAGAUCUGAGCCUGGGAGCUCUCUGGCUAAC
UAGGGAACC−3’

VA_I full length:
5’−GGGCGAAUUUCCGUGGUCUGGUGGAUAAAUUCGCAAGGGUAUCAUGGC
GGACGACCGGGGUUCGAACCCCGGAUCCGGCCGUCCGCCGUGAUCCAUGCG
GUUACCGCCCGCGUGUCGAACCCAGGUGGCGACGUCAGACAACGGGGAUGC
GCUCCUUU−3’

VA_IΔTS (wt):
5’−GGCAAGGGUAUCAUGGCGGACGACCGGGGUUCGAACCCCGGAUCCGGCC
GUCCGCCGUGAUCCAUGCGGUUACCGCCCGCGUGUCGAACCCAGGUGUGCC
−3’

Δloop:
5’−GGCAAGGGUAUCAUGGCGGACGACCGGGGUUCGAACCCCGGAUCCGGCC
GUCCGCCGUGAUCCAUGCGGUUCGCCGCGUGUCGAACCCAGGUGUGCC−3’

Δbulge:
5’−GGCAAGGGUAUCAUGGCGGACGACCGGGGUUCGAACCCCGGAUCCGGCC
GUCCGCCGUGACCCAUGCGGUUACCGCCCGCGUGGGACCCAGGUGUGCC−3’

ΔCD:
5’−GGCAAGGGUAUCAUGGCGGACGACCGGGGUUCGAACCCCGGAUCCGGCC
GUCCGCCGUGAACCCAGGUGUGCC−3’

ΔGU:
5’−GGCAAGGGUAUCAUGGCGGACGACCGGGGUUCGAACCCCGGAUCCGGCC
GUCCGCCGUGAUCCACGCGGUUACCGCCCGCGUGUCGAACCCAGGUGUGCC
−3’

ΔCD2bp:
5’−GGCAAGGGUAUCAUGGCGGACGACCGGGGUUCGAACCCCGGAUCCGGCC
GUCCGCCGUGAUCCACGGUUACCGCCCGUGUCGAACCCAGGUGUGCC−3’

ΔCD4bp:
5’−GGCAAGGGUAUCAUGGCGGACGACCGGGGUUCGAACCCCGGAUCCGGCC
GUCCGCCGUGAUCCAGUUACCGCCUGUCGAACCCAGGUGUGCC−3’

VA_I-AS:
5’−CCCATGGCGGACGACCGGGGTTCGAACCCCGGATCCGGCCGTCCGCCGTG
GGGTA−3’

Mini or Maxi protocols (Thermo scientific, USA) were followed to purify the desired quantity of template DNA required for either protein expression or *in vitro* transcription. The cells were grown overnight in manufacturer recommended volume of LB media containing appropriate antibiotic for selectivity. Prior to performing the *in vitro* RNA transcription, the desired plasmid was linearized using BstZ17I or BsaI restriction enzyme (NEB) and over night digestion was performed at 37°C. This digestion step is followed by adding an equal volume of phenol/chloroform/isoamyl alcohol (25:24:1) required for extraction of linearized plasmid from the organic layer containing the polymerase. The upper aqueous layer is transferred into a new tube followed by DNA precipitation with 3 M sodium acetate and addition of 2.5 - fold excess of cold 95% ethanol. DNA pellet was obtained by centrifugation at 21000 x g on a tabletop centrifuge (Thermo scientific). After a quick wash with 70% ethanol to remove residual salt, the DNA pellet was dissolved in HPLC-grade water to a concentration of 500 µg/mL.

HIV-1 TAR, Adenovirus VA_I RNA and its truncated versions were prepared by *in vitro* transcription from a linearized template plasmid under control of the T7 RNA polymerase promoter. The reaction was prepared by mixing 50 µg/mL of linearized plasmid with 1X T7 polymerase buffer (100 mM Tris-HCl (pH 8.10 at 37 °C), 10 mM spermidine, 1% w/v Triton X-100, 1 mM dithiothreitol and HPLC water), 8 mM nucleotide triphospahte (NTP) mix, 10 mM $MgCl_2$, and 1µL T7 RNA polymerase. The reaction was incubated at 37 °C for 3 h. Following the incubation, the reaction mixture was spun by centrifugation at room temperature (2700 x g for 5 min) to remove the pyrophosphate precipitate. The reaction is then quenched by adding excess EDTA (50 mM) to chelate the remaining Mg^{2+}. An equal volume of phenol/chloroform/isoamyl

alcohol (25:24:1) was added, and the mixture was transferred into a phase lock gel kit (5 PRIME, Hamburg, Germany). Centrifugation at 1500 x g ensures that the organic phase is removed from the aqueous layer by phase separation. The aqueous layer is then transferred onto a 10-DG desalting column (BioRad) to remove traces of phenol/chloroform and small molecule contaminants (salts and NTPs). The final purification of RNAs is performed by SEC using a HiLoad 26/60 Superdex 75 gel filtration column (2.6 x 60 cm, GE Healthcare Life Sciences, USA) in the absence [50 mM Tris (pH 7.50), 100 mM NaCl] or presence of $MgCl_2$ [50 mM Tris (pH 7.50), 100 mM NaCl, and 5 mM $MgCl_2$]. The purity of the transcribed RNA was verified by native polyacrylamide gel electrophoresis (in 1 X TBE buffer) and concentration was determined spectrophotometrically (NanoDrop2000c, Thermo Scientific), monitoring at 260 nm using the calculated extinction coefficients (ε_{VAI}=1552300, $\varepsilon_{VAI\Delta TS}$=975000 $cm^{-1}M^{-1}$, $\varepsilon_{\Delta loop}$=948500 $cm^{-1}M^{-1}$, $\varepsilon_{\Delta bulge}$=963000 $cm^{-1}M^{-1}$, $\varepsilon_{\Delta CD}$=712000 $cm^{-1}M^{-1}$, $\varepsilon_{\Delta GU}$=975000 $cm^{-1}M^{-1}$, $\varepsilon_{\Delta CD2bp}$=937125 $cm^{-1}M^{-1}$, $\varepsilon_{\Delta CD4bp}$=902000 $cm^{-1}M^{-1}$, $\varepsilon_{VAI\text{-}AS}$=511200 $cm^{-1}M^{-1}$, ε_{TAR}=548000 $cm^{-1}M^{-1}$).

2.3 PURIFICATION OF RNA-PROTEIN COMPLEXES

TAR-$PKR_{1\text{-}169}$, VA_I-AS-$PKR_{1\text{-}169}$, $VA_I\Delta$TS-PKR, and Δloop-$PKR_{1\text{-}169}$ complexes were prepared by incubating purified proteins in the presence of a 1.1-fold excess of RNA in a buffer containing 50 mM Tris (pH 7.50) and 100 mM NaCl or the same buffer supplemented with 5 mM $MgCl_2$ for 15 minutes at room temperature. After incubation, the mixture was applied on a HiLoad 26/60 Superdex 75 gel filtration column (2.6 x 60 cm, GE Healthcare Life Sciences, USA). Elution fractions for both complexes were assayed for the presence of RNA-protein complex via in-line spectrophotometer (at 260

and 280 nm simultaneously), and confirmed by native polyacrylamide gel electrophoresis. Fractions containing RNA-protein complex were pooled and concentrated in Millipore concentrators (*Mw* cut off 10000, Millipore, USA). The purity of the complexes was assessed by the native polyacrylamide gel electrophoresis, whereas the concentration was determined using the extinction coefficients of protein and RNA.

2.4 ELECTROPHORETIC MOBILITY SHIFT ASSAY (EMSA)

EMSAs were performed by titrating RNA at 100 nM with increasing concentration (0-1000 nM) of full length PKR or $PKR_{1\text{-}169}$ in 50 mM Tris, 100 mM NaCl (pH 7.0) and 5 mM $MgCl_2$. RNA and protein were mixed and incubated at room temperature for 10 minutes followed by addition of native load dye [0.02% bromophenol blue, 0.01% xylene cyanol FF, 10% glycerol in 1X Tris/Borate/EDTA (TBE)]. The samples were loaded onto native TBE-PAGE gels and electrophoresis was performed at 80V and 4° C. The electrophoresis system (mini-protean 3 cell, Biorad) and the buffer (0.5X TBE) are kept on ice during for the length of the experiment. The experiment takes approximately 3 hours for sufficient separation. To visualize RNA-containing species, gels were stained with SybrGold (Invitrogen Inc.) for 5 minutes and imaged by the FluorChem Q System (ProteinSimple, Inc.), and normalized data was used for determining of K_D by fitting the fraction of bound RNA against the protein concentration using the Hill equation:

$$Y = \frac{B_{\max} \times X}{\left(K_D + X\right)} + NS \times X + Background \qquad \textbf{(Equation 2.1)}$$

Where Y is fraction bound, Bmax is the maximum specific binding in the same units as Y, K_D is a equilibrium constant, X is the concentration of ligand (protein), NS is the slope

of non-specific binding, Background is the amount of non-specific binding with no added ligand.

2.5 SDS/PAGE GELS AND WESTERN BLOTTING

Equal amounts of PKR were resolved by SDS/PAGE. Protein concentration was calculated using the known extinction coefficient as measured by UV-Vis spectrophotometry (NanoDrop2000c, Thermo Scientific, USA). 5x SDS loading dye (0.313 M Tris pH6.8, 50% glycerol, 10% SDS 0.05% bromophenol blue) was added to the protein samples to obtain the loading dye concentration of 1X, and samples were loaded into the wells of stacking gel. The loading volume was adjusted to load 15 ng of protein per lane for SDS/PAGE and Western blotting. Protein was separated on a 10% polyacrylamide resolving segment and the gel electrophoresis was performed in 1x Tris-Glycine SDS running buffer (3.03g Tris, 14.4g Glycine, 1g SDS brought to 1 L) in a mini-protean 3 cell (Biorad). Gels were run at 150V (constant voltage) for migration through the stacking gel and at 200V while in the separating gel (10% acrylamide). After completion of SDS/PAGE, proteins on the polyacrylamide gels were transferred to polyvinyl difluoride (PVDF) membranes (Hybond P, GE Healthcare, Piscataway, NJ, US). A wet transfer apparatus (Biorad) was used and the transfer was performed at a constant voltage of 100V for 1 hour at ~4°C keeping the current below 350 mAmp. Membranes were blocked with 5% skim milk powder dissolved in Tris buffered saline containing 0.1% Tween-20 (TBS-T) for 1 hour at room temperature on a shaker. Primary PKR antibody (anti-PKR or Anti-PKR phospho T446) were used in 1:4000 and 1:3000, respectively, dissolved in 5% milk TBS-T and the membrane was incubated at room temperature for an hour. The primary antibodies used are anti-PKR antibody (mouse,

ab32052, Abcam, with 1:5000 dilution), and anti-PKR (phospho T446) antibody (rabbit, ab47377, Abcam, with 1:2000 dilution). Following incubation with primary antibody, the membrane is washed in TSB-T (3X 5 minute washes) and then incubated for an hour with appropriate horseradish peroxidase (HRP) conjugated secondary antibody (anti-mouse secondary antibody when anti-PKR primary antibody was used and anti-rabbit secondary antibody when anti-PKR phospho T446 antibody was used both antibodies diluted 1:10000 in 5% milk TBS-T). The membrane was washed (4X 10 minutes) and then 2 mL of Luminata™ Forte Western HRP substrate (Milipore) was applied directly on it. The chemiluminiscence generated by the HRP (conjugated to the secondary antibody) acting on the HRP substrate is visualized using FluorChem Q System (Cell Biosciences) with typical exposure of 1.5 min.

2.6 PKR ACTIVATION/INHIBITION ASSAY

The *in vitro* PKR activation assay was carried out as follows. RNA samples at various concentrations (0-1000 nM) were pipetted into microcentrifuge tubes on ice. Next, to make a final buffer concentration of 1xa reaction, a mixture of 5x activation buffer (250 mM Tris at pH 7.5, 125 mM NaCl, 25 mM $MgCl_2$, and 5 mM ATP), supplemented with PKR (100 nM) was added to tubes containing RNA. For the control reaction, RNA samples were replaced by 0.0002 μg Poly I:C. The tubes were incubated at 30 °C for 15 minutes and quenched by adding the 5x sodium dodecyl sulfate (SDS) load mixture to the reactions. 15 ng of Protein was loaded on 10% sodium dodecyl sulfate/polyacrylamide gel and transferred onto polyvinyl difluoride membrane to monitor PKR phosphorylation using Anti-PKR phospho Thr446 antibody by means of

western blot analysis as previously described in section **2.5**. In addition, anti-PKR antibody was also used for western blot analysis to monitor a loading control.

Inhibition assays were carried out in similar manner: 100 nM PKR was pre-incubated with the inhibitory RNAs ranging from 0-1500 nM for 10 minutes at room temperature. A mixture of 5x activation buffer and PolyIC was added, and reactions were incubated at 30 °C for 15 minutes and quenched by addition of 5x SDS load mixture. The western blot was developed as previously described in section **2.5**, and visualized using FluorChem Q System. Quantitation of PKR phosphorylation was performed using Alpha Imager Software.

2.7 ANALYTICAL ULTRACENTRIGUGATION (AUC)

AUC experiments for VA_I were carried out by our collaborator Dr. Stephen Harding group at NCMH Laboratory, School of Biosciences, University of Nottingham, UK. The sedimentation velocity (SV) experiment for the VA_I RNA was performed using an Optima XL-I analytical ultracentrifuge (Beckman Instruments, USA) with an An60-Ti rotor at 20.0 °C as described previously [335]. Standard 12 mm double sector cells were used where VA_I [at 0.2 mg/mL in 50 mM Tris, 100 mM NaCl and (pH 7.5)] and buffer were loaded in appropriate channels. SV data were collected at 28-minute intervals at 40,000 rpm using the Rayleigh interference optical system. Data were analyzed using the SEDFIT program [336, 337] to obtain the sedimentation coefficients at each concentration ($s_{20,b}$) which were then corrected to standard solvent conditions ($s_{20,w}$) using SEDNTERP [338]. From the (weight average) sedimentation coefficient of (5.46 ± 0.10 S), and the (z-average) r_H from DLS the (weight average) molecular weight, M_w of VA_I RNA was calculated by using the following form of the Svedberg equation:

$$M_w = \frac{6\pi\eta_0 r_H s^0_{20,w}}{1 - \bar{\nu}\rho_0}$$ (**Equation 2.2**)

Where $\bar{\nu}$ is the partial specific volume, η_o is the solvent viscosity and ρ_o is the solvent density.

2.8 DYNAMIC LIGHT SCATTERING (DLS)

Samples were dialyzed for 2 hours at 4 ˚C against 50 mM Tris (pH 7.50) and 100 mM NaCl or the same buffer with addition of 5 mM $MgCl_2$ prior to DLS analysis. After dialysis, samples were subjected to filtration through a 0.1μm filter (Millipore, USA) and equilibrated at 20 ˚C. The (z-average) hydrodynamic radius r_H and homogeneity (distribution of r_H) of each sample was examined using the Zetasizer Nano S system (Malvern Instruments Ltd., Malvern, UK) equipped with a 4 mW laser (λ = 633 nm) at scattering angle of 173° as previously described [339]. The molecular weight of each molecule was calculated using the same principal as in AUC experiment by employing Svedberg equation adjusted to include the equivalent hydrodynamic radius r_H in place of the translational diffusion coefficient. The DLS experiments for each sample were performed at multiple concentrations: 2.50-6.50 mg/mL for $PKR_{1\text{-}169}$, 0.70-1.30 mg/mL for TAR, 0.80-1.90 mg/mL for VA_I-AS, 0.30-1.10 mg/mL for the $PKR_{1\text{-}169}$-TAR complex, 0.70-1.30 mg/mL for $PKR_{1\text{-}169}$-VA_I-AS complex, 0.60-1.50 mg/mL for wt ($VA_I\Delta TS$), 1.20-1.60 mg/mL for full length VA_I, 1.00-1.75 mg/mL for $VA_I\Delta TS$-$PKR_{1\text{-}169}$ complex, 4.00-8.00mg/mL for PKR, and 1.00-4.00 mg/mL for $VA_I\Delta TS$-PKR complex (all in 50 mM Tris (pH 7.50) and 100 mM NaCl).

For samples prepared in 50 mM Tris (pH 7.50), 100 mM NaCl and 5 mM $MgCl_2$,

DLS experiments are performed at multiple concentrations as follows: 2.20-3.70 mg/mL for wt ($VA_I\Delta TS$), 1.00-1.40 mg/mL for Δloop, 0.40-0.80 mg/mL for Δbulge, 1.50-3.10 mg/mL for ΔCD, 0.70-1.30 mg/mL for ΔGU, 1.80-2.80 mg/mL for ΔCD2bp, 0.40-0.80 mg/mL for ΔCD4bp, 1.10-1.70 mg/mL for wt-PKR_{1-169} complex, and 1.00-1.50 mg/mL for Δloop-PKR complex.

2.9 SMALL ANGLE X-RAY SCATTERING (SAXS)

Recently, SAXS has emerged as a reliable technique for determining size and shape of macromolecules in solution as well as very good complimentary tool to X-ray crystallography and NMR. I employed SAXS extensively for modeling of PKR_{1-169}, $VA_I\Delta TS$ as well as other RNAs. **Figure 2.2** is a schematic representation of collecting and processing SAXS data, as well as *ab initio* model generation of macromolecules. Following section covers more detailed overview of SAXS theory and data processing.

2.9.1 Theory and background

Small angle X-ray scattering (SAXS) is a solution scattering technique where X-ray interacts with the assemblies of electrons in the molecule resulting in scattering that is recorded at very low angles [340, 341]. X-rays are electromagnetic waves with high-energy. When an X-ray hits an electron, the electron resonates with the frequency of the X-ray and emits coherent secondary waves. If these secondary waves or scattered waves have the same wavelength (λ) as the original X-ray (0.5 to 2.0 Å) it is referred to as elastic scattering [341, 342]. In SAXS, elastic scattering contributes to the scattering data almost entirely. Inelastic scattering is ignored as it is too weak and does not interfere with

the elastic scattering.

Consider a situation where there are two electrons that scatter light that reaches the detector. At the time of the arrival, if these two rays are in phase then they produce a dark spot (constructive interference) and if they are out of phase they produce a lighter spot (deconstructive interference) that are recorded on the detector [342]. The electrons basically act as a source of a secondary X-ray wave [341]. The pattern on the detector encodes information on distance between the two electrons under consideration because the intensity of the spot on the detector contains information on amplitude. The amplitude will have information on the phase difference of the two secondary waves under consideration, which in-turn depends on path difference of the two. If the path distances (the distances between the spot recorded on the detector and the secondary wave sources or a pair of electrons) is very large compared to the path difference in them then the sources are considered parallel to the detector [341, 343].

2.9.2 SAXS data collection

The software program PRIMUS [344] is used to convert this scattering pattern into a 1D SAXS scattering curve, both of which are in reciprocal space. This curve has the log of intensity *I(q)* plotted against the momentum transfer (**Figure 2.2**) [345].

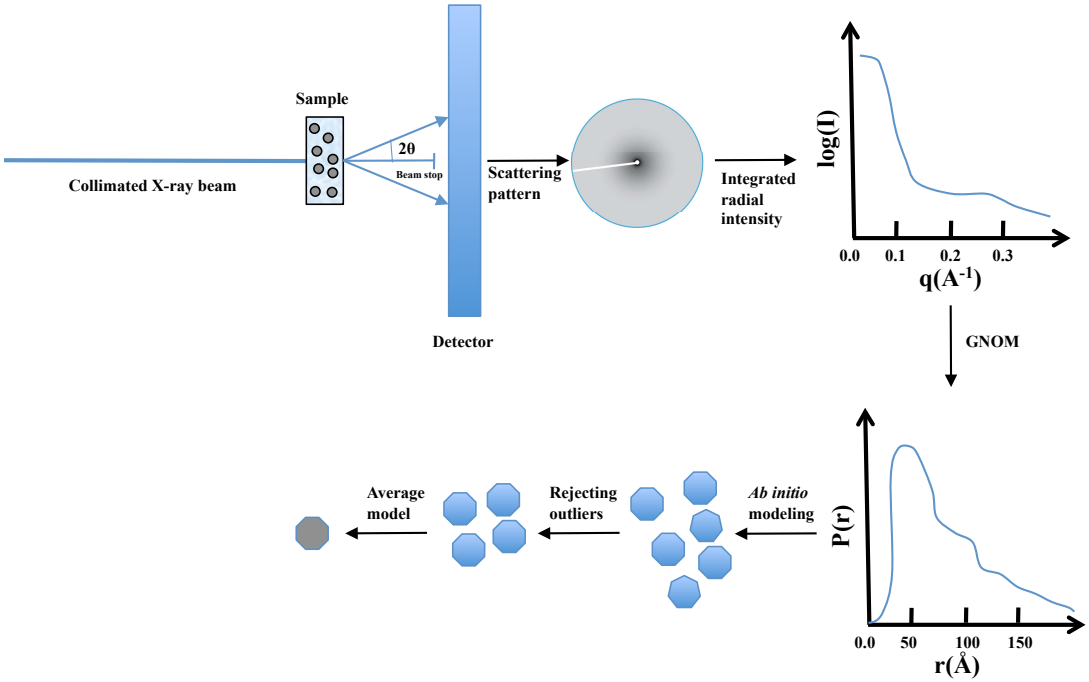

Figure 2.2: Schematic representation of Small angle X-ray scattering. The sample scatter collimated X-ray beams (Cu Kα radiation) that are registered on the detector as a circular scattering pattern that is in reciprocal space. Integrating the radial intensity of this circular scattering pattern generates the SAXS scattering curve. The scattering curve is converted to a pair distribution function curve *P(r)* that is in real space. From the *P(r)* plot a number of *ab initio* models are built. Outlier models are rejected and an averaged model is obtained.

$$(s) = 4\pi \sin\frac{\theta}{\lambda} \qquad \textbf{(Equation 2.3)}$$

Here the θ is the scattering angle and λ is the wavelength of the X-ray radiation. At larger scattering angles (θ), destructive interference resulting from secondary waves emitted from all electrons that include waves in all possible phases will lead to no scattering with directionality of θ [346, 347]. However, at smaller scattering angles the phase difference between the scattered waves will be smaller, limiting destructive interference and enabling scattering in the direction of the small angle to be recorded on the detector [348]. Ideally, we would have no interference at zero angle but the collection of data is

not performed at zero angle due to the beam stop to protect the detector from direct X-ray damage [341, 349].

2.9.3 Data analysis

The pair distribution function *P(r)* is a distribution of distances between all pairs of electrons (source of secondary waves) in a molecule based on its electron density [350]. This curve is generated by inverse Fourier transform that deconvolute distance information on electron pairs performed by the program GNOM [350, 351].

Using the schematic representation of an electron pair (Figure 2.1), it can be said that the: $\gamma_O(r_{ij})$ is the probability of finding (j) at a distance (r) from point (i), number of possible i is directly proportional to volume (V) of the molecule, where the number of possible (j) is directly proportional to r_{ij}^2. The number of electron pairs (i,j) with a distance r between them is directly proportional to $\rho^2\ \gamma_O(r_{ij})\ Vr^2$. The pair distribution is given by [345].

$$P(r) = r^2\gamma_0(r)V\rho^2 = r^2\gamma(r) \qquad \textbf{(Equation 2.4)}$$

The P(r) plot provides us with the information on shape and maximum particle dimension (*Dmax*) of the molecule. *Dmax* is described by the distance on the X-axis from the origin to the end-point where the curve meets the X-axis again. Another valuable parameter determined from the P(r) plot is the radius of gyration (r_G). Radius of gyration is the mean square distance to the center of mass weighted by the contrast of electron density and is obtained from GNOM using following equation:

$$rG^2 = \frac{\int v_r \Delta\rho(r) r^2 dVr}{\int v_r \Delta\rho(r) dVr} \qquad \textbf{(Equation 2.5)}$$

Where V is the volume of the particle or sample, $\Delta\rho$(r) the contrast in electron density between sample and solvent, r is the distance from the reference point (i) to a particle or electron at another point (j), r_{ij}^2 is the square of distance between an electron pair [345].

Major limitations of SAXS are the loss of phase of the X-ray due to the sample being in solution and usability in one/two phase systems only. It is also important to include the assumptions made for SAXS analysis including the monodispersity of sample and its infinite dilution (no effect on the sample behavior because of change in sample concentration) [343]. Another limitation of the technique is that sample is isotropic and the vectorial (3D) scattering intensity distribution i(q) reduces to a scalar (1D) intensity distribution i(q). This entails a loss of information, which constitutes the most severe limitation of the method.

2.9.4 *Ab initio* model construction

Ab initio modeling with the scattering data obtained begins with finding a particle (usually a sphere) that has the closest X-ray scattering pattern to that of sample. This sphere (assume its radius as R) is then filled with N number of densely packed small spheres (dummy atoms) of radius r. The number of dummy atoms (N) is usually close to 1000, set by default in processing software. Then the connectivity, which is denoted by the number of non-solvent atoms, an atom under consideration is in contact with, for each dummy atom is defined. This approach to *ab initio* modeling has been discussed extensively and the software programs are called bead-modeling programs [349, 352]. These programs employ energy minimization through a simulated annealing protocol [353]. The use of a simulated annealing protocol in this context can be generally explained as heating the system, allowing random modification and slowly cooling-down

the system and verifying whether these modification results in decreasing the energy of the system. A*b initio* modeling software uses the determined r_G and *Dmax*, which provides the constraints for the models generated. The predicted scattering of the model molecule after every energy minimization step is calculated and compared with the experimental scattering profile of the sample to check for conformity with it. This is usually referred to as "goodness of fit" (Chi or χ) between the *ab initio* model and experimentally determined scattering curve [354, 355]. Typically, a Chi value of 1 or less represents a good fit. To obtain the average structure of the *ab initio* model, multiple runs with random seed are performed. Another parameter that determines best alignment and measures similarities between the individual models from the same run is called normalized spatial discrepancy (NSD) [356]. For ideally superimposed similar objects, NSD tends to 0, but typically values less then 1 show good agreement. The simulated annealing protocol employs a high temperature in the beginning of the energy minimization steps and the changes are almost random, which may generate both high and low energy configurations, but towards the end of the protocol the temperature is much lower, and a configuration with nearly minimum energy is reached [349, 352].

2.9.5 SAXS processing and modeling of full length PKR, PKR1-169, HIV-1 TAR, VA_I, VA_I mutants, TAR-PKR_{1-169}, VA_I-AS-PKR_{1-169}, $VA_I\Delta TS$-PKR_{1-169}, and Δloop-PKR_{1-169} complexes

SAXS data for proteins (wild type PKR and PKR_{1-149}), and RNAs including HIV-1 TAR, VA_I-AS, full length VA_I, $VA_I\Delta TS$, and truncated versions of $VA_I\Delta TS$ ($VA_I\Delta Loop$, $VA_I\Delta Bulge$, $VA_I\Delta CD$, $VA_I\Delta GU$, $VA_I\Delta CD_{2bp}$, $VA_I\Delta CD_{4bp}$) were collected using an in-house Rigaku instrument (Rigaku S-MAX3000) as described previously

[357]. The SAXS data for TAR were collected at 0.7, 1.0, 1.3 mg/mL, for VA_I-AS at 1.0, 1.4, and 1.9 mg/mL, for PKR_{1-169} at 3.5, 4.5, and 5.5 mg/mL, for PKR_{1-169}-TAR complex at 0.80, 1.20, and 2.10 mg/ml, and PKR_{1-169}-VA_I-AS complex at 0.60, 0.9, and 1.63 mg/mL (all in 50 mM Tris pH 7.50, 100 mM NaCl buffer). SAXS data for $VA_I\Delta TS$ were collected at 0.7, 1.2 and 1.5 mg/mL and at 0.6, 0.9 and 1.2 mg/mL for VA_I (all in 50 mM Tris pH 7.0, 100 mM NaCl buffer). The $VA_I\Delta TS$-PKR_{1-169} SAXS data were collected at 1.0, 1.25, 1.5 and 1.75 mg/mL in 50 mM Tris pH 7.50, 100 mM NaCl buffer. In addition, SAXS data for PKR were collected at 3, 4, 5, 7 and 8 mg/mL whereas for $VA_I\Delta TS$-PKR complex, data were collected at 1.5, 1.6, 3, and 5 mg/mL. SAXS data for wt were collected at 1.00, 1.90 and 3.10 mg/mL, 1.00, 3.00, and 4 mg/mL for Δloop, 0.40, 0.60, 0.80 mg/mL for Δbulge, 1.00, 1.50, and 2.20 mg/mL for ΔCD, 1.30, 1.80, 2.30 mg/mL for ΔGU, 1.30, and 1.70 mg/mL for ΔCD2bp, 1.40, 1.90, 2.40 mg/mL for ΔCD4bp, 1.30, 1.50, and 1.70 mg/mL for wt-PKR_{1-169} complex, and 1.25 and 1.50 mg/mL for Δloop-PKR_{1-169} complex (all in 50 mM TRIS (pH 7.50), 100 mM NaCl, and 5 mM $MgCl_2$). The instrument is equipped with a Rigaku MicroMax+002 microfocus sealed tube (Cu Kα radiation at 1.54 Å) and a Confocal Max-Flux (CMF) optics system operating at 40 W (Rigaku). It has a 200-mm multiwire two-dimensional detector to record generated scattering data. The data for all RNA and protein samples and buffer(s) were collected for 3 h for each sample within the range of $0.008 \leq s \leq 0.26$ $Å^{-1}$ and processed according to the method previously described in section 2.9.2, where we used momentum transfer (s) = $4\pi\sin\theta/\lambda$. Here the θ is the scattering angle and λ is the wavelength of the X-ray radiation. SAXS data for all samples were collected at multiple concentrations. Prior to data collection, samples were subjected to DLS experiments to confirm that all the

samples were highly pure and suitable for data collection. Wild type PKR is prepared in 50 mM Tris pH 8.0, 100 mM NaCl, 5 % Glycerol w/w, and 5mM 2-β-mercaptoethanol), PKR_{1-149} is prepared in 50 mM Tris pH 7.50, 100 mM NaCl, and 5mM 2-β-mercaptoethanol), and RNAs are made in 50 mM Tris pH 7.50, 100 mM NaCl buffer, or 50 mM Tris pH 7.50, 100 mM NaCl supplemented with 5 mM $MgCl_2$. Primary data analysis was performed using program PRIMUS [344], followed by the merging of buffer subtracted data for all concentrations of each sample and the complex. The data were further processed using the GNOM program [358] to obtain radius of gyration (r_G) and maximal particle dimension (D_{max}).

The *ab initio* modeling for protein and individual RNA molecules was performed using the program DAMMIN [359]. The program MONSA [359] was employed to calculate *ab initio* models of protein-RNA complexes by fitting data for protein, RNA and the complex simultaneously. The quality of the models was verified by the goodness of fit parameter (χ value) after each model calculation. *Ab initio* models for each sample and the complex were then rotated and averaged using the program DAMAVER [360]. Sample quality was confirmed after SAXS experiments by gel electrophoresis.

The hydrodynamic properties for each individual protein and RNA models, and complexes were calculated using the program HYDROPRO [361]. The atomic element radius of 2.9 Å was considered for HYDROPRO calculations according to the HYDROPRO manual. The density (1.0038 g/mL) and viscosity (1.026 cPoise) of buffer was calculated using SEDNTERP [338] whereas the molecular weights and partial specific volume were calculated using NucProt Calculator [362]. The partial specific

volumes of $VA_I\Delta TS\text{-}PKR_{1\text{-}169}$ and $VA_I\Delta Loop\text{-}PKR_{1\text{-}169}$ complexes were calculated using Equation 2.6.

$$\bar{v}_{complex} = \frac{(M_{PKR}\bar{v}_{PKR} + M_{RNA}\bar{v}_{RNA})}{(M_{PKR} + M_{RNA})} \qquad \textbf{(Equation 2.6)}$$

Hydrodynamic parameters are summarized in Chapters 3, 4, and 5.

2.10 COMPUTATIONAL MODELING OF TERTIARY STRUCTURE

High-resolution modeling was performed in collaboration with Dr. Janusz Bujnicki, director of the Laboratory of Bioinformatics and Protein Engineering, International Institute of Molecular and Cell Biology, Warsaw, Poland. Here is the overview of the approach taken for the modeling. The tertiary structure of $VA_I\Delta TS$ was modeled using SimRNA, a method for RNA folding simulations by the Monte Carlo approach that uses a coarse-grained representation and a statistical potential [363]. Predicted secondary structure without any assumptions about possible pseudoknots [364] was used as restraints. First, a series of Replica Exchange Monte Carlo simulations were carried out, starting from extended sequence of $VA_I\Delta TS$ RNA, and low-energy decoys were collected. These decoys were then clustered based on their mutual geometric similarity, and the central member of the largest cluster was selected as a representative model. For these models, full-atom representations were generated using a routine from the SimRNA toolkit, and their local geometry (bond lengths, angles, and steric interactions) was refined using phenix.refine [365].

Modeling of the $VA_I\Delta TS$ alone and in complex with the dsRBMs of PKR was carried out using PyRy3D (an in-house method under development in the Bujnicki laboratory; http://genesilico.pl/pyry3d/). First, *ab initio* reconstructions of the $VA_I\Delta TS$

alone and in complex with PKR_{1-169} were converted into pseudo EM-maps with sfall and fft programs from the CCP4 suite [366]. For the protein-RNA complex, two complementary maps were obtained. Second, RNA and protein models were divided into rigid and flexible regions. Individual helices of RNA (together with hairpin loops at their ends) were modeled as rigid bodies, restrained at the junction to maintain the continuity of the nucleotide chain. For the protein-RNA complex, the pseudoknot was also retained. For modeling of the $VA_I\Delta TS$ complex with $PKR_{1-169,}$ individual dsRBM domains taken from the experimentally determined structure (PDB code: 1QU6) [367] were treated as rigid bodies. The N-terminus (residues 1-13) and the linker between dsRBMs (residues 87-103) were modeled as flexible chains.

For RNA alone, and for protein-RNA complex, separate Monte Carlo simulations were conducted with PyRy3D to optimize the fit of the starting models to the corresponding pseudo-densities derived from SAXS measurements. The above-mentioned rigid elements connected to each other were allowed to move around, aiming to fill out as much as possible of the volume inside the map, minimize the complex volume outside of the map, minimize the violation of restraints, and minimize steric conflicts between the individual components. In the case of the protein-RNA complex, the RNA molecule was fitted first, following by fitting of the protein moiety in the presence of best-fit RNA model. The medoid structure from the largest cluster obtained from 100 independent simulations was selected for further processing. The final models of the RNA alone and of the RNA-protein complex were obtained following a refinement with phenix.refine [365], with restrains on $VA_I\Delta TS$ pseudo-density map.

CHAPTER 3: RECOGNITION OF VIRAL RNA STEM LOOPS BY THE TANDEM DOUBLE-STRANDED RNA BINDING DOMAINS OF PKR

Chapter 3 of the thesis was adapted from: Dzananovic, E., Patel, T. R., Deo, S., McEleney, K., Stetefeld, J. and McKenna, S. A. (2013) Recognition of viral RNA stem-loops by the tandem double-stranded RNA binding domains of PKR. RNA. 19, 333-344. E.Dz primarily carried out the preparation and writing of manuscript. In addition, E.Dz. was responsible for designing and performing the experiments as well as analyzing experimental data. T.P. gave assistance with carrying out ab initio modeling of macromolecules. S.D. contributed to preparation of protein, RNAs, and buffers. K.M. was responsible for operating the Small angle X-ray instrument. S.M. and J.S. are principal investigators.

3.1 Background

Human PKR is a 551-residue enzyme containing three distinct regions, each with specific functional roles in the response to dsRNA. N-terminal tandem dsRBMs adopt a canonical fold containing a 3-stranded antiparallel β-sheet flanked by 2 α-helices with the tandem dsRBMs joined by a 23 amino acid linker [157]. The C-terminal region encompasses a Ser/Thr kinase domain responsible for target substrate recognition and phosphorylation. The kinase domain is connected to dsRBMs by a second domain, an 80 residue long flexible linker implicated in PKR self-association [194-196]. Binding of dsRNA to the dsRBMs significantly enhances the kinase activity of PKR [232]. The molecular basis for the interaction has been studied extensively with a variety of synthetic and biological dsRNA molecules, although no high-resolution structure of PKR in complex with RNA exists. Productive interaction requires residues from both dsRBM1

and 2 as well as the linker that joins them [226]. Structures of a single dsRBM from proteins other than PKR in complex with perfectly duplexed dsRNA indicate that approximately 1.5 turns (~15 bp) of the A-form RNA helix comprising consecutive minor-major-minor grooves are recognized, and that contacts are mediated primarily through the 2'-hydroxyl groups of the ribose sugar, explaining the observed selectivity [169, 170, 180-183]. In addition to a minimum length requirement (~15 bp), specific structural (bulges, loops, *etc.*) and nucleotide modifications (*i.e.* 5'-phosphorylation state) have been observed to be accommodated by PKR, and in some cases significantly affect both the affinity for and activation of PKR [226-231]. As there is scant structural information about imperfectly duplexed RNA in complex with PKR, a detailed understanding how PKR accommodates these deviations remains an unanswered question.

A well-characterized viral dsRNA activator of PKR is the HIV-1 transactivation response (TAR) element, an RNA stem-loop structure spanning nucleotides +1 to +59 of the newly synthesized viral mRNA [233]. TAR adopts an A-form RNA helix with distortions including a trinucleotide bulge and hexaloop [239, 240]. HIV-1 TAR RNA has been established as a potent activator of PKR kinase activation, where high affinity interaction requires the presence of 16 base pairs proximal to the loop as well as both the bulge and hexaloop [226, 251, 252]. Given that each individual dsRBM requires approximately 15 bp for interaction, it is unclear how the tandem dsRBM domains of PKR are interacting with TAR RNA. High-resolution information on a tandem dsRBM-dsRNA complex has been difficult to obtain, likely due to the established flexibility of both the linker between dsRBM1 and 2 and the inherent flexibility of stem-loop RNA

structures. Here, I present the solution conformation of tandem dsRBMs of PKR in complex with an imperfectly base-paired viral dsRNA using small-angle X-ray scattering. *Ab initio* analysis of PKR_{1-169}, HIV-1 TAR, and the protein-RNA complex were determined to investigate how each dsRBM orients and interacts with TAR RNA. Dynamic light scattering (DLS) was employed to (1) investigate the homogeneity of macromolecules at various concentrations, (2) measure the hydrodynamic radius of individual macromolecules as well as their complexes and (3) compare the calculated values from SAXS models with experimentally determined values. This experimental approach was repeated using a second model RNA ligand, the apical stem of adenovirus VA_I RNA, in order to confirm the validity of the results with a second known activator of PKR. Together, these results provide a plausible framework for the recognition of short, imperfectly base-paired RNA ligands by the tandem dsRBMs of PKR and highlight the effectiveness of small-angle X-ray scattering approaches for systems with highly flexible components.

3.2 RNA-protein complex purification and characterization

In perfectly duplexed dsRNA, the tandem dsRBMs of PKR require a minimum of 15 bp (1.5 turns of the A-RNA helix) for interaction, and yet based on existing structures it would be expected that each dsRBM would require the entire 15bp. Additionally, PKR is capable of tolerating, and in some cases requires, deviations from prefect duplexes including bulges, internal loops, and loops for high affinity binding. In order to study the structural basis for these interactions, I sought to determine the solution conformation of two dsRNA-PKR complexes by small angle X-ray scattering (SAXS). Complexes were

assembled with purified recombinant PKR_{1-169}, which contains both dsRBM1 and 2 and retains identical binding affinity to the full-length PKR (**Figure 3.1**).

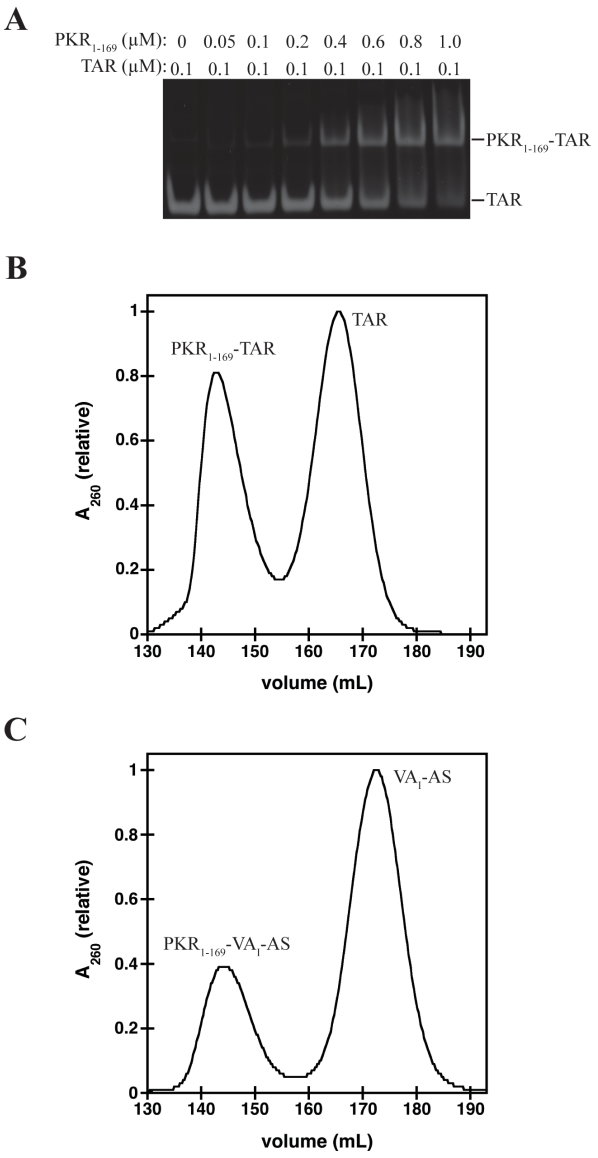

Figure 3.1: EMSA and size exclusion chromatography profile showing the ability of dsRBD to bind to both TAR and VA-AS RNAs. (A) EMSA of dsRBD with TAR RNA confirming the binding between the protein and the RNA. The concentration of protein ranges from 0 to 1 μM (lane 1 to 8), concentration of RNA is 0.1 μM in all of the lanes. The samples were incubated at room temperature for 10 minutes and run on 8 % native TBE gels at 4° C. The gel was stained by Syber Gold dye. (B) Size exclusion chromatography profile of dsRBD-TAR complex. Peak corresponding to elution of complex is at 142 mL, which precedes the TAR RNA alone peak at 164 mL. (C) Size exclusion chromatography profile of dsRBD-VA-AS complex. Peak

corresponding to elution of complex is at 144 mL, which precedes the VA-AS RNA alone peak at 172 mL.

The dynamic light scattering experiments were performed to study homogeneity of all macromolecules and to determine the hydrodynamic radius (r_H) of each species being studied at multiple concentrations. $PKR_{1\text{-}169}$ displays a narrow distribution of hydrodynamic radii at all concentrations examined, consistent with a monodisperse sample (2.80 ± 0.10 nm) (**Fig. 3.2A**). A linear distribution of r_H over multiple concentrations (2.50-6.50 mg/mL) was observed suggesting minimal concentration dependence on the Stokes radius (**Figure 3.2B**).

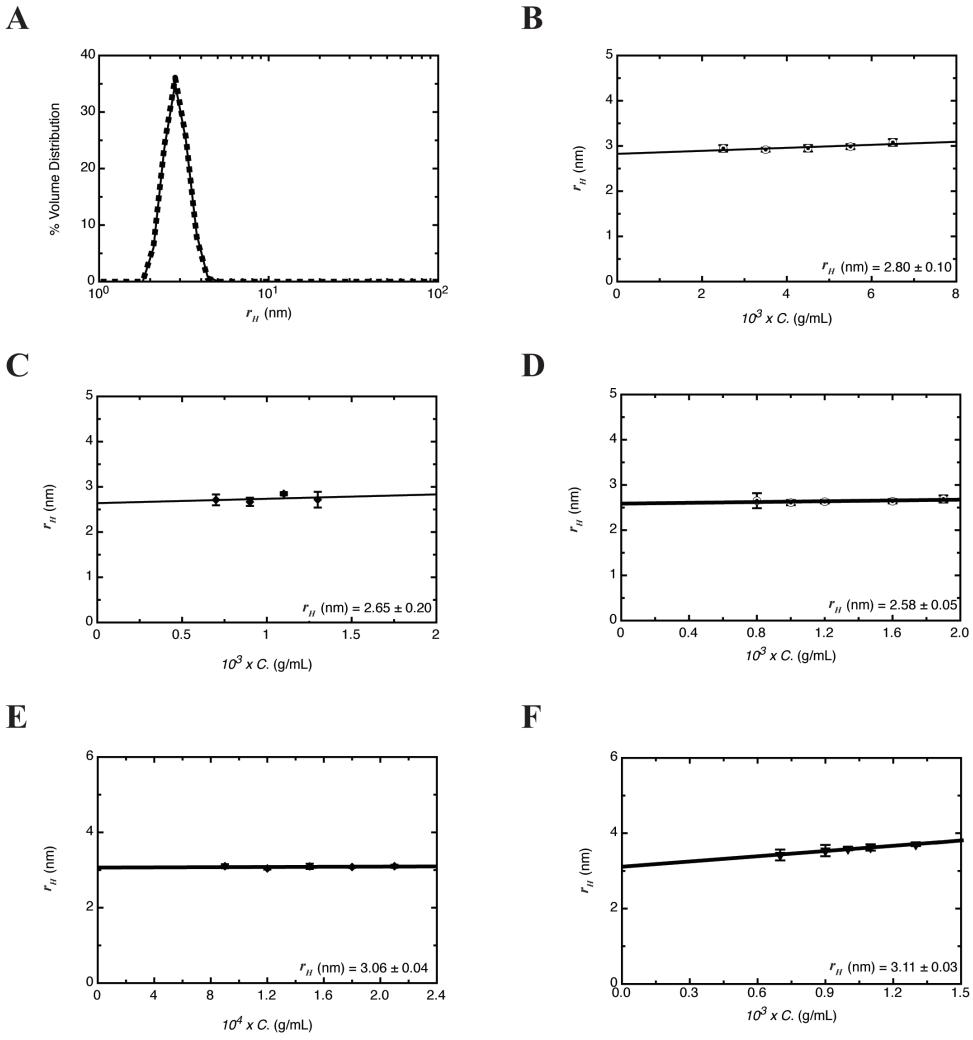

Figure 3.2: Confirming the quality of dsRBD's, TAR, VA-AS, and complexes by DLS. (A) DLS profile of dsRBD at 3.50 mg/mL, before (−, solid line) and after (•••, dotted line) SAXS data collection. (B) Concentration dependence of the Stokes radius (*Rh*) deduced from the peaks of DLS profiles for dsRBD shows linear fit with *Rh* = 2.80 ± 0.10 nm. (C) Concentration dependence of the Stokes radius (*Rh*) deduced from the peaks of DLS profiles for TAR shows data in linear range with calculated *Rh* of 2.65 ± 0.20 nm. (D) Concentration dependence of the Stokes radius (*Rh*) deduced from the peaks of DLS profiles for VA-AS showing all concentration being in linear range with respect to *Rh* of 2.58 ± 0.05 nm. (E) Concentration dependence of the Stokes radius (*Rh*) deduced from the peaks of DLS profiles for dsRBD-TAR complex showing all concentration being in linear range with respect to *Rh* of 3.06 ± 0.04 nm. (F) Concentration dependence of the Stokes radius (*Rh*) deduced from the peaks of DLS profiles for dsRBD-VA-AS complex shows data in linear range with calculated *Rh* of 3.11 ± 0.03 nm.

RNA model ligands were selected based on (i) their high affinity (~100 nM) for $PKR_{1\text{-}169}$ (**Figure 3.1A**), (ii) their ability to stimulate autophosphorylation and kinase activity of PKR, and (iii) that they are short, imperfectly base-paired dsRNA stem loops. Based on these criteria, I selected HIV-1 TAR RNA (57 nt) and the apical stem of adenovirus VA_I RNA (52 nt) (**Figure 1.6 and 1.7**). Both RNAs were *in vitro* transcribed from linearized template, purified by size exclusion chromatography, and subjected to native gel electrophoresis. Both TAR (**Figure 3.1A, lane 1**) and VA_I-AS (not shown) behave as a single species based on this analysis. DLS confirmed the r_H value consistent with monomeric TAR (2.7 ± 0.2 nm) over the concentration range examined, indicating minimal concentration dependence on Stokes radius, thus excluding the possibility of presence of aggregation **(Figure 3.2C)**. Identical observations were made for VA_I-AS (r_H = 2.58 ± 0.05 nm) that has similar size to that of TAR suggesting that both RNA have similar shape in solution as r_H depends on size and shape of macromolecules **(Figure 3.2D)**. The determined hydrodynamic radii of the RNA species being studied are within error of each other, consistent with their size exclusion chromatography elution profiles.

Complexes containing PKR_{1-169} and either TAR or VA_I-AS were assembled in the presence of excess RNA to minimize non-specific protein binding and maximize 1:1 stoichiometry. At low concentrations, electrophoretic mobility shift assays (EMSA) confirm the emergence of a single higher molecular weight species upon incubation of TAR with increasing concentrations of PKR_{1-169} (**Fig 3.1A**). Identical results were obtained with VA_I-AS-containing complex (data not shown). Complexes were then assembled at high concentration (μM range), and purified away from free RNA by size exclusion chromatography (**Figures 3.1B, C**). Given that solution conformation data quality by SAXS is sensitive to sample heterogeneity, this step is essential to ensure the removal of uncomplexed dsRNA. The elution profile for both complexes show two distinct peaks: a higher molecular weight peak corresponding to RNA-protein complex followed by a lower molecular weight peak corresponding to free RNA.

The DLS profiles of complexes are also linear with respect to increasing concentration, showing no signs of aggregation across the concentration range at which the experiments were performed (**Figures 3.2E, F**). PKR_{1-169} in complex with either TAR (r_H = 3.06 ± 0.04 nm) or VA_I-AS TAR (r_H = 3.11 ± 0.03 nm) are monodisperse and within error demonstrate similar r_H values, consistent with their elution profiles from size exclusion chromatography. As expected, an increase in r_H is observed in the complex compared to the individual components, although relative to the largest component (PKR_{1-169}) these increases were relatively moderate for TAR (9%) and VA_I-AS (11%). Taken together, these results confirm complex homogeneity and suggest a stacked orientation of both RNA-protein complexes.

3.3 The dsRNA-binding domain of PKR adopts an extended conformation in solution

To understand the behavior of dsRNA-PKR_{1-169} complexes in solution, I first studied the individual protein and RNA components in solution using SAXS. As our starting point, I first examined PKR_{1-169} as the high-resolution structure of this protein has already been determined in solution [157], and will serve to validate the quality of SAXS results. SAXS data collected at multiple concentrations were merged to generate a single scattering profile for PKR_{1-169} for further data analysis (**Figure 3.3A, red circles**).

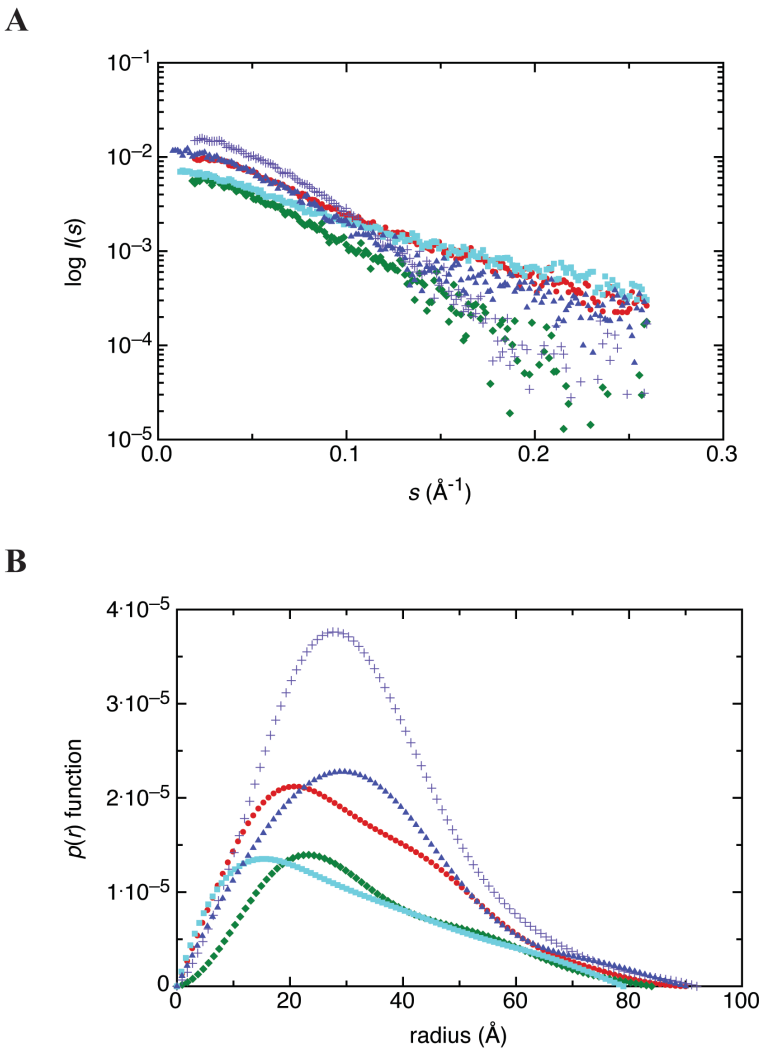

Figure 3.3: Small angle scattering experimental data. (A) Scattering profile curves for dsRBD (•), TAR (◆), dsRBD-TAR (+), VA-AS (■), and dsRBD-VA-AS complex (▲).
(B) Pair distribution function profile of dsRBD (•), TAR (◆), dsRBD-TAR (+), VA-AS (■), and dsRBD-VA-AS complex (▲) providing the information on the overall shape of molecules.

First, the scattering data was used to generate a distance distribution plot that presents a frequency histogram of all observed electron pairs in the molecule, enabling determination of key parameters including the radius of gyration (r_G) and the maximum particle dimension (D_{max}) using the program GNOM [351]. A skewed bell-shaped distance distribution function was observed typical for elongated molecules that may contain flexible regions (**Figure 3.3B, red circles**). The experimentally calculated r_G and D_{max} for PKR_{1-169} are 2.53 ± 0.04 nm and 9.0 nm respectively (**Table 3.1**). Based on the scattering data, multiple *ab initio* solution conformations for PKR_{1-169} were generated using the program DAMMIF [352] and superimposed using program DAMAVER [368] to generate an average surface envelope of the protein (**Figure 3.4A**).

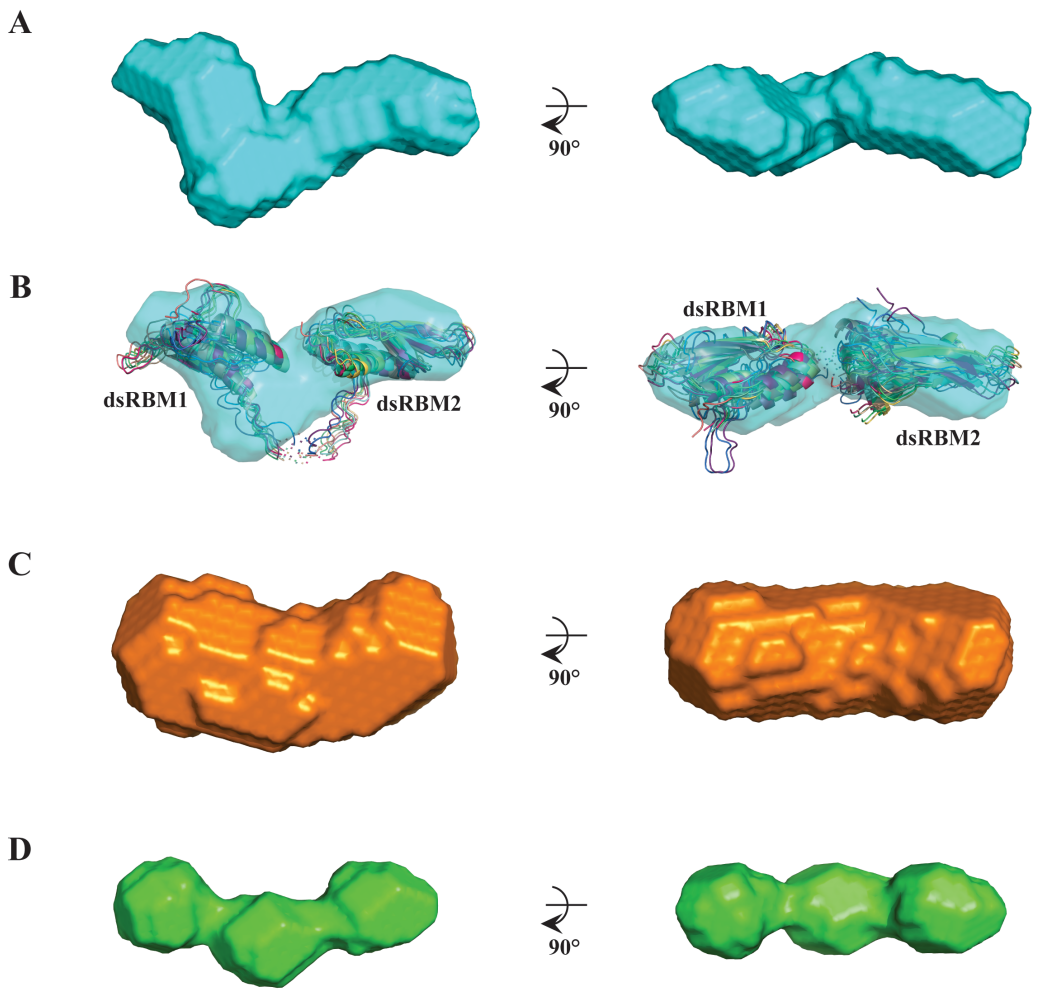

Figure 3.4: SAXS modeling of dsRBD's, TAR, and VA-AS. (A) Averaged solution *ab initio* model of dsRBD obtained from DAMMIF (top left) and 90° rotation (top right) around its major axis. The model suggests extended and flexible conformation of dsRBD in solution. (B) Fitting of high-resolution NMR structures into SAXS model. SAXS model dimensions have a good agreement with the known NMR structure. (C) Averaged solution *ab initio* model of TAR obtained from DAMMIF, and its 90° rotation around its major axis. SAXS solution model of TAR suggests extended and flexible conformation. (D) Averaged solution *ab initio* model of VA-AS obtained by DAMMIF (bottom left), and its 90° rotation (bottom right) around its major axis. There are three distinct bulges that can be seen in VA-AS model. This suggests that VA-AS takes upon more rigid conformation in solution then TAR.

The molecule adopts an extended structure that appears to orient the individual dsRBMs at opposite ends joined by the interdomain linker. However, the relatively uniform broadness of the entire molecule (including both the dsRBMs and linker) is

consistent with the flexible nature of the linker. The χ value obtained for individual *ab initio* models was ~ 0.9 illustrating an excellent agreement between experimental data and that obtained from the *ab initio* calculation. Furthermore, the normalized spatial discrepancy parameter (NSD) of 0.80 ± 0.04 amongst the *ab initio* models generated to create the average model indicates very little differences between individual PKR_{1-169} models. In order to validate the *ab initio* calculations, the program HYDROPRO [369] was employed to calculated hydrodynamic parameters. The r_G of 2.62 ± 0.02 nm, D_{max} of 9.5 ± 0.05 nm and r_H of 2.76 ± 0.06 nm are in good agreement with experimentally calculated hydrodynamic properties (**Table 3.1**). Identical DLS results were obtained after SAXS data collection, confirming absence of any radiation damage to the sample after exposure to X-rays (**Figure 3.2A**).

To validate our *ab initio* modeling approach and to determine the orientation of individual dsRBMs within the solution conformation, I took advantage of the existing high-resolution solution structure of PKR_{1-169} (PDB ID: 1QU6) [157]. This was accomplished by employing program BUNCH [370] that is able to utilize high-resolution information and finds optimal positions and orientations of individual domains (dsRBMs) for which the high-resolution structural information is available as well as place the dummy residues for the part of the domains where the high-resolution information is missing (linker). In order to prevent model bias, the linker was severed in the center such that each dsRBM could rotate freely. All the structures calculated using BUNCH (3D domain structures) were nearly identical to each other as well as to *ab initio* models that does not incorporate information from high-resolution data in terms of their solution conformation (**Figure 3.4B**). Overall, the *ab initio* model comfortably accommodates

each dsRBM, and strongly suggests that the interdomain linker can adopt a number of different configurations. BUNCH data analysis also strongly indicates that the dsRBM1 is positioned into the shorter arm while dsRBM2 is positioned in longer arm of the SAXS model. The hydrodynamic parameters calculated from *ab initio* models as well as for 3D structures from program BUNCH are not only nearly identical within error to each other but also agrees very well with those parameters determined experimentally validating our modeling approach (**Table 3.1**).

		PKR_{1-169}		TAR		TAR-PKR_{1-169}		VA_I-AS		VA_I-AS-PKR_{1-169}	
Hydrodynamic parameters	Experimental	HYDROPRO		HYDROPRO		HYDROPRO		HYDROPRO		HYDROPRO	
		DAMMIF	BUNCH	Experimental	DAMMIF	Experimental	MONSA	Experimental	DAMMIF	Experimental	MONSA
r_H (nm)[a]	2.8(±0.1)	2.76(±0.06)	2.80(±0.05)	2.7(±0.2)	2.90(±0.06)	3.06(±0.04)	3.00(±0.06)	2.58(±0.05)	2.40(±0.05)	3.11(±0.1)	3.1(±0.1)
r_G(nm)[b]	2.53(±0.04)	2.62(±0.02)	2.63(±0.01)	2.60(±0.05)	2.66(±0.01)	2.58(±0.03)	2.53(±0.02)	2.45(±0.02)	2.50(±0.02)	2.66(±0.04)	2.60(±0.01)
D_{max}(nm)[b]	9.0	9.5(±0.05)	9.8(±0.05)	8.4	9.2(±0.05)	9.2	9.00(±0.04)	7.9	8.80(±0.07)	9.0	9.1(±0.04)
r_G/r_H	0.9(±0.01)	0.95(±0.08)	0.94(±0.06)	1.0(±0.2)	0.92(±0.07)	0.84(±0.07)	0.84(±0.08)	0.95(±0.07)	1.04(±0.07)	0.86(±0.07)	0.8(±0.1)
χ	-	0.9	1.1	-	1.0	-	1.0/1.4/1.0[c]	-	1.0	-	1.0/1.1/1.1[c]
NSD	-	0.80(±0.04)	0.9(±0.1)	-	0.7(±0.1)	-	0.58(±0.03)	-	0.7(±0.1)	-	0.76(±0.02)

[a] fromDLS data
[b] from SAXS data
[c] values from protein/RNA/complec respectively

Table 3.1: Comparison of experimental and predicted hydrodynamic parameters

3.4 Solution conformation of HIV-1 TAR and adenovirus VA_I-AS RNA

SAXS data for TAR and VA_I-AS were collected at multiple concentrations and merged to generate their respective scattering profiles (**Figure 3.3A**). The resultant distance distribution functions for both TAR and VA_I-AS demonstrate a bell-shaped curve with an extended tail that is consistent with an elongated stem-loop conformation (**Figure 3.3B**). The experimentally determined values of r_G and D_{max} are 2.60 ± 0.05 nm and 8.4 nm, respectively. The pair-distance distribution plot was utilized for *ab initio* analysis to obtain the solution conformation of the RNA. The χ value of ~1.0 was obtained for each model indicating good agreement between SAXS experimental data and the data calculated for each *ab initio* model. The NSD parameter of 0.7 ± 0.1 for *ab*

initio models also suggests that individual *ab initio* models agree with each other almost perfectly. The averaged solution conformation presents an extended shape with slight curvature. Interestingly, the model lacks significant definition in terms of distinct structural features such as the loop or internal bulge (**Figure 3.4C**). The r_H (2.90 ± 0.06 nm), r_G (2.66 ± 0.01 nm) and D_{max} (9.2 ± 0.05 nm) values for the TAR models were calculated using HYDROPRO and are consistent with experimentally determined values (**Table 3.1**). As with the free protein ($PKR_{1\text{-}169}$), no significant sample deterioration due to radiation damage was observed by DLS after SAXS data collection (data not shown).

For the VA_I-AS RNA, r_G of 2.45 ± 0.02 nm and D_{max} of 7.9 nm was obtained from the distance distribution function that was further employed to generate several *ab initio* solution conformations. The resultant χ values of those models of ~1.0 and the NSD parameter of 0.7 ± 0.1 provides a high level of confidence with our data analysis. SAXS data analysis of VA_I-AS suggests that it adopts and extended shape with slight curvature, but with more pronounced definition in terms of three distinct bulges (**Figure 3.4D**). VA_I-AS RNA is significantly more compact than TAR, which suggests that VA_I-AS adopts a more rigid conformation in solution than TAR. The slightly smaller r_G and D_{max} values may be due to the smaller RNA size (52 versus 57 nucleotides). The r_H (2.40 ± 0.05 nm), r_G (2.50 ± 0.07 nm) and D_{max} (8.80 $\pm$ 0.07 nm) values for the VA_I-AS models were calculated using HYDROPRO and are consistent with experimentally determined values (**Table 3.1**). DLS results pre and post data acquisition were identical, confirming that no significant sample deterioration due to radiation damage occurred (data not shown).

3.5 PKR_{1-169} interacts with TAR via both the stem and loop regions

To determine the molecular basis for the interaction between PKR and TAR RNA, I subjected the purified complex to SAXS analysis. The merged scattering data from multiple concentrations of complex were used to generate the distance distribution function, which indicates an extended structure with corresponding r_G (2.58 ± 0.03 nm) and D_{max} (9.2 nm) values (**Figures 3.3A, B**). The experimentally determined D_{max} for the complex is within error of each of the individual RNA and protein components, consistent with a stacked as opposed to end-to-end orientation of the complex. Individual *ab initio* solution conformations of the PKR_{1-169}-TAR complex were determined using the MONSA software suite, which exploits the differential scattering intensity of RNA and protein components to allow visualization of each molecule in the complex. A representative individual best-fit model is shown in **Figure 3.5A**.

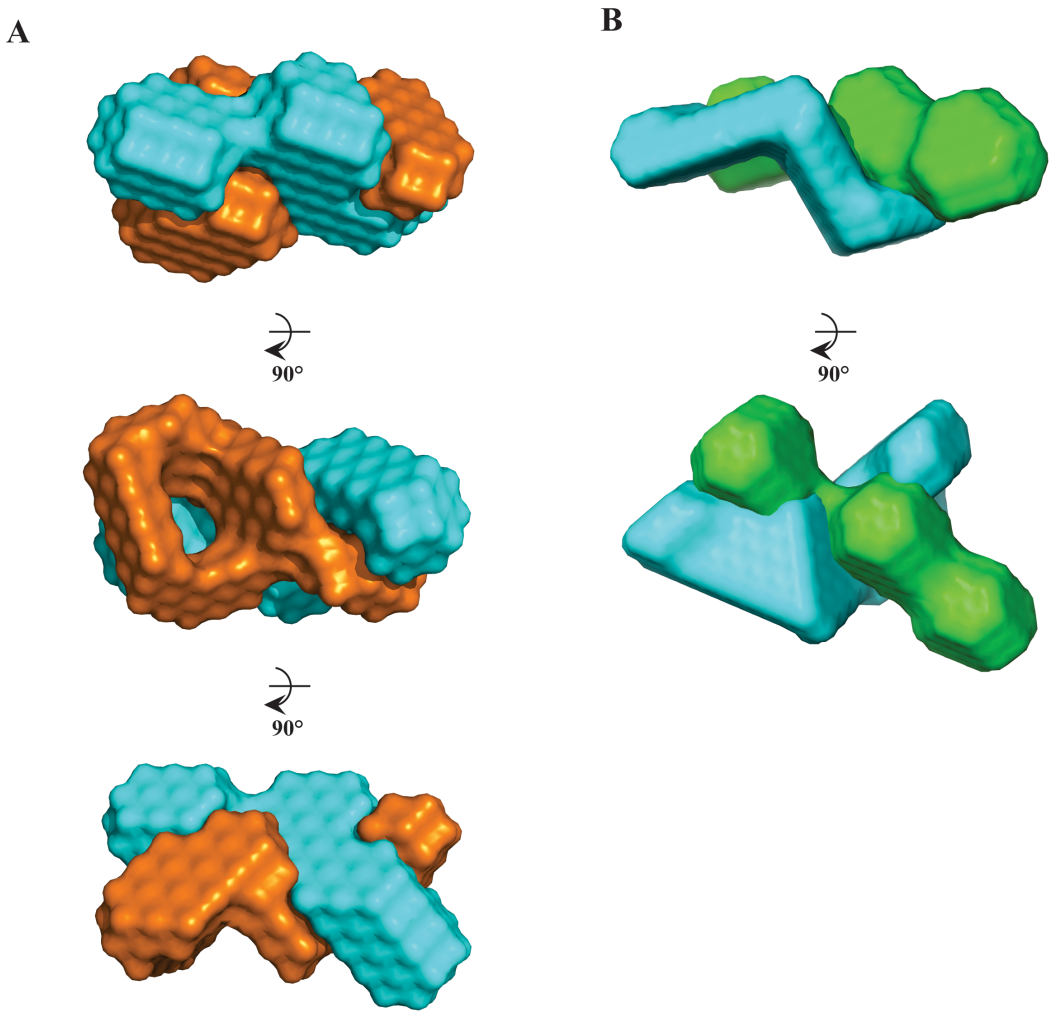

Figure 3.5: Modeling of complexes with MONSA. MONSA uses scattering data information for individual components and complex to resolve the structure of complex. (A) Averaged solution *ab initio* model of dsRBD-TAR. In MONSA model we can clearly distinguish between protein and RNA component. The model has an extended structure in solution, and TAR wraps around the dsRBD. Whole of TAR is required to interact with tandem dsRBD's. In this model TAR loop can be seen suggesting that TAR in complex is more rigid structure. (B) Averaged solution *ab initio* model of dsRBD-VA-AS. Again both RNA and protein part can be seen. For this binding too the whole RNA is required to bind the tandem of dsRBD's. The complex has extended structure in solution and protein wraps around the RNA. In VA-AS three distinct regions are still present, and RNA takes upon rigid conformation like when found free in solution.

The RNA-protein interface curves along the length of the extended complex structure, with both dsRBMs and the linker region between them are required for the interaction with the RNA. As opposed to the free TAR RNA model, the RNA stem loop is clearly visualized upon complex formation with PKR_{1-169}, and both the loop and stem regions of the RNA are involved in the interaction. Once in complex, TAR adopts a significantly more defined conformation than observed in individual models for the free RNA. The overall solution conformation of PKR_{1-169} is similar to that of the free protein, and therefore it appears as though dsRBM1 is responsible for interaction with the loop of TAR, with the linker and dsRBM2 primarily mediating the interaction with the stem region of the RNA. Finally, the solution conformation is consistent with 1:1 stoichiometry, as other stoichiometries tested were unable to sustain reasonable fits to the raw data. For comparison, the average solution conformation from the individual MONSA fits is significantly less information-rich, yet defines a disc-shaped surface envelope (**Figure 3.6A**).

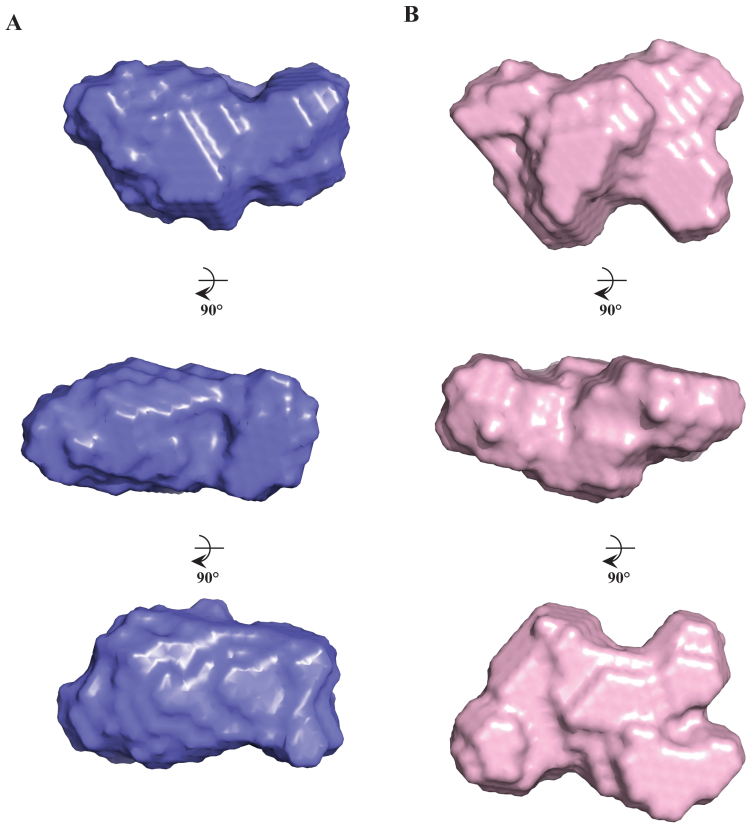

Figure 3.6: DAMFILT models of complexes. (A) Averaged solution *ab initio* model of dsRBD-TAR (top left), and its 90° rotation (bottom left) around its major axis. In solution, dsRBD-TAR complex takes upon extended shape. (B) Averaged solution *ab initio* model of dsRBD-VA-AS (top right), and its 90° rotation (bottom right) around its major axis. In solution dsRBD-VA-AS takes upon extended shape. In solution dsRBD-TAR model takes upon more rigid conformation then dsRBD-VA-AS model.

The determined χ values of ~1.0 and NSD value of 0.58 ± 0.03 for the complex indicates a quality fit between the calculated individual solution structures and the raw scattering data. Model-based parameter determinations are in good agreement with experimentally determined values, including the SAXS model-based and DLS-determined r_H values (**Table 3.1**).

3.6 VA_I-AS and TAR adopt similar overall conformations in complex with PKR_{1-169}

Finally, I performed SAXS experiments on purified PKR_{1-169}-VA_I-AS to determine whether a similar solution conformation could be observed to the PKR_{1-169}-

TAR complex. Experimental hydrodynamic parameters based on the distance distribution function calculated from the raw scattering data are within error of those determined for the TAR-containing complex (**Figure 3.3 & Table 3.1**). The overall topology of individual surface conformation models present and extended structure in which, again, the dsRBMs of PKR track the length of the VA_I-AS RNA molecule (**Figure 3.5B**). The entire length of the PKR_{1-169} protein mediates the interaction, presumably via the dsRBMs and linker joining them. Unlike in the TAR-containing complex, the loop region of the VA_I-AS RNA was not pronounced, and no significant conformation change is observed in the RNA molecule upon protein binding. However, the overall disc-shaped topology is similar between the two complexes, as illustrated by the comparison of the solution conformations (**Figure 3.6B**). As with all other molecules examined by SAXS, the model validation parameters (χ; NSD) and hydrodynamic parameters (r_H; r_G; D_{max}) are also consistent with an accurate model determination approach.

3.7 Discussion

The structure of individual dsRBMs from proteins other than PKR in complex with synthetic RNA duplexes suggest that the A-RNA helix is recognized in a sequence-independent manner via the 2'-hydroxyl groups of the ribose sugar in the minor groove and nonbridging oxygen residues of the phosphodiester backbone in the intervening major groove [169, 170, 181-183]. The separate structure of each of ADAR2's (dsRNA-binding enzyme that performs RNA editing) tandem dsRBMs bound to its stem-loop RNA ligand additionally demonstrated the direct readout of the RNA primary sequence in the minor groove accounting for the sequence specificity of each dsRBM [180]. To

date, no high-resolution structure of the dsRBMs of PKR in complex with either synthetic or natural ligands exists, nor does a clear understanding exist of how PKR is capable of interacting with imperfectly duplexed RNA ligands. Therefore, I sought to structurally characterize the interaction between the tandem dsRBMs of PKR and two viral dsRNA ligands, HIV-1 TAR and a stem-loop form adenovirus VA_I (VA_I-AS) (**Figures 1.6 and 1.7**).

I examined the conformation of individual components and complexes by SAXS, a solution-based structural technique that allows low-resolution determination of molecular shape and importantly can accommodate systems that are dynamic. All protein, RNA, and complexes were purified by size exclusion chromatography to remove heterogeneity and were confirmed monodisperse by DLS prior to SAXS experiments (**Figures 3.1 & 3.2**). All samples demonstrated a linear dependence of r_H on sample concentration, confirming their suitability for SAXS experiments (**Figure 3.2**). Confidence statistics (χ~1 in all cases) on individual models indicate an excellent fit with the raw scattering data. NSD values (< 0.9 in all cases) confirm that the individual models share similar structural features. Model-based calculations of hydrodynamic parameters are within error of the experimentally determined values, and importantly are cross-validated with the independently determined r_H values from DLS experiments. DLS experiments performed after SAXS data collection for each sample demonstrated absence of any sample degradation due to radiation damage. Finally, using BUNCH modeling with the known NMR solution structure of $PKR_{1\text{-}169}$, it was possible to recapitulate the determined SAXS model and even orient the individual dsRBMs to specific regions of the model.

Models of RNA-protein complexes were determined using MONSA, software that ultimately allows for the separate visualization of both protein and RNA components. The experimentally determined solution structure of TAR in complex with the tandem dsRBMs of PKR (PKR_{1-169}) highlights that nearly the entire length of the protein tracks a curved path to form contacts with the RNA stem-loop, involving both dsRBMs and the linker that joins them (**Figure 3.5A**). This is consistent with the observation that high affinity binding to TAR requires both dsRBMs of PKR, and NMR chemical shift perturbation experiments that have identified the binding interface to involve both dsRBMs and the linker [226]. A striking feature of the model is the apparent decrease in flexibility of TAR RNA upon interaction with PKR_{1-169} and the ability to visualize both the stem and loop portions of TAR RNA. Based on our modeling results of the free protein, I propose that dsRBM1 is responsible primarily for interaction with the loop, whereas the linker and dsRBM2 primarily interact with the stem region of TAR RNA. The model also suggests that the C-terminal end of the protein (dsRBM2) may be oriented such that the 80-residue interdomain linker and kinase domain are not directly affected by interaction with the RNA; similar observations have been made previously [197]. The RNA sequesters the tandem dsRBMs entirely, which would preclude the RNA from interacting with another molecule of PKR or an interaction between the dsRBMs and kinase domains from a single PKR molecule.

The observed TAR loop structure is striking but also suggests that a region larger than the expected hexaloop is involved in loop formation. While the model resolution is not sufficient to confirm the nucleotides involved, the TAR RNA hexaloop is highly dynamic [371], and has been shown to adopt significantly different conformations

depending on its association with ligands including small molecules, peptides, proteins, and other nucleic acid molecules [372, 373]. Concerted motions in TAR RNA have been suggested as the basis for access to bound state conformations [374]. HIV-2 TAR undergoes similar conformational changes [375]. Other dsRBM-containing proteins such as *S.cerevisiae* Rnt1p [376] and *Drosophila* Staufen [181] have shown a preference for loop regions, and mutation of the TAR hexaloop, bulge, or stem results in a significant reduction in binding affinity to PKR [226]. Therefore, there is significant experimental basis for recognition of the TAR loop via the dsRBMs of PKR.

Our SAXS, DLS, and size exclusion chromatography data are all consistent with a 1:1 complex stoichiometry under the concentration range and buffer conditions employed in this study or under the conditions in which the experiments were performed. With the experimentally determined hydrodynamic parameters, it was not possible to fit the acquired scattering data to any other complex stoichiometry. These results are consistent with previous NMR experiments in which the same complex stoichiometry is observed [197, 226]. It is important to stress that this study has been focused on a bound conformation of the PKR-TAR complex, and no comment can be made on whether this complex represents an active conformation, which remains our goal for further study. TAR RNA dimerization has been suggested as a potential mechanism required for activation [254], and while our data cannot preclude this possibility it does not directly support it either.

I additionally examined a second viral dsRNA stem-loop, VA_I-AS, in order to determine the generality of our results. Previously performed NMR experiments have indicated that identical amino acid residues in PKR are responsible for the interaction

with both TAR and VA_I-AS, and that similar regions of the stem-loop structure are responsible for interaction with PKR [227]. Free VA_I-AS is more conformationally constrained than TAR, and the same trend is observed once bound to $PKR_{1-169,}$ as VA_I-AS undergoes only moderate conformation changes (**Fig. 3.4, 3.5**) However, the SAXS envelope of TAR and VA_I-AS containing complexes have similar overall domain orientations and hydrodynamic parameters, consistent with a similar mode of interaction supporting previous studies [227].

Overall, the work presented demonstrates how tandem dsRBMs are capable of tolerating a wide range of sequence and structural motifs to function in the innate immune response to viral infection.

CHAPTER 4: SOLUTION CONFORMATION OF ADENOVIRUS VIRUS ASSOCIATED RNA-I AND ITS INTERACTION WITH PKR

The writing of Chapter 4 was adopted from: Dzananovic, E., Patel, T. R., Chojnowski, G., Boniecki, M. J., Deo, S., McEleney, K., Harding, S. E., Bujnicki, J. M. and McKenna, S. A. (2014) Solution conformation of adenovirus virus associated RNA-I and its interaction with PKR. J Struct Biol. 185, 48-57. E.Dz. was responsible for writing the manuscript, and designing and carrying out experiments including analysis of experimental data. T.P. contribution involved assistance with AUC experiments as well helping with ab initio modeling. Members of J.B. group, G.C. and M.B. contributed to in silico modeling of RNAs, proteins, and their complexes. S.D. contributed to preparation of protein, RNAs, and buffers. K.M. was responsible for operating the Small angle X-ray instrument. S.H. provided the access and assistance with operating the AUC instrument. S.M. is a principal investigator

4.1 Background

PKR, a Ser/Thr kinase, is a key component of the interferon-stimulated innate immune response that interacts with dsRNAs originating from replication by-products, mRNA transcripts, or the viral genome itself via its tandem N-terminal double-stranded RNA binding motifs (dsRBMs, residues 1-169) [228]. Once viral dsRNA binds to PKR, it can either activate or inhibit the protein. A number of studies have suggested that VA_I RNA acts as an inhibitor of PKR and prevents its self-association [160, 234, 235, 290-292]. During the late stages of viral infection, adenovirus synthesizes non-coding virus associated (VA) RNAs by host RNA polymerase III that accumulate to high concentration [377, 378]. VA_I mediates its effect in part through enabling efficient

translation of viral mRNA during late stages of infection [322, 379]. VA_I RNA has been determined to consist mainly of a double-stranded RNA (dsRNA) with three major domains; an apical stem-loop (AS), a central stem-loop (CS), and a terminal stem (TS) (**Figure 1.7**) [321, 323, 324]. The role of the apical and central stems of VA_I is well established; the apical stem directly involved in the interaction with the tandem dsRBMs, and the central stem prevents self-association of PKR [160, 274, 291, 292]. PKR autophosphorylation assays, isothermal calorimetry, NMR studies and RNA footprinting have demonstrated that the central stem of VA_I does not make a high affinity interaction with any region of PKR [160, 274, 291, 292]. In the absence of a high-resolution structure of the RNA-protein complex, the most straightforward interpretation would be that the central stem serves as a steric block to self-association of two PKR molecules. In addition, a truncated version of VA_I that lack the terminal stem (nucleotides 1-29 and 132-159) called $VA_I\Delta TS$, can still bind to PKR with full affinity and prevent its self-association.

As a precursor to understanding the molecular mechanisms of inhibition, biophysical and structural characterization of VA_I and its protein-binding partners are a required first step. In this study, I have *in vitro* transcribed and purified both VA_I and VA_I lacking the terminal stem ($VA_I\Delta TS$) by SEC. The solution conformation of these RNAs were determined using SAXS, and results were cross-validated by both dynamic light scattering and analytical ultracentrifugation. Using a similar experimental approach, I determined the solution conformation of $VA_I\Delta TS$ in complex with the tandem dsRBMs of PKR. I have then used SAXS data as restraints for computational modeling of $VA_I\Delta TS$ - free and in complex with the dsRBMs of PKR. Taken together, the results presented

provide insight of the structural features of VA_I that enable recognition and inhibition of PKR.

4.2 Homogeneity of VA_I, $VA_I\Delta TS$, and $VA_I\Delta TS$-PKR_{1-169}

I first sought to determine the solution conformation of VA_I by SAXS. A prerequisite for this approach and its validation is a pure, monodisperse sample that displays similar hydrodynamic properties over a range of concentrations. I initially investigated 3 species purified by SEC: VA_I, VA_I lacking the terminal stem ($VA_I\Delta TS$), and $VA_I\Delta TS$ in complex with the dsRBMs of PKR (PKR_{1-169}). The elution profiles of the RNAs (not shown) and the RNA-protein complex (**Figure 4.1A**) indicate the presence of a single species. The SEC purified samples were subjected to dynamic light scattering to further investigate purity of *in vitro* transcribed VA_I and $VA_I\Delta TS$, as well as $VA_I\Delta TS$-PKR_{1-169} complex.

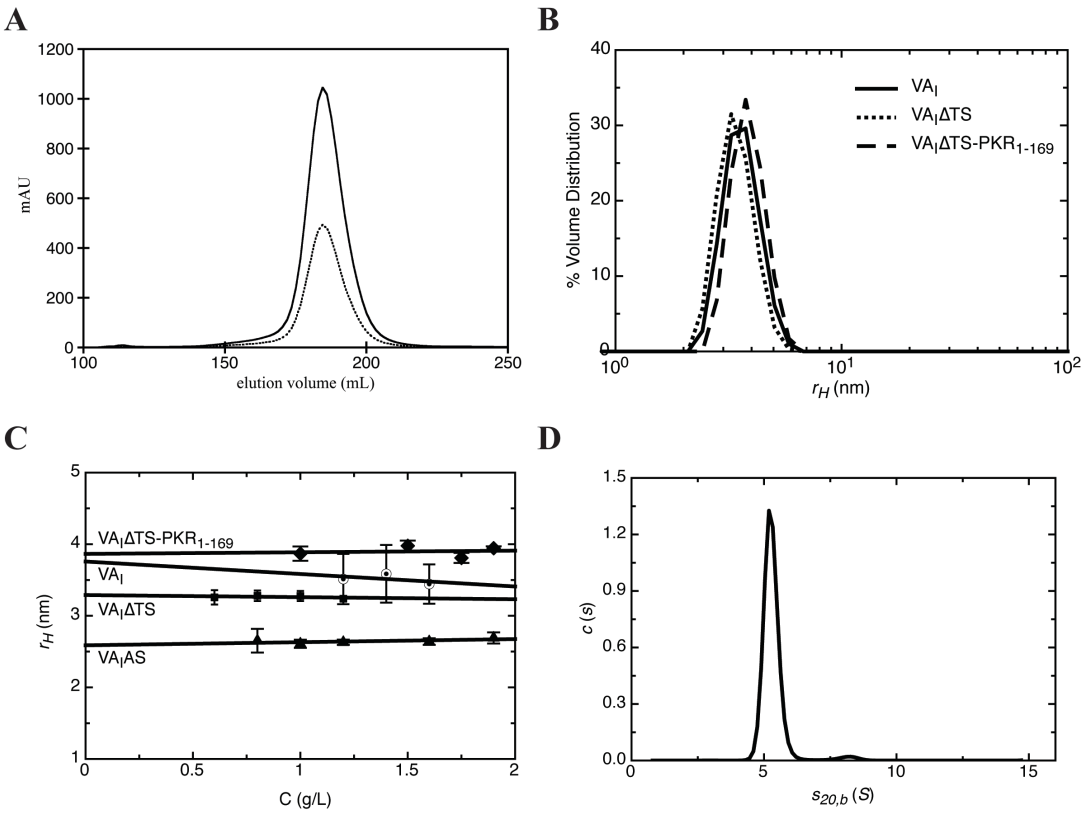

Figure 4.1: Homogeneity of $VA_{I\Delta}TS$, $VA_{I\Delta}TS$-PKR_{1-169} complex and VA_I RNA. (A) The elution profile of $VA_{I\Delta}TS$-PKR_{1-169} complex from SEC indicating the purity of the complex. A_{260} (solid line) and A_{280} (dashed line) values are shown. (B) Hydrodynamic radius distribution for $VA_{I\Delta}TS$, $VA_{I\Delta}TS$-PKR_{1-169} complex and VA_I RNA at 1.2, 1.0 and 1.2 mg/mL, respectively confirming the purity of RNAs and complex. (C) Dynamic light scattering data for $VA_{I\Delta}TS$, $VA_{I\Delta}TS$-PKR_{1-169} complex and VA_I RNA are presented at multiple concentrations. For comparison purposes, DLS data for VA_IAS has also been presented. An increase in hydrodynamic radius from VA_IAS to $VA_{I\Delta}TS$-PKR_{1-169} complex is clearly evident with increase in molecular mass of these macromolecules. (D) Sedimentation coefficient distribution of VA_I RNA at 0.20 mg/mL indicating that the RNA is of high purity.

The DLS profiles of both RNAs as well as the complex indicated monodisperse sample preparation (**Figure 4.1B**). Linear distribution over multiple concentrations suggested minimal concentration dependence of the Stokes radius (**Figure 4.1C**). The hydrodynamic radius (r_H) values obtained from the DLS measurements at multiple concentrations for $VA_I\Delta TS$ and VA_I are (3.30 ± 0.04) and (3.80 ± 0.04) nm, respectively. As expected, the size of the truncated versions of the VA_I RNA ($VA_I\Delta TS$ and VA_I AS [380] is smaller than the wild type and molecular weight and r_H are positively correlated for the three RNAs. The respective elution volumes on SEC further supported this observation, where the full length RNA elutes first followed by $VA_I\Delta TS$ and VA_IAS (data not shown). As expected, VA_I ΔTS-PKR_{1-169} complex presented an increase in r_H (3.90 ± 0.20 nm) compared to $VA_I\Delta TS$ alone. The sedimentation velocity experiment for the VA_I RNA was carried out at a single concentration (0.2 mg/mL). The sedimentation velocity analysis (**Figure 4.1D**) suggested that VA_I RNA is monodisperse, supporting the SEC and DLS results in terms of its purity. The $s_{20,b}$ (S) for VA_I RNA was corrected to standard solvent conditions using program SEDNTERP to $s_{20,w}$ (S) of (5.46 ± 0.10) S. Taken together, the results suggest all three samples are appropriate for SAXS. The results have been summarized in the Table 4.1.

4.3 SAXS studies on $VA_I\Delta TS$ and VA_I

While there is currently no high-resolution structural information available on VA_I, its secondary structure consists primarily of A-RNA stem-loops interrupted periodically by internal bulges, a junction, and non-canonical base pairing (**Figure 1.7**). In order to determine the solution conformation of VA_I and its Dicer processed version ($VA_I\Delta TS$), I performed SAXS experiments. The stability of each sample was assessed by denaturing gels pre- and post-SAXS experiments (data not shown). The solution scattering profiles were collected at multiple concentrations and evaluated for self-association at individual concentrations by calculating the radius of gyration (r_G). The output files at individual concentrations were then merged to obtain a single profile, from which the $p(r)$ distribution function was determined (**Figure 4.2A**). The merged data were also utilized for Guinier analysis to obtain radius of gyration [381] (**Figure 4.2B**). The $p(r)$ function of previously published VA_IAS is also presented in **Figure 4.2C** [380].

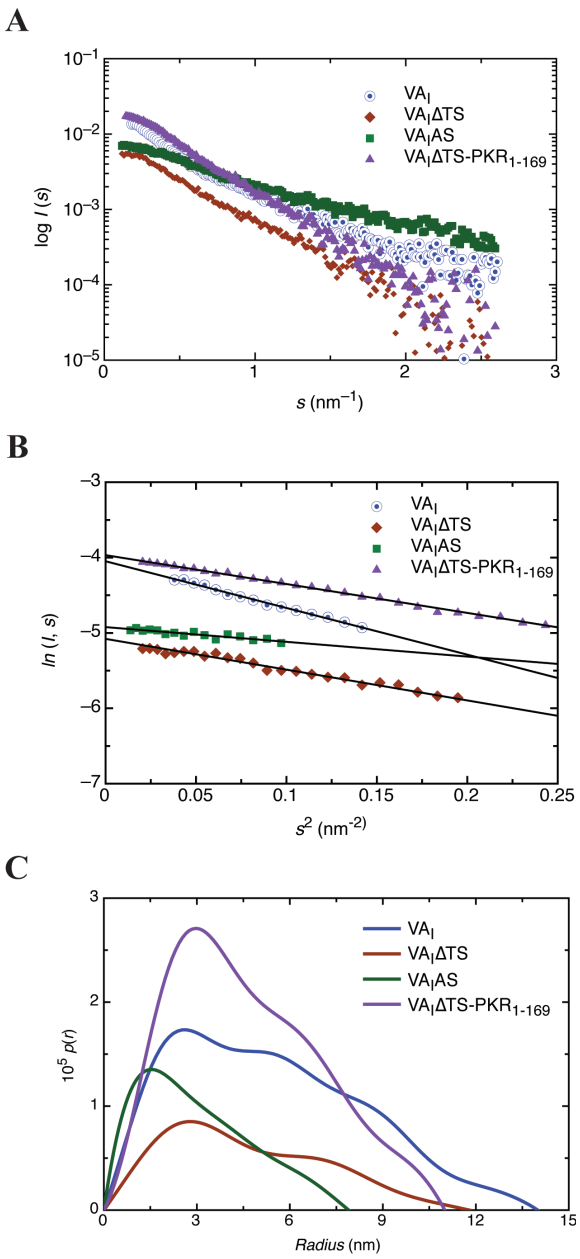

Figure 4.2: SAXS data analysis. (A) Merged raw SAXS data for individual macromolecules. (B) Guinier analysis of merged data for individual macromolecules. (C) The pair distribution function analysis of VA_I RNA, $VA_{I\Delta}TS$, $VA_{I\Delta}TS$-PKR_{1-169} complex and VA_IAS are presented.

Each profile adopts a skewed bell shape that is typical for elongated molecules, and the extended tails of each of the distribution functions are distinct suggesting structural differences between these three RNAs. From the scattering profiles, I obtained

the r_G for VA_I and $VA_I\Delta TS$ of (4.35 ± 0.07) nm, and (3.71 ± 0.06) nm respectively. The r_G for all species obtained from GNOM analysis were comparable to those obtained from Guinier analysis (Table 4.1). I also obtained the D_{max} values of 14.0 and 11.8 nm for VA_I and $VA_I\Delta TS$ respectively (Table 4.1). As expected, the r_G and D_{max} values for VA_I and $VA_I\Delta TS$ are consistent with that of the VA_IAS (r_G - 2.45 ± 0.02 and D_{max} – 7.9 nm) as the full length RNA behaves as largest species followed by $VA_I\Delta TS$ and VA_IAS.

4.4 Solution conformation of $VA_I\Delta TS$

Based on the experimentally determined r_G and D_{max} values, *ab initio* models for $VA_I\Delta TS$ were determined using the program DAMMIN [359]. Twelve models for $VA_I\Delta TS$ were calculated using the merged scattering data obtained from multiple concentrations. A χ value of ~0.8 was obtained for individual models of $VA_I\Delta TS$, indicating an excellent agreement between the experimental data and data calculated from *ab initio* models (**Table 4.1**).

Hydrodynamic parameters	VA_I		$VA_I\Delta TS$		$VA_I\Delta TS\text{-}PKR_{1\text{-}169}$	
	Experimental	HYDROPRO DAMMIN[e]	HYDROPRO Experimental	HYDROPRO DAMMIN[e]	Experimental	HYDROPRO MONSA[e]
r_H (nm)[a]	3.8(±0.4)	3.65(±0.02)	3.30(±0.04)	3.43(±0.03)	3.9(±0.2)	3.78(±0.04)
r_G(nm)[b]	4.4(±0.1)	-	3.7(±0.1)	-	3.4(±0.2)	-
r_G(nm)[c]	4.35(0.07)	4.33(±0.03)	3.71(±0.06)	3.78(±0.06)	3.60(±0.03)	3.42(±0.04)
D_{max}(nm)[c]	14.0	14.20(±0.02)	11.8	12.2(±0.06)	11.0	10.50(±0.01)
χ	-	0.8	-	0.8	-	1.0/0.8/1.1[d]
NSD	-	0.71(±0.01)	-	0.63(±0.02)	-	0.75(±0.03)

[a] experminetally determined fromDLS data, with error obtained from linear regression analysis.
[b] experimentally determined r_G from Gunier analysis.
[c] experimentally determined from P(r) analysis by GNOM
[d] values for protein/RNA/complexes respectively
[e] model-based parameters calculated from HYDROPRO, with errors obtained as the standard deviation from multiple models

Table 4.1: Summary of hydrodynamic data (with error in parentheses)

Ab initio models of $VA_I\Delta TS$ were then rotated, aligned, averaged and filtered using program DAMAVER that provided a normalized spatial discrepancy (NSD) of 0.64 ± 0.02, suggesting a strong agreement between the individual models (**Figure 4.3A**). The *ab initio* model of $VA_I\Delta TS$ shows two distinct elongated domains possibly coinciding with apical and central stem-loops. The structure exhibits an elongated conformation, which agrees with experimental data from the pair distribution function.

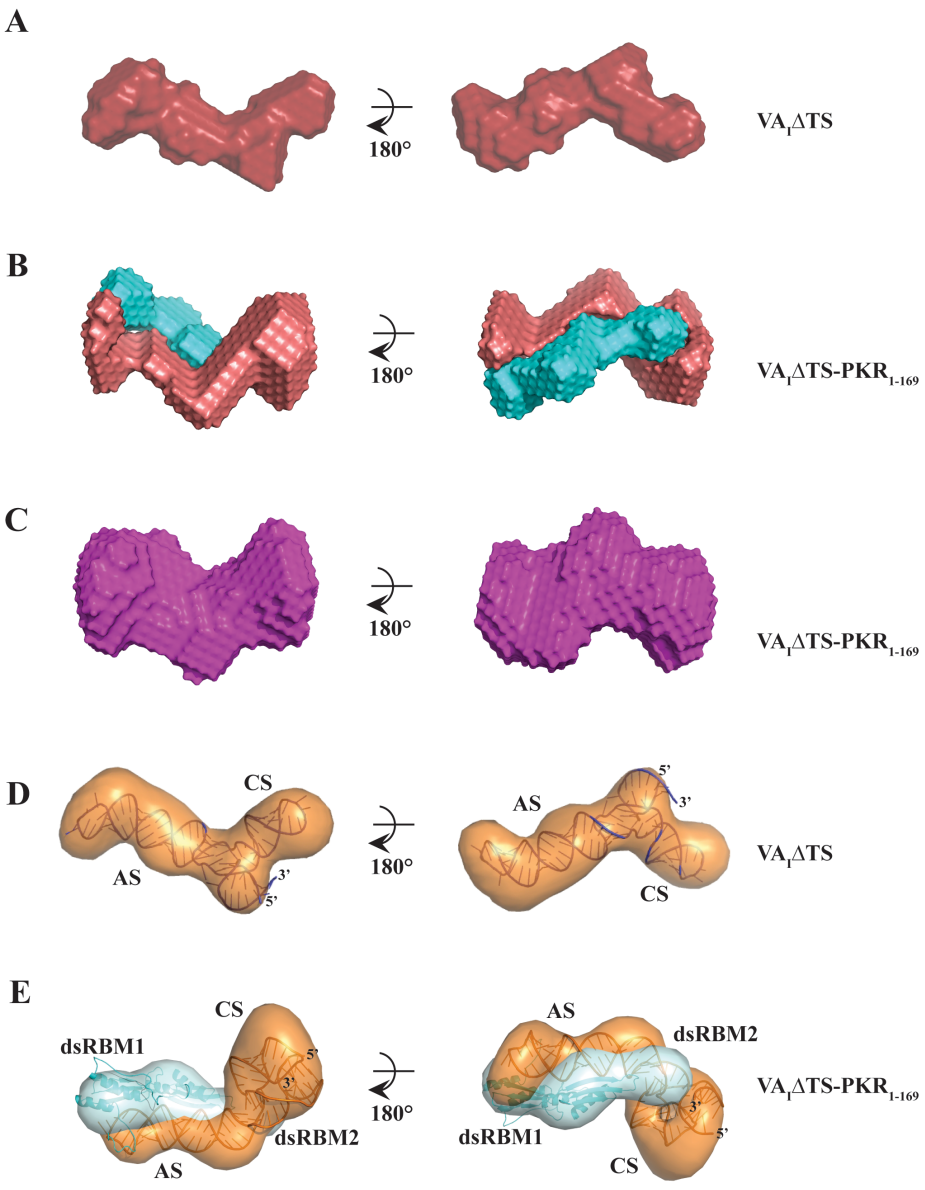

Figure 4.3: *Ab initio* analysis of VA$_I$ΔTS. (A) Solution conformation of VA$_I$ΔTS obtained from *ab initio* analysis using DAMMIN program. (B) A representative *ab initio* model of VA$_I$ΔTS-PKR$_{1-169}$ complex calculated using MONSA program. The PKR$_{1-169}$ is presented in cyan color whereas VA$_I$ΔTS is in orange color. (C) A filtered model of VA$_I$ΔTS-PKR$_{1-169}$ complex obtained form 15 *ab initio* calculations indicating overall shape of the complex in solution. (D) *In silico* model of VA$_I$ΔTS based on *ab initio* solution conformation determination. A high-resolution RNA model was obtained from SimRNA program and built into the reconstructions using PyRy3D. (E) Model of the VA$_I$ΔTS-PKR$_{1-169}$ build based on the *ab initio* reconstructions of protein (cyan) and RNA (orange) components of the complex. Atomic coordinates of the models are available from ftp://genesilico.pl/iamb/models/VA-RNA/.

4.5 Solution conformation of $VA_I\Delta TS$-PKR_{1-169} complex

VA_I lacking the terminal stem is the shortest RNA sufficient for binding and inhibition of PKR, and therefore I chose this RNA as our PKR binding partner. Prior to performing SAXS experiments, the $VA_I\Delta TS$-PKR_{1-169} complex was purified by means of SEC to separate the complex from any unbound individual components. The purity of the complex was further assessed by DLS (**Figure 4.1B**) before SAXS data collection. SAXS experiments were performed at multiple concentrations and the raw data were merged (**Figure 2 inset**). An r_G of 3.60 ± 0.03 nm and D_{max} of 11 nm was obtained from the bell-shaped pair distribution function plot that is characteristic of an extended molecule. Both the r_G and D_{max} of the complex are slightly smaller than those of the RNA alone, indicating a potential minor conformational change in the RNA upon protein binding. To obtain *ab initio* models, the previously published scattering data for PKR_{1-169} [380] was used as an input dataset along with the scattering data for $VA_I\Delta TS$ and $VA_I\Delta TS$-PKR_{1-169} complex to determine the solution conformation of the complex using the MONSA program. χ values of 1.0, 0.8, and 1.1 were obtained for PKR_{1-169}, $VA_I\Delta TS$ and $VA_I\Delta TS$ PKR_{1-169} complex respectively, demonstrating the agreement between experimental scattering data and data calculated from the models. **Figure 4.3B** presents an individual *ab initio* model calculated for the $VA_I\Delta TS$-PKR_{1-169} complex where PKR_{1-169} and $VA_I\Delta TS$ interact in a side-by-side orientation that involves entire PKR_{1-169} molecule. It is also evident that $VA_I\Delta TS$ undergoes a slight conformational change upon its interaction with PKR_{1-169}. The DAMAVER processed averaged model of the complex obtained from multiple *ab initio* models is presented in **Figure 4.3C**. The NSD parameter of 0.75 ± 0.03 was obtained indicating that the individual models are highly similar to each other.

4.6 In silico tertiary structure prediction based on *ab initio* models

To further visualize the conformations of $VA_I\Delta TS$ both RNA alone and in complex with $PKR_{1\text{-}169}$, a set of preliminary tertiary structure models were obtained using the SimRNA program. Simulations were carried out with restraints on predicted secondary structure [364]. SAXS solution conformations were then used as a restraint to filter the resulting low-energy models to select structures for further refinement. Based on the filtered SimRNA results, modeling with restraints derived from experimental data was carried out using PyRy3D, a tool for modeling of macromolecular complexes where individual parts with defined structures can be represented as either rigid bodies or as flexible chains. PyRy3D models were generated by minimizing the violation of restraints including distances between individual elements or their parts, shapes, contacts, exposure on the surface. Here, segments of $VA_I\Delta TS$ RNA and $PKR_{1\text{-}169}$ predicted to be rigid were treated as rigid bodies, and spatial restraints included shapes obtained from SAXS *ab initio* reconstructions, and continuity of the nucleotide and polypeptide chains. For $VA_I\Delta TS$ alone, the overall dimensions of the *in silico* structure and SAXS *ab initio* model are self-consistent (**Figure 4.3D**). An extended conformation was observed with clearly defined apical and central stems oriented roughly perpendicular to each other. For the protein-RNA complex, the *in silico* structure supports that both dsRBMs mediate the interaction with the apical stem while making no significant contacts with the central stem (**Figure 4.3E**). The dsRBM1 is situated at the loop end of the apical stem, whereas dsRBM2 primarily contacts the apical stem at is base near the junction with the central stem. The mode of interaction between either of the dsRBM domains and the RNA is consistent with the typical RNA-binding mode of essentially all dsRBDs studied to date

[382]. In the context of the RNA-protein complex, the central and terminal stems of $VA_I\Delta TS$ adopt a pseudoknot conformation by base pairs that were not restrained in the simulation.

4.7 Solution conformation of VA_I RNA

To investigate the structural importance of the terminal stem, *ab initio* models for VA_I were calculated using the DAMMIN program that provided models with χ values of ~0.7. Individual models adopt an extended conformation and show three distinct domains that, at low resolution, may correspond to the predicted stem loop regions of VA_I (**Figure 4.4A**).

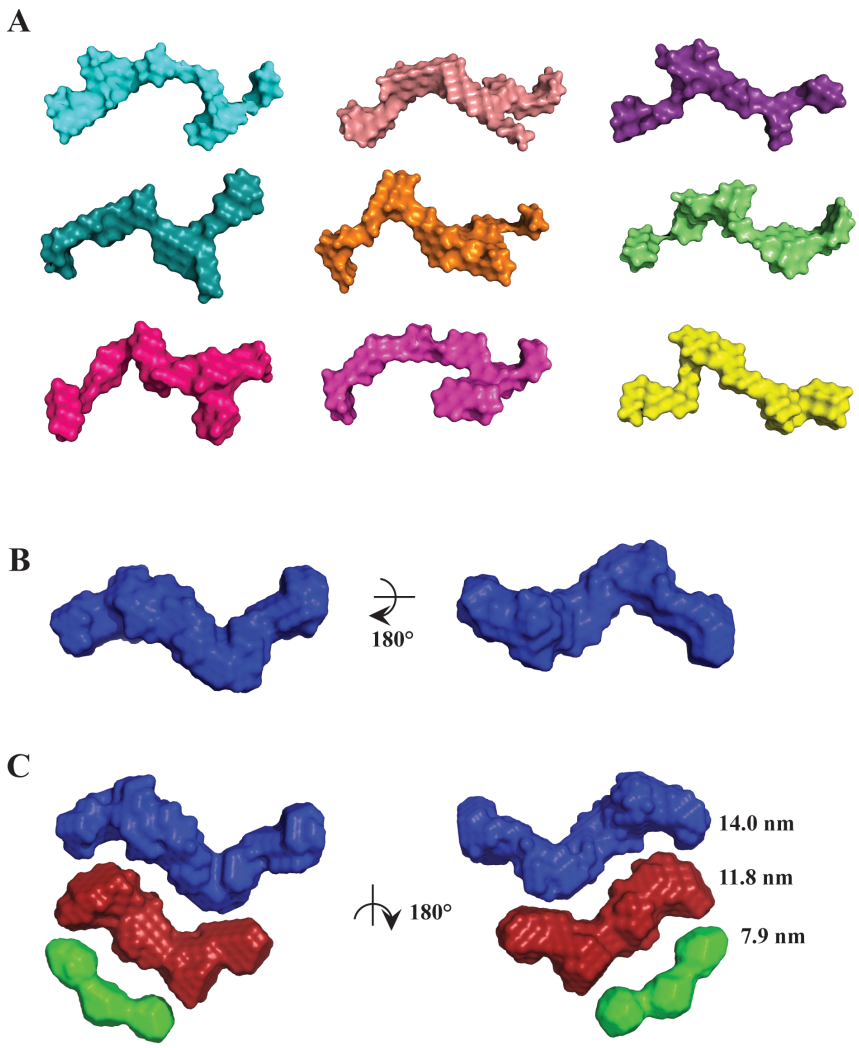

Figure 4.4: *Ab initio* analysis of VA_I RNA. (A) Solution conformations of VA_I RNA obtained from DAMMIN program. (B) A filtered model of VA_I RNA obtained from DAMAVER program using 15 *ab initio* models. (C) Comparison of solution conformations of VA_I RNA (blue), $VA_I\Delta TS$ (red) and VA_IAS (green) RNAs.

The average model for VA_I RNA (from DAMAVER) was determined with a resulting NSD value of 0.79 ± 0.01 (**Figure 4.4B**). By comparison to $VA_I\Delta TS$ and the previously published VA_IAS model [380], VA_I RNA is the largest RNA followed by the $VA_I\Delta TS$, which lacks 21 base pairs in the terminal region of the VA_I, followed by the VA_IAS which does not contain the central or the terminal stem (**Figure 4.4C**).

4.8 Solution conformation of PKR and PKR-$VA_I\Delta TS$

The original focus of our study was to characterize PKR and PKR-$VA_I\Delta TS$ complex using SAXS. PKR was expressed and purified followed by dynamic light scattering analysis at a wide range of concentrations to evaluate its purity. Although the protein was found to be monodisperse up to 8 mg/mL (highest concentration used in the current study), the r_H at concentrations above 2 mg/mL increased dramatically (data not shown). The r_H for PKR up to 2 mg/mL was found to be independent of concentration (**Figure 4.5A**) and a linear extrapolation of r_H from 0.5 to 2 mg/mL provided a value of 5.8 ± 0.03 nm. Interestingly, r_H of 7.6 ± 0.3 nm was obtained for PKR at 8 mg/mL, suggesting self-association behavior (data not shown). Further evidence of PKR's self-association was obtained from SAXS studies performed at multiple concentrations. The radius of gyration and maximal particle dimension obtained from pair distribution function analysis of SAXS data for PKR from 3 to 8 mg/mL (**Figure 4.5 (B) and (C)**) clearly indicates that PKR self-associates. Therefore, an attempt was not made for either *ab initio* or rigid body modeling for PKR. I was also able to prepare PKR-$VA_I\Delta TS$ complex and purify by SEC. The purity of complex was analyzed using dynamic light

scattering at multiple concentrations and a value of 6.7 ± 0.2 nm was obtained (**Figure 4.5D**). The pair distribution function analysis for PKR-VA$_I$ΔTS complex suggested minor increase in r_G and D_{max} from ~1.5 mg/mL to 3.2 mg/mL that prevented any further model building to study low-resolution shape (**Figure 4.5E**).

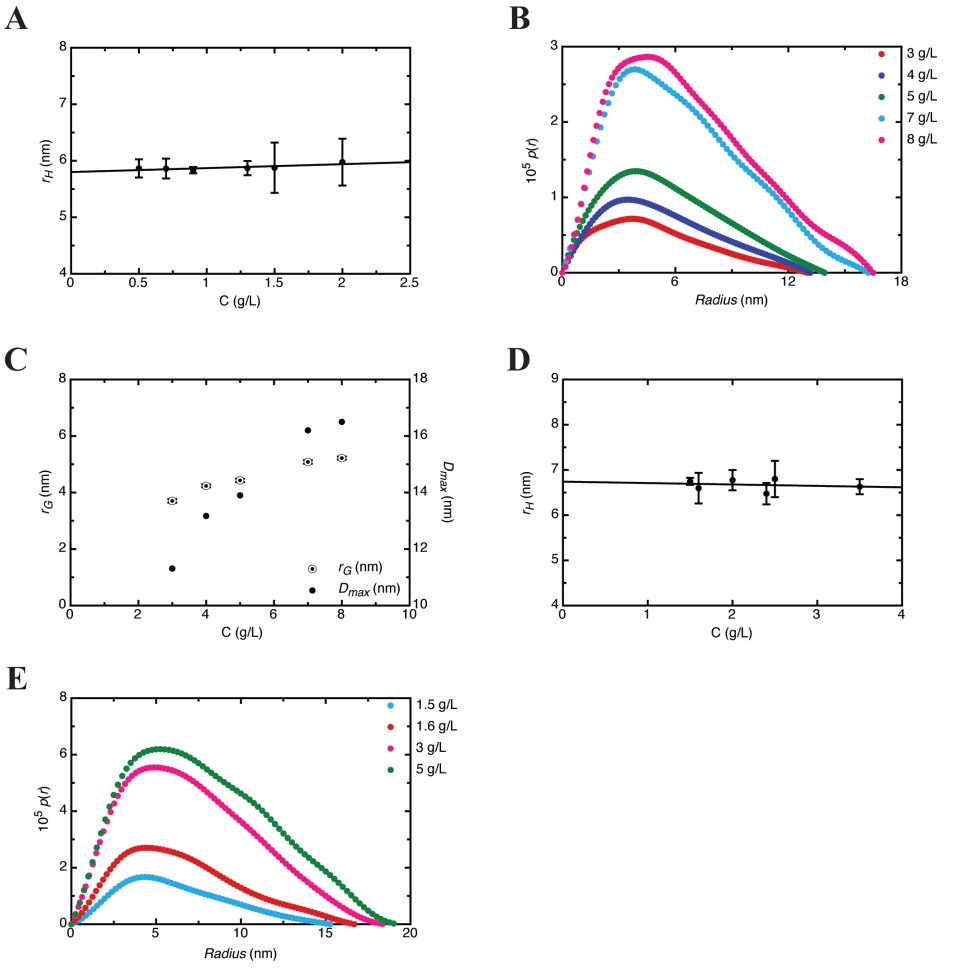

Figure 4.5: Hydrodynamic studies on PKR and PKR-VA$_{I\Delta}$TS complex. (A) Hydrodynamic radius of PKR measured at dilute concentrations (up to 2 mg/mL). (B) Pair distribution function analysis of PKR at multiple concentrations. (C) Dependence of r_G and D_{max} on PKR concentration. (D) Hydrodynamic radius distribution of PKR-VA$_{I\Delta}$TS complex at multiple concentrations. (E) Pair distribution function analysis of PKR-VA$_{I\Delta}$TS complex at multiple concentrations indicating increase in radius of gyration and maximal particle dimension with increase in concentration.

4.9 Calculation of hydrodynamic parameters from ab initio models

In order to further validate the *ab initio* solution conformations by SAXS, I compared experimentally determined hydrodynamic parameters (r_G, r_H and D_{max}) with those calculated from the models (Table 4.1). Using this approach, the r_H, r_G and D_{max} values obtained from *ab initio* models of $VA_I\Delta TS$ are 3.43 ± 0.03 nm, 3.78 ± 0.06 nm, and 12.2 ± 0.06 nm respectively, which are in excellent agreement with the experimentally determined data. The $VA_I\Delta TS\text{-}PKR_{1\text{-}169}$ complex *ab initio* models provided the r_H, r_G and D_{max} values of 3.42 ± 0.04 nm, 3.78 ± 0.04 nm and 10.50 ± 0.01 nm respectively which are also consistent with the experimental data. An excellent agreement was also obtained for VA_I RNA, where the r_G of 4.33 ± 0.03 nm, r_H of 3.65 ± 0.02 nm and D_{max} of 14.2 ± 0.02 nm was obtained from *ab initio* models.

4.10 Discussion

As a countermeasure to host innate immunity, adenovirus transcribes VA_I RNA in host cells to enable viral growth. This effect is at least in part mediated through the interaction with and inhibition of PKR, a key interferon-stimulated protein. The apical stem of VA_I interacts with the tandem dsRBMs of PKR while the central stem plays a pivotal role in inhibition of PKR autophosphorylation. VA_I lacking its terminal stem ($VA_I\Delta TS$) is sufficient to mediate inhibition *in vitro*, and suggests maintenance of its secondary structure. In order to investigate these features, I investigated the solution conformation of $VA_I\Delta TS$, $VA_I\Delta TS\text{-}PKR_{1\text{-}169}$ complex, and the full length VA_I RNA by small angle X-ray scattering (SAXS). Prior to solution conformation determination by SAXS, RNA was purified by SEC and characterized by DLS. For both VA_I and $VA_I\Delta TS$ a highly pure and homogenous sample preparation was observed (**Figure 4.1**).

Additionally, the purity of VA_I RNA was also confirmed using the analytical ultracentrifugation. From the sedimentation coefficient of VA_I RNA (5.46 ± 0.10 S), the molecular weight of 54.2 kDa was calculated by taking advantage of the r_H of 3.80 ± 0.40 nm using equation 1. The sedimentation coefficient obtained for VA_I agrees with a value of ~5 S obtained from previous study [332]. This agrees with the sequence molecular weight of 48.2 kDa for a monomer. Therefore, I am confident in my sample quality prior to SAXS analysis.

The *ab initio* models of $VA_I\Delta TS$ suggested it adopts an extended conformation with two roughly perpendicular protrusions that are consistent with the previously predicted secondary structure of VA_I RNA (**Figure 1.7 and Figure 4.3A**). The $VA_I\Delta TS$ *in silico* tertiary structure superimposes nicely on the *ab initio* models, and I propose that the longer stem represents the apical stem-loop, while the shorter one coincides with the central stem (**Figure 4.3D**). Individual *ab initio* models for full length VA_I also presented an extended conformation, but with three distinct domains (**Figure 4.4A**). Based on comparison to the solution conformations of VA_IAS [380] and $VA_I\Delta TS$, the longer stem of VA_I resembles the apical stem and the terminal stem extends beyond the envelope assigned to the central stem. Unfortunately, the results prevented the structural resolution of the central from terminal stems in the context of VA_I, and will await high-resolution structure determination. Models are in agreement with the independently determined experimental data, and model validity is further supported by the determined χ and NSD values (**Table 4.1**).

Our attempts to study the solution conformation of full-length PKR, free or in complex with $VA_I\Delta TS$, were unsuccessful. An examination of the r_G and D_{max} values at

multiple concentrations indicated a concentration-dependent increase in both parameters. Interestingly, previous SAXS study on PKR was carried out at 1, 2 and 4 mg/mL and reported a radius of gyration of 4.2 ± 0.02 nm at 4 mg/mL that also agrees with the r_G I determined at 4 mg/mL. The current study involves wider range of concentrations (**Figure 4.5B**) that provides evidence for self-association at higher concentrations. Although, the r_G value of 4.2 ± 0.05 nm at 4 mg/mL from this study is comparable with that from VanOudenhove et al. [195]. This result is not unexpected for full length PKR, as numerous studies have established the dynamic nature of the linker joining the dsRBMs to kinase domain [194-196]. That similar behavior was observed for the PKR-$VA_I\Delta TS$ complex may suggest that the interaction with inhibitory RNA does not significantly reduce the interdomain linker flexibility. Additionally, this data serves as a cautionary tale as to the limitations of using SAXS approaches at a single concentration, particularly in systems where self-association is known to occur.

A recent study from our group provided additional support for the recognition of the apical stem RNA construct (VA_IAS) by the dsRBMs of PKR, where the dsRBMs track the entire length of the RNA [380]. Here, I have extended the studies to include the solution conformation of VA_I lacking the terminal stem ($VA_I\Delta TS$) in complex with the dsRBMs of PKR (PKR_{1-169}) in order to determine the structural contributions of the central stem. The complex adopts an extended conformation where RNA and protein present a side-by-side interaction (**Figure 4.3B,E**). Based on (*i*) comparison of the SAXS envelopes of VA_I-AS and $VA_I\Delta TS$ (**Figure 4.3C**), (*ii*) the computationally predicted tertiary structure of the complex (**Figure 4.3E**), and (*iii*) the previously published VA_I-AS -PKR_{1-169} data from SAXS, I propose that the dsRBMs track the length of the apical

stem but do not interact extensively with the central stem of VA_I. While speculative based on the resolution afforded by SAXS, our results indicate that the loop of apical stem is involved in the interactions with one of the dsRBMs (presumably dsRBM1) leaving the other dsRBM (dsRBM2) of PKR to interact with base of the apical stem, thus supporting previously reported mode of recognition between the RNA and PKR [380]. The central stem is oriented roughly perpendicular to the helical axis of the apical stem, which suggests a potential structural basis for the inhibition of PKR via steric prevention of PKR self-association.

CHAPTER 5: THE STRUCTURAL INTEGRITY OF THE CENTRAL STEM-LOOP OF ADENOVIRUS VA_I RNA IS ESSENTIAL FOR PKR INHIBITION

Chapter 5 is an adaptation of a manuscript titled "The structural integrity of the central stem-loop of adenovirus VA_I RNA is essential for PKR inhibition" that is in the process of being submitted for publication. Co-authors on this manuscript include Edis Dzananovic, Trushar R. Patel, Soumya Deo, Grzegorz Chojnowski, Astha, Evan P. Booy, Kevin McEleney, Janusz M. Bujnicki, Sean A. McKenna. E.Dz was primarily involved in carrying out the preparation and writing of manuscript. In addition, E.Dz. was responsible for designing and performing the experiments including analysis of experimental data. T.P. assisted with ab initio modeling of macromolecules. S.D. contributed to preparation of protein, RNAs, and buffers. High-resolution modeling is to be performed by members of J.B. group, G.C. and Astha (data not included in thesis). E. B. contributed by providing technical assistance with western blotting. K.M. was responsible for operating the Small angle X-ray instrument. S.M. is a principal investigator.

5.1 Background

To evade the host innate immune system, some viral countermeasures include transcription of small non-coding RNAs that inhibit PKR via direct binding to the dsRBMs of PKR to prevent autophosphorylation [274]. Adenovirus uses the host RNA polymerase III to transcribe virus associated RNA-I (VA_I) that accumulates during the late stages of infection to inhibit PKR [160, 234, 235, 290-292]. At the secondary structure level, VA_I consists of two stem-loops, apical (AS) and central (CS) (**Figure 1.7**) and a terminal stem (TS) region [321, 323, 324, 383]. Functionally, the apical stem of

VA_I is responsible for interaction with the dsRBMs of PKR, while the central stem plays a pivotal role in the inhibition of PKR autophosphorylation. The terminal stem appears dispensable for PKR inhibition, as VA_I lacking the terminal stem ($VA_I\Delta TS$) has no impact on affinity for or inhibition of PKR *in vitro* [328]. Moreover, $VA_I\Delta TS$ may represent a biologically relevant structure based on results demonstrated by the Dicer-processing of VA_I by the RNA interference machinery [328].

The central stem is hypothesized to prevent PKR self-association and autophosphorylation through steric means, through formation of a pseudoknot that adopts a structure favorable to inhibition, or a combination of both [227, 383, 384]. Although it is evident that the central domain of the VA_I is critical for the inhibition of PKR [160, 274, 291, 292], contradictory results suggest that the central stem is dispensable [385, 386]. Instead the central stem's overall organization as a three-helix junction found at the base of the three stems plays a crucial role for the activation [386]. The interaction between the PKR and the RNA is mediated through dsRBMs of PKR and the apical stem of RNA, while the RNA-mediated inhibition of PKR is accomplished through the central stem-loop of $VA_I\Delta TS$ [321, 323, 324]. Recently, several studies have questioned the role of central stem-loop in the inhibition of PKR by $VA_I\Delta TS$ [386]. Magnesium ions have been shown to play multiple roles required for the function of VA_I RNA. The binding stoichiometry to PKR is modulated by the presence of Mg^{2+} ions [387], and PKR requires the presence of the divalent ion for its function [160, 190, 193, 291]. In addition, it has been observed that Mg^{2+} is required for the formation of pH-dependent tertiary structure in the central stem of the RNA [387]. Furthermore, Mg^{2+} ions are present under the

physiological condition within the cell. Based on these observations we decided to perform experiments in presence of Mg^{2+} ions.

As of now there is no high-resolution structure of PKR, VA_I/$VA_I\Delta TS$, or the complexes involving these molecules. However the high-resolution structures of PKR_{1-169} [157] and kinase domain [165] together with SAXS models of full length PKR [158] as well as PKR_{1-169} alone and in complex with short viral dsRNAs [380, 383] give insight into mechanism of activation/inhibition of PKR. NMR studies of PKR_{1-169} show that each dsRBM from PKR adopts a canonical fold required for dsRNA recognition, containing a 3-stranded antiparallel β-sheet flanked by 2 α-helices with the tandem dsRBMs joined by a 23 amino acid linker [157]. The C-terminal region of PKR encompasses a Ser/Thr kinase domain involved in PKR autophosphorylation and recognition and phosphorylation of target substrate. Structural studies on the kinase domain in complex with eIF2α detailed the overall Ser/Thr kinase fold including the Thr446 and Thr451 residues in activation loop overhanging the kinase active site that lead to PKR autophosphorylation and activation as well as the features required for target substrate interaction [165, 380, 383]. The dsRNA binding and kinase domains are joined by a third region, a flexible interdomain linker (80-residue), implicated in PKR self-association [158, 159]. Previous studies have shown that significant flexibility in the two linkers (one between the dsRBMs, the other between the dsRBMs and kinase domains) exist, allowing for two distinct conformations of PKR; an extended "open" conformation where dsRBMs and kinase domains are not in contact, and a collapsed "closed" conformation [158, 161, 196-198].

The solution conformation of VA_I and $VA_I\Delta TS$ reveal that the RNA takes upon an extended shape in solution [383, 388]. The *ab initio* model of VA_I and $VA_I\Delta TS$ shows two distinct elongated domains coinciding with apical and central stem-loops consistent with the previously predicted secondary structure. Tertiary structure computational models of $VA_I\Delta TS$ show an extended conformation was observed with clearly defined apical and central stems oriented roughly perpendicular to each other [383]. SAXS modeling together with chemical probing reveal the presence of pseudoknot in $VA_I\Delta TS$ formed between the loop of central stem and a single-stranded region near the three-way junction of the AS, CS, and TS [388]. In addition, a solution conformation of PKR_{1-169} in complex with apical stem of VA_I (VA_I-AS) and $VA_I\Delta TS$ determined by SAXS show an extended shape in solution with small decrease in size of $VA_I\Delta TS$ suggestion a change in RNA conformation upon binding to PKR_{1-169}. VA_I-AS and $VA_I\Delta TS$ are shown to interact in a side-by-side orientation that involves entire PKR_{1-169} molecule. dsRBMs track the length of the apical stem but do not interact extensively with the central stem of VA_I. Both the loop and stem region of each RNA are involved in the interaction with both dsRBMs and the linker region between them. *In silico* model of $VA_I\Delta TS$-PKR_{1-169} structure supports that both dsRBMs mediate the interaction with the apical stem while making no significant contacts with the central stem.

In this study we have investigated the role of the central stem-loop in the mechanism of inhibition of PKR by the $VA_I\Delta TS$ RNA. In order to establish the importance of various structural features in the inhibitory central stem to PKR inhibition, we produced and purified $VA_I\Delta TS$ RNA and $VA_I\Delta TS$ with modest in the central stem of $VA_I\Delta TS$ designed to not drastically affect the overall tertiary structure of the RNA and

retain full binding affinity for PKR. Electrophoretic mobility shift assays (EMSAs) were performed to confirm that the mutations do not affect binding affinity. Dynamic light scattering (DLS), and small-angle X-ray scattering (SAXS) were used to determine the impact of mutation on global tertiary structure. *In vitro* autophosphorylation assays were then performed to determine the impact of mutation of the central stem on PKR, and suggest that preservation of the pseudoknot structure, and not steric hindrance represents the mechanism of PKR inhibition. Finally, VA_I-PKR complexes were compared structurally to determine the impact of mutation on complex structure.

5.2 Purification of $VA_I\Delta TS$ derivatives to probe central stem structure

To study the effect of specific structural features of the central stem-loop (CS) of $VA_I\Delta TS$ on its ability to inhibit PKR, we *in vitro* transcribed $VA_I\Delta TS$ RNA (used as a wt RNA in this study) and six mutant versions of the RNA that all retained the apical stem (AS) (**Figure 1.7**). The mutants probe the CS heptaloop by mutation to UUCG (Δloop), CS bulge at its base by conversion to perfect duplexed (Δbulge), mid-CS GU bp by conversion to a canonical GC basepair (ΔGU), CS length by stem shortening by two (ΔCD2bp) or 4 bp (ΔCD4bp), or complete CS truncation (ΔCD). *In vitro* transcribed RNAs were purified using non-denaturing size-exclusion chromatography (SEC) in a Mg^{2+}-containing buffer (Buffer, 50 mM Tris pH 7.5, 100 mM NaCl, 5 mM $MgCl_2$.) (**Figure 5.1A**).

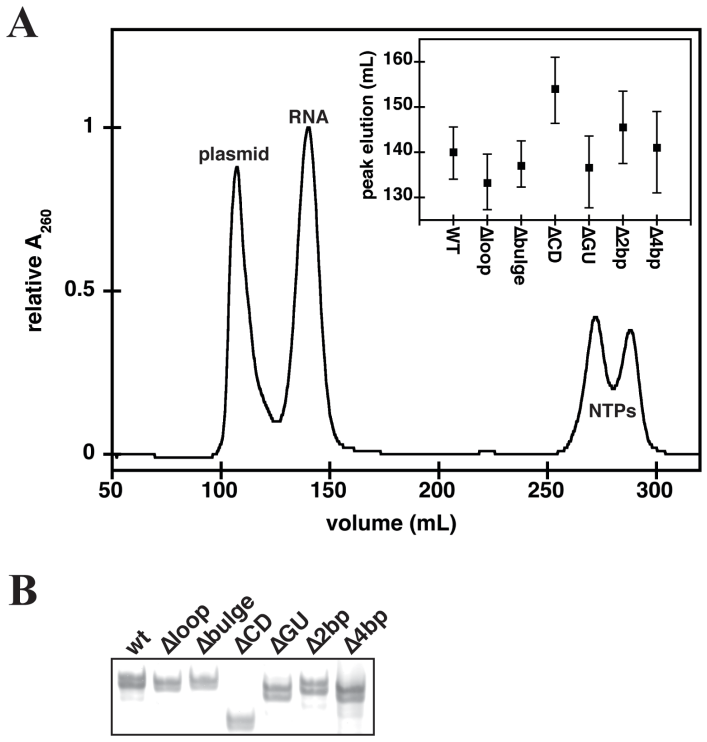

Figure 5.1: Purification of $VA_I\Delta TS$ and its mutant versions by size exclusion chromatography. (A) HiLoad 26/60 Superdex 75 size exclusion chromatography purification of RNA. The elution range for the peak volume of each RNA (insert) (B) Native gel electrophoresis of $VA_I\Delta TS$ and its mutants. 2 µg of each RNA was loaded on 8% native TBE gel. Gels were stained with Toluidin blue for total RNA. Concentration of elution fractions was monitored by in-line spectrophotometric detection at 260 and 280 nm simultaneously.

This method allows separation of template plasmid and small molecule contaminants from the desired RNA. The elution profiles demonstrate good separation and that all RNAs elute in a similar volume range as the wt ($VA_I\Delta TS$), with the notable exception of ΔCD that lacks the CS and is of smaller size. Sample purity of the samples was verified using native gel electrophoresis, where again all RNAs share similar features to wt with the exception of the smaller ΔCD (**Figure 5.1B**).

Dynamic light scattering (DLS) analysis of each sample was performed to ensure sample monodispersity over a range of RNA concentrations (**Figure 5.2**), and was used

to determine the hydrodynamic radius (r_H) for each RNA by extrapolation to infinite dilution (**Table 5.1**).

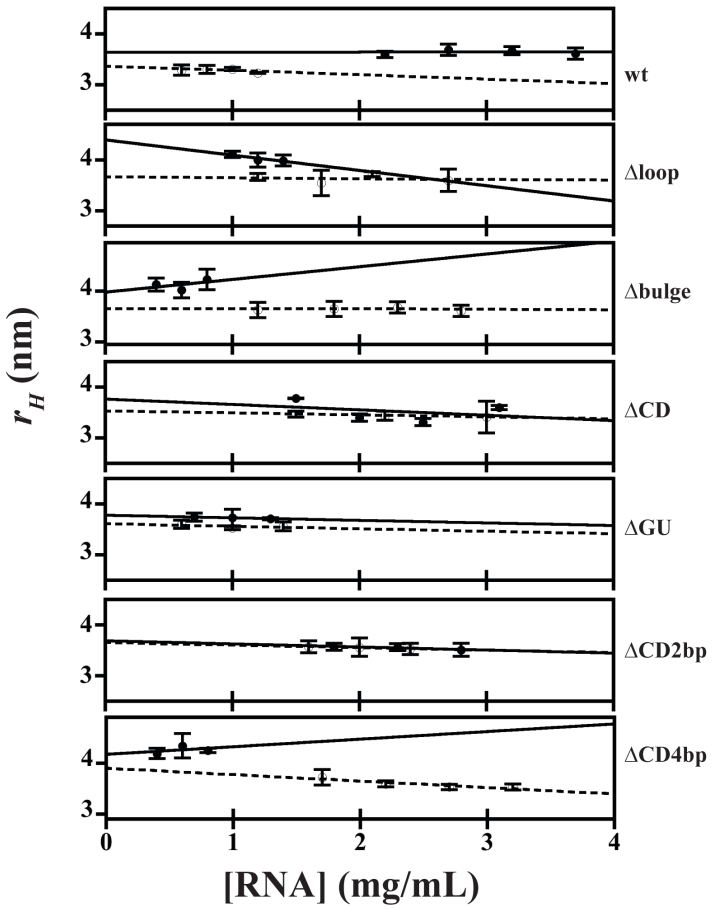

Figure 5.2: Homogeneity of $VA_I\Delta TS$ and its mutant versions. The concentration dependence of the hydrodynamic radius (r_H) was determined by DLS. For comparison purposes, DLS experiments were carried out in Tris-based buffer in presence (solid line) and absence (dashed line) of Mg^{2+}.

Samples displayed no observable change in r_H consistent with self-association over the concentration range examined, suggesting that subsequent solution structure experiments using small-angle x-ray scattering (SAXS) were feasible. Reasonably comparable r_H values for the mutant and wt $VA_I\Delta TS$ suggest absence of any drastic conformational changes of mutated/truncated RNA molecules. Identical experiments were repeated using RNAs prepared in buffer lacking Mg^{2+} (Buffer 2) and some

noticeable differences were observed when compared to samples containing Mg^{2+} (Table 5.1, Fig. 5.2, open circles). For the majority of RNAs, the absence of Mg^{2+} resulted in a minor but significant decrease in r_H values, with the notable exceptions ΔCD, ΔGU and Δ2bp where no change in r_H is observed. Given that Mg^{2+} would be present under physiological conditions, all subsequent studies were performed in its presence.

5.3 Specific central stem mutations affect the solution conformation of VA_IΔTS

To obtain structural insights of the impact of modest mutations on the structure of the CS, we performed SAXS experiments on each of the wt and derivatives in the presence of Mg^{2+}. The scattering profiles of individual concentrations were merged to obtain a single scattering profile (**Figure 5.3A**), from which the $p(r)$ distribution function (distribution of electron pair distances in the sample), maximum particle dimension (D_{max}) and radius of gyration (r_G) were determined using GNOM analysis. The $p(r)$ distribution function of these RNAs show profiles that adopt a skewed bell shape at short radii with an extended tail that is typical of an elongated molecule (**Figure 5.3B**).

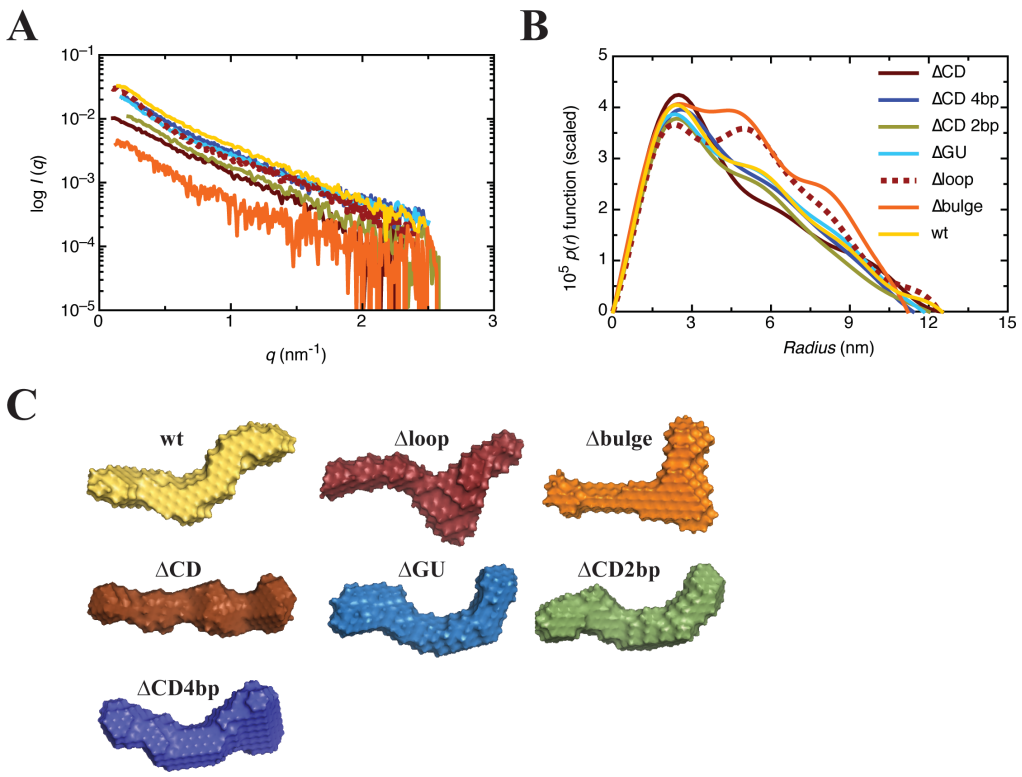

Figure 5.3: Characterization of complexes by SAXS. (A) SAXS scattering profiles for $VA_I\Delta TS$ and its mutant versions. Each data point represents the merged raw data from multiple sample concentrations. (B) Dependence of the pair distribution function upon particle radius for each of the samples outlined in A. (C) Averaged ab initio model of $VA_I\Delta TS$ and its mutants obtained from DAMMIF.

The extended tails observed in the $p(r)$ distribution functions from each RNA have different shapes suggesting structural differences between these RNAs. While the wt and majority of the mutants display little definition in the tail, Δloop and Δbulge present distinctive definition in the tail suggestive of specific subdomain formation that is distinct. The r_G values determined for all RNAs obtained from GNOM analysis were comparable to each other (3.60-3.96 nm), although the largest results were observed for Δloop and Δbulge (**Table 5.1**). D_{max} values determined were also relatively similar amongst the RNAs (11.2-12.5 nm) with Δbulge at the smaller end and wt/ΔCD at the

larger (**Table 5.1**). Taken together, these results were suggestive that introduction of modest mutations, to the loop and bulge in particular, was having a significant impact on VA_I structure.

RNA	Experimental					HYDROPRO		
	R_h (nm)	R_g (nm)	D_{max} (nm)	Chi	NSD	R_h (nm)	R_g (nm)	D_{max} (nm)
ΔCD	3.77 ± 0.40	3.70 ± 0.06	12.5	1	0.58 ± 0.03	3.40 ± 0.04	3.71 ± 0.04	12.6 ± 0.02
ΔCD 4bp	4.27 ± 0.08	3.63 ± 0.03	11.4	0.91	0.77 ± 0.04	3.68 ± 0.02	3.67 ± 0.03	11.5 ± 0.1
ΔCD 2bp	3.68 ± 0.06	3.60 ± 0.04	12.0	0.91	0.72 ± 0.03	3.55 ± 0.03	3.64 ± 0.04	12.1 ± 0.01
ΔGU	3.76 ± 0.01	3.75 ± 0.04	11.8	1	0.80 ± 0.03	3.63 ± 0.03	3.78 ± 0.03	12.1 ± 0.01
Δloop	4.07 ± 0.07	3.96 ± 0.05	12.4	1	0.95 ± 0.08	3.84 ± 0.03	4.00 ± 0.06	13.2 ± 0.12
Δbulge	4.12 ± 0.02	3.87 ± 0.06	11.2	0.92	1.1 ± 0.06	3.84 ± 0.04	3.90 ± 0.05	11.7 ± 0.06
VA_IΔTS	3.64 ± 0.14	3.77 ± 0.05	12.5	1	0.78 ± 0.02	3.57 ± 0.04	3.78 ± 0.06	12.7 ± 0.02
ΔLoop/ PKR_{1-169}	5.30 ± 0.08	4.27 ± 0.10	13.0	1, 1.1, 1	0.80 ± 0.05	4.02 ± 0.10	3.87 ± 0.10	12.5 ± 0.20
TSΔ21/ PKR_{1-169}	3.90 ± 0.28	3.95 ± 0.07	13.2	1, 1.2, 1.1	0.53 ± 0.04	4.23 ± 0.10	3.95 ± 0.02	13.0 ± 0.14

Table 5.1: Comparison of experimental and predicted hydrodynamic parameters

To determine the average solution conformation of VA_IΔTS and mutants, the experimentally determined $p(r)$ plot, r_G and D_{max}, were used as constraints for generating *ab initio* models. Twenty models for each RNA were determined using the program DAMMIF [352]. The calculated χ value for individual models for each RNA was ~1 indicating good agreement between the experimental data and data calculated from *ab initio* models (**Table 5.1**). *Ab initio* models were then rotated, aligned, averaged and filtered using program DAMAVER [368] that provided a normalized spatial discrepancy (NSD) of ~1 suggesting a strong agreement between the individual models. DLS experiments were carried out before (**Figure 5.2**) and after (**data not shown**) the SAXS experiments to ensure sample quality. An elongated solution conformation of wt VA_IΔTS with a modest bend near the midpoint of the structure was observed, and is consistent with a previously determined model [383] (**Figure 5.3C, yellow**). Noticeably, no obvious regions corresponding to the AS and CS are observed. When compared to the wt *ab initio*

model, ΔGU and Δ2bp present a similar overall shape to wt, suggesting that these mutations have no discernable effect on VA_I conformation (**Figure 5.3C, blue and green**). ΔCD while adopts a completely linear extended conformation, consistent with an RNA that lacks the central stem and is almost completely A-RNA conformation along its length (**Figure 5.3C, brown**). Δ4bp adopts a conformation that is slightly less elongated and more globular at one end relative to wt (**Figure 5.3C, purple**) Δloop and Δbulge show a large protuberance in the form of a distinct junction that is not observed in the wt (**Figure 5.3C, crimson and orange**). Δbulge, in particular, displays an enveloped consistent with AS and CS in a perpendicular orientation. Together the data are consistent with VA_IΔTS adopting a compact structure wherein either the AS and CS are aligned in an end-to-end orientation mimicking an elongated A-RNA helix, or the CS is collapsing down and directly interacting with the rest of the RNA.

5.4 Mutations in the central stem-loop of VA_IΔTS do not significantly impair binding affinity to PKR

Previous studies have shown that the CS does not make a high-affinity interaction with any region of PKR, and that the AS of VA_I is solely responsible for the interaction with the PKR [160, 227, 274, 291, 292]. Therefore, we would expect that the CS mutants would interact PKR and with similar affinity as wt. To assess binding stoichiometry and affinity of RNAs to PKR, EMSAs were performed at a single concentration of RNA (100 nM) and protein (500 nM) (**Figure 5.4A**).

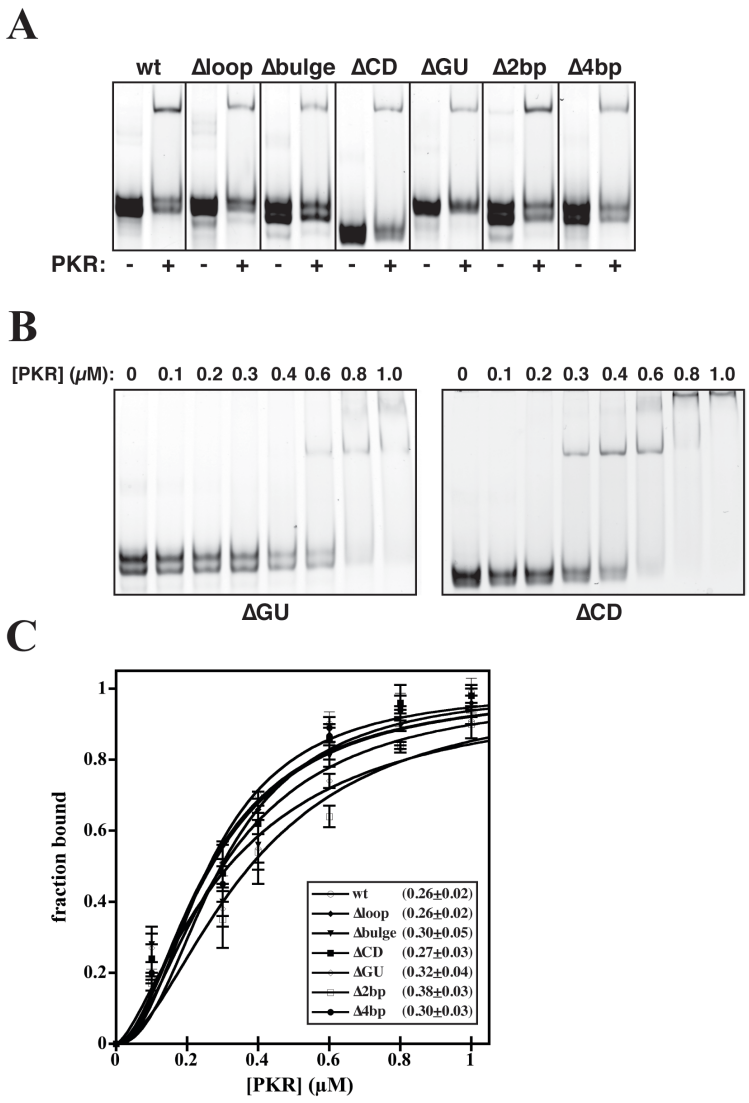

Figure 5.4: EMSA performed to assess binding stoichiometry and affinity of RNAs to PKR. (A) EMSAs performed at a single concentration of RNA (100 nM) and protein (500 nM). (B) EMSA of PKR (0–1000 nM) binding to ΔGU (left) and ΔCD (right) (100 nM) confirming the formation of a single complex. Quantification of free RNA bound to PKR. Curve fitting and calculation of K_D was performed as described in section 2.4.

Under these conditions, all RNAs interact with PKR. To compare the affinity of the mutants to that of $VA_I\Delta TS$, RNAs were incubated with increasing concentrations of PKR and a gradual shift to higher molecular weight species was observed. **Figure 5.4B** shows representative EMSAs for two of the RNAs, ΔCD and ΔGU. Identical experiments

were performed for all of the RNAs, and the fraction bound was plotted against the protein concentration to determine the relative affinity of the RNAs for PKR (**Figure 5.4C**). Within error nearly identical binding curves were observed for each RNA, indicating that the mutations introduced to the CS are not impacting the AS structure.

5.5 Mutations in the CS that disrupt the potential pseudoknot attenuate the inhibition of PKR

Recombinant human PKR activation loop autophosphorylation was assessed by incubation with $VA_I\Delta TS$ and mutants in the presence of ATP/Mg^{2+} with detection of Thr446 phosphorylation using immunoblotting (**Fig. 5.5A**).

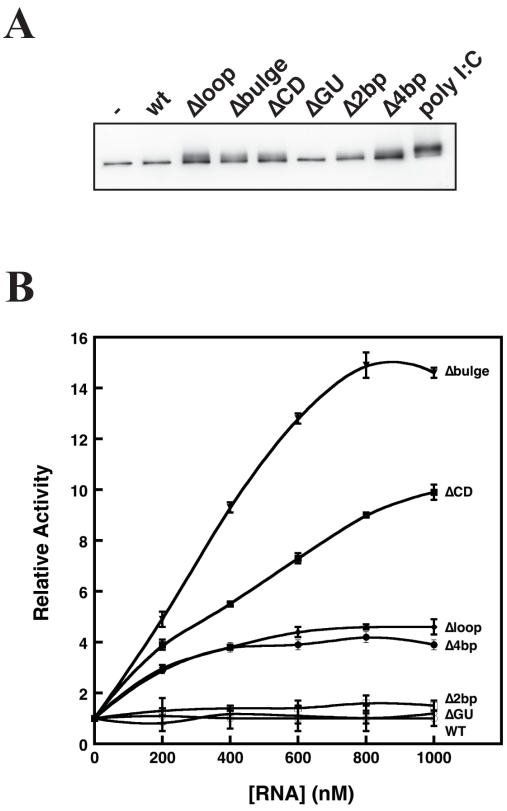

Figure 5.5: Activation of PKR in presence of $VA_I\Delta TS$ (wt) and its mutant versions. (A) PKR (100 nM) and RNAs (500 nM) were incubated for 15 min at 30 °C. PKR autophosphorylation assays were performed, as previously described in section 2.6. The phosphorylation levels of PKR monitored by Anti-PKR Thr446 specific antibodies. (B) Quantification of PKR autophosphorylation in presence of variable

concentrations of RNAs. Quantification of phosphorylated PKR was performed by using Alpha Imager Software.

In the absence of RNA (negative control), basal levels of PKR phosphorylation were observed. In the presence of synthetic dsRNA (poly I:C, positive control), an increase in antibody intensity and a slight change in migration on the gel are observed, both characteristic of PKR autophosphorylation. Consistent with its established role as a PKR inhibitor, $VA_I\Delta TS$ does not lead to PKR activation above negative control levels. ΔGU and Δ2bp, which show similar solution structures to $VA_I\Delta TS$, also do not lead to PKR activation. As expected, ΔCD, which lacks the inhibitory CS, acts as an activator of PKR. Interestingly, mutation to Δloop, Δbulge and Δ4bp also lead to PKR activation *in vitro*, suggesting that these RNAs have lost their inhibitory potential (**Figure 5.5A**). To directly compare the relative activity of these RNAs with respect to PKR, autophosphorylation was measured over a concentration series (**Figure 5.5B**). As expected ΔCD behaves as a potent activator of PKR, but surprisingly Δbulge led to higher autophosphorylation at all concentrations. Δloop and Δ4bp led to similar intermediate activation well above the negative control. $VA_I\Delta TS$, ΔGU, and Δ2bp were within error of the negative control even at high RNA concentrations. To confirm that ΔGU and Δ2bp retained their ability to inhibit PKR (as opposed to not activating), increasing concentrations of these RNAs were pre-incubated with PKR and then challenged with a potent dsRNA activator, poly I:C (**Figure 5.6A,B**). As expected, $VA_I\Delta TS$ increasingly inhibits PKR at higher concentrations, as do ΔGU and Δ2bp to a similar extent.

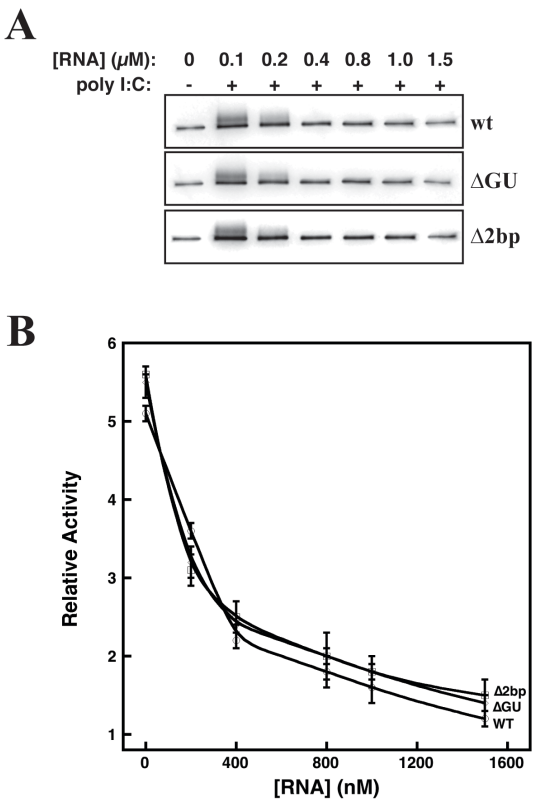

Figure 5.6: Inhibition of PKR by $VA_I\Delta TS$ (wt), ΔGU, and Δ2bp. (A) PKR (100 nM) and variable concentrations of RNAs were preincubated for 10 min at room temperature, followed by addition of 10 µg/ml polyI:C. Reaction mixture was incubated for further 15 min at 30 °C. PKR autophosphorylation assays were performed, as previously described in section 2.6. (B) Quantification of PKR autophosphorylation in presence of inhibitors. Quantification was performed as described in section 2.6. The percent inhibition was calculated relative to a sample containing no inhibitory RNA.

Together, the activation and inhibition assays clearly highlight that although all RNAs examined bind PKR with similar affinity, inhibition of PKR by $VA_I\Delta TS$ depends upon a specific structural conformation of the CS, in particular the bulge at the base of the CS, and to a lesser extent the loop composition and stem length.

5.6 Solution conformations of the dsRBMs of PKR in complex with $VA_I\Delta TS$ and Δloop adopt subtly different conformations

It has been suggested that structure of $VA_I\Delta TS$ is stabilized by pseudoknot formation between the loop of CS and a single stranded region adjacent to the CS, and that the interaction between $VA_I\Delta TS$ and PKR is modulated by the Mg^{2+} ions [386, 388]. In Chapter 4 we have shown an *ab initio* SAXS model for the $VA_I\Delta TS$-PKR_{1-169} complex in the absence of Mg^{2+} where PKR_{1-169} (dsRBMs alone) and $VA_I\Delta TS$ interact in a side-by-side orientation that involves entire PKR_{1-169} . The calculated hydrodynamic properties for this complex showed that the complex is slightly smaller than that of the RNA alone, suggesting a probable minor conformational change in the RNA. We extended our studies on $VA_I\Delta TS$-PKR_{1-169} complex in the presence of 5 mM $MgCl_2$ (Buffer 1) in order to examine the effect of Mg^{2+} ions on overall structure and stability of the $VA_I\Delta TS$-PKR_{1-169} complex. The pair distribution function in the presence of Mg^{2+} is very similar to that previously determined in the absence of Mg^{2+} (**Figure 5.7A,B**).

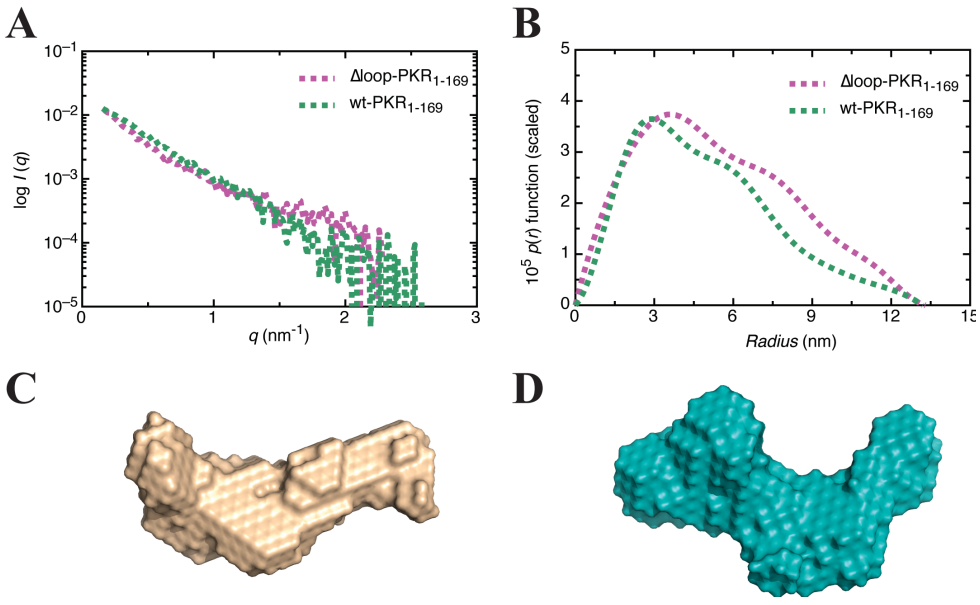

Figure 5.7: Characterization of complexes by SAXS. (A) SAXS scattering profiles for wt-PKR_{1-169}, and Δloop-PKR_{1-169} complexes. Each data point represents the merged raw data from multiple sample concentrations. (B) The pair distribution function analysis of wt-PKR_{1-169}, and Δloop-PKR_{1-169} complexes. (C) A filtered model of wt-PKR_{1-169} complex. (D) A filtered model of Δloop-PKR_{1-169} complex

obtained form *ab initio* calculations indicating overall shape of the complex in solution.

The MONSA derived ab *initio* model shows a one-to-one complex where $VA_I\Delta TS$ and PKR_{1-169} interact in a side-by-side orientation with both dsRBMs and the linker of PKR_{1-169} being involved in the interaction (**Figure 5.7C**). The calculated χ values show good agreement between the experimental and model derived hydrodynamic parameters, and NSD values show excellent agreement indicating that the individual models are in good agreement with each other (**Table 5.1**). Computational models of the complex reinforce that the entire length of the RNA molecule, including pseudoknot, are mediating the interaction with the dsRBMs of PKR (**Figure 5.7C**).

Our SAXS and activation data show that a mutation in the loop of the CS has a significant impact on the overall conformation and function of $VA_I\Delta TS$. To examine the structural importance of the CS loop in pseudoknot formation and PKR interaction, we conducted SAXS experiments on purified Δloop-PKR_{1-169} complex in the presence of Mg^{2+} (**Figure 5.7A**). While exhibiting similar D_{max} values, the pair distribution function of Δloop-PKR_{1-169} complex has distinct differences when compared to that obtained for $VA_I\Delta TS$-PKR_{1-169}, reflected in an r_G for Δloop-PKR_{1-169} being slightly larger than the $VA_I\Delta TS$-PKR_{1-169} + Mg^{2+} complex (**Figure 5.7B, Table 5.1**). The *ab initio* model of Δloop-PKR_{1-169} complex generated by MONSA shows an extended structure in solution as suggested by the bell-shaped distribution function with a long tail (**Figure 5.7D**). The *ab initio* model obtained by MONSA show that overall structure of Δloop-PKR_{1-169} + Mg^{2+} complex is different from the $VA_I\Delta TS$-PKR_{1-169} + Mg^{2+} complex.

5.7 Discussion

The antiviral properties of PKR are well established [142, 225, 234, 290]. Viruses

have evolved various strategies to circumvent host immunity. In the case of PKR, viruses produce small non-coding dsRNAs, including VA_I, that interact with PKR and prevent its self-association, thereby inhibiting its antiviral effects. The structural mechanism of inhibition of PKR by $VA_I\Delta TS$ is not fully understood; however, previous *in vitro* studies have highlighted the importance of the CS of VA_I in the inhibition of PKR self-association [160, 234, 235, 290-292]. Recent studies have suggested that a pseudoknot forming between the CS and a single-stranded region (nucleotides 123-127, **Figure 1.7**) plays an important role in stabilizing the overall VA_I structure and may be functionally required for inhibition [386, 388]. Isothermal calorimetry, NMR and RNA footprinting studies previously suggested that the CS of $VA_I\Delta TS$ does not make a direct high affinity interaction with any region of PKR [160, 274, 291, 292]. Therefore, while it is clear that the CS is required to sequester PKR in a 1:1 complex incapable of trans-autophosphorylation, it is unclear whether this is due to the CS imposing a steric block to PKR dimerization, or the CS being crucial to proper folding at the three-way junction of the AS, CS, and TS so that inhibitory complex formation with PKR occurs. We therefore studied $VA_I\Delta TS$ and CS mutants to understand the mechanism of PKR inhibition. Binding affinity of these RNAs for PKR were all within error of each other and consistent with previously published data [160, 387, 389]. Therefore, the structural and activity differences observed for different $VA_I\Delta TS$ mutants cannot be accounted for by a simple increase or decrease in affinity.

Overall, the SAXS models of $VA_I\Delta TS$ and mutants, when considered in conjunction with the previously determined computational tertiary structures of $VA_I\Delta TS$ and $VA_I\Delta TS$-PKR_{1-169} complex strongly suggest the formation of a pseudoknot requiring

specific structural features of the CS. Instead of observing the predicted perpendicular orientation of the CS and AS based on secondary structural information, $VA_I\Delta TS$ adopts an extended conformation in solution suggesting that the AS and CS form a more compact structure (**Figure 5.3C**). Although the Δ4bp, Δloop and Δbulge mutants contain minor changes in the wt structure, their low-resolution models present a clear conformational difference when compared to $VA_I\Delta TS$ (**Figure 5.3**). We observe a clear conformational change in overall shape of Δloop, where a hexaloop is replaced with a UUCG tetraloop, suggesting that the loop sequence is important for the overall $VA_I\Delta TS$ fold. While converting the CS bulge to a perfectly double stranded stem (Δbulge) was expected to introduce a more rigid conformation, a large protuberance in the three-way junction region of this mutant was observed suggesting disruption of an important tertiary interaction. Interestingly, mutation of a GU bp to the more conformationally restricted GC bp in the CS had no such structural impact. Activation assays reinforce that mutations that disrupt the compact $VA_I\Delta TS$ fold behave as activators, and not inhibitors, of PKR (**Figure 5.5**). Complete truncation of the CS (ΔCD), in fact shows substantially higher phosphorylation levels than $VA_I\Delta TS$. Disruption of the compact pseudoknot structure with Δloop and Δbulge results the loss of PKR inhibition despite increasing the potential for steric prevention of PKR autophosphorylation, arguing that a specific $VA_I\Delta TS$ conformation, as opposed to steric features of VA_I, is responsible for inhibition of PKR. In addition to the loop composition and presence of the bulge for RNA function, the length of the stem has also been shown to be crucial for PKR inhibition, [291], and while deletion of 2 bp in the stem has no impact on structure or inhibition of PKR, the more aggressive deletion of 4 bp impacts the structure and inhibition to a significant degree.

We propose that these mutants are able to activate PKR instead of inhibiting PKR due to the loss of structural integrity of the central stem.

It has been reported that Mg^{2+} ions are required for tertiary stability of VA_I, and that PKR-VA_IΔTS complex formation is enhanced in the presence of Mg^{2+} ions [386, 388]. The solution conformation of VA_IΔTS in the presence of Mg^{2+} does not show any significant conformational change relative to the previously determined SAXS structure of VA_IΔTS in the absence of Mg^{2+} (**Figure 4.3A**), although in the presence of Mg^{2+} a slightly larger D_{max} is observed for the dsRBD-RNA complex. When comparing VA_IΔTS + Mg^{2+} *ab initio* model to VA_IΔTS + Mg^{2+} solution model determined by Launer-Felty et al. [388], both models show extended structure in solution. However, the overall shape of two RNAs is remarkably with model presented here showing a well-defined apical and central domain.

Since no significant change was observed in overall conformation of VA_IΔTS + Mg^{2+} when compared to the previously determined structure of VA_IΔTS [383], we investigated the VA_IΔTS-$PKR_{1\text{-}169}$ + Mg^{2+} complex and compared it to the previously determined VA_IΔTS-$PKR_{1\text{-}169}$ complex (**Figure 4.3B**), to examine if the complexes differ in the presence and absence of Mg^{2+}. SAXS data analysis suggests that the complex of wt-$PKR_{1\text{-}169}$ + Mg^{2+} adopts an extended conformation with side-by-side interaction of RNA and protein where $PKR_{1\text{-}169}$ follows the entire length of an apical stem of RNA (**Figure 5.7**).

Due to the facts that (*i*) Δloop has very distinguishable solution conformation compared to the rest of the mutants (**Figure 5.3**), (*ii*) it acts as an activator of PKR (**Figure 5.5**) and (*iii*) it is involved in pseudoknot formation, we also investigated Δloop-

PKR_{1-169} complex in the presence of Mg^{2+} to study how dsRBMs recognize Δloop. The *ab initio* model of Δloop-PKR_{1-169} + Mg^{2+} complex displays an extended and curved conformation compared to that of wt-PKR_{1-169} + Mg^{2+} (**Figure 5.7D**). Since the interaction between Δloop and PKR_{1-169} involves interaction between different regions of RNA and the protein, it possibly points towards the formation of a pseudoknot in the context of the RNA-protein complex.

Taken together, it can be argued that Mg^{2+} ions do not have a significant impact on overall structure of the VA_IΔTS-PKR_{1-169} complex. The individual structure of Δloop together with that one of the Δloop-PKR_{1-169} complex in support by the activation assays confirm that the loop of the central stem is crucial for the structural integrity and the function of VA_IΔTS. Central stem loop of VA_IΔTS is a dynamic structure that is very important for overall structural integrity of RNA and its function in the context of viral survival within the hosts cell. Overall our data presented here show that in addition to previously proposed role of the central stem-loop of VA_IΔTS in PKR inhibition, the length of the central domain structure as well as its nucleotide composition are very important for the stability and the function of VA_IΔTS as an inhibitor of PKR.

CHAPTER 6: CONCLUSIONS AND FUTURE DIRECTIONS

6.1 Conclusions

PKR, a product of an ISG, is a key protein in the innate immune system involved in the initial response to pathogens [142]. PKR binds to viral double-stranded RNA (dsRNA), and after initial binding PKR self-associates and then it becomes autophosphorylated. In turn, PKR phosphorylates its substrate eukaryotic initiation factor 2α, which slows the translation of viral proteins. In addition to PKR's role in innate immunity, PKR is shown to be involved in cell-signaling pathways, such as signal transduction, differentiation and apoptosis [151]. Latent PKR interacts directly with dsRNA from replication by-products, mRNA transcripts, or the viral genome itself [232]. In addition to viral dsRNA, PKR can be activated by heparin, dextran sulfate, chondroitin sulfate, and poly-L-glutamine [390]. PKR interacts with its binding partners through tandem double-stranded RNA-binding motif (dsRBM). The recognition of dsRNA by dsRBMs is mainly mediated through consecutive minor-major-minor grooves of the RNA helix, and approximately 1.5 turns (~15 bp) of the A-form RNA helix is required for the interaction with single dsRBM [169, 170, 180-183]. Both dsRBMs of PKR are required for the high affinity interaction with dsRNA [160]. In addition to a minimum length requirement, specific structural (bulges, loops, *etc.*) and nucleotide modifications (*i.e.* 5'-phosphorylation state) have been observed to be accommodated by PKR, and in some cases significantly affect both the affinity for and activation of PKR [226-231]. Regulation of PKR activity by RNA secondary structure is best observed in PKR's interaction with two imperfectly base-paired viral dsRNAs: HIV-1 transactivation response (TAR) element, and adenovirus VA (viral associated) RNA I (VA_I).

HIV-1 TAR is viral dsRNA activator of PKR [233]. TAR adopts a 23 bp RNA stem-loop structure with distortions including a trinucleotide bulge and hexaloop [239, 240]. HIV-infected cells treated with interferon demonstrate a decreased production of HIV proteins as well as HIV particles due to the activity of PKR [249]. A study has suggested that a dimeric form of TAR activates PKR [254]. However, the biological basis for TAR dimerization remains a topic for debate. Adenovirus VA_I is a non-coding RNA implicated in viral growth. VA_I dsRNA consists of three major short imperfectly base-paired stem-loop regions with different functions; an apical stem-loop (dsRBM-binding stem); the central stem-loop domain that is responsible for PKR inhibition; and a terminal stem structure that contains important transcription signals but is entirely dispensable or the PKR kinase inhibition activity of VA_I [321, 323, 324]. PKR has been identified as one of the key enzymes responsible for an overall decrease in protein synthesis in host cells in the absence of VA_I RNA [234, 290]. VA_I binds to PKR *via* its apical stem with similar affinity as TAR and other activators, but prevents PKR self-association and autophosphorylation through its central stem-loop thus prolonging the viral infection in the host [160, 234, 235, 290-292, 322, 379]. It has been suggested that VA_I structure is stabilized by Mg^{2+} ions [387, 391], and that central stem-loop is stabilized by pseudoknot [384, 386, 388], which could potentially be important for its function. VA_I lacking its terminal stem ($VA_I\Delta TS$) is the shortest version of VA_I sufficient to bind to PKR with full affinity and mediate its inhibition *in vitro* [184, 274, 291, 332]. The apical stem of VA_I (VA_I-AS) alone binds PKR_{1-169} with high affinity and it contains the ability to stimulate autophosphorylation and kinase activity of PKR *in vitro* [160].

The work presented in this thesis focused on understanding how the interaction between PKR and imperfectly basepaired viral dsRNA ligands regulates the enzymatic activity of PKR. Together, the results also present an experimental approach to combine hydrodynamic measurements, SAXS, and computational structural predictions to study protein–RNA interactions. This work has recently been recognized in a review articles by one of the leading experts in biological SAXS [392].

In order to understand the interaction between PKR and short imperfectly basepaired viral dsRNA, I sought to investigate how each dsRBM orients and interacts with TAR and VA_I to provide a plausible framework for the recognition of RNA substrate by the tandem dsRBMs (PKR_{1-169}). In addition, I studied the structural features of $VA_I\Delta TS$ that enable recognition and inhibition of PKR self-association. Both TAR and VA_I form a high-affinity interaction with PKR. Using small-angle X-ray scattering analysis, I have shown for the first time a structure of tandem dsRBMs in complex with imperfectly base paired viral dsRNAs. *Ab initio* models of TAR-PKR_{1-169} and $VA_I\Delta TS$-PKR_{1-169} complexes determined by SAXS highlights the role of linker between dsRBMs in PKR_{1-169}, as well as of bulges and loops in viral dsRNAs for recognition of imperfectly duplexed RNA. I have shown, in agreement with previous studies, that central stem-loop of VA_I has no binding affinity for PKR, yet tertiary organization of three-way junction and central stem-loop of RNA is crucial for structural integrity and its function in PKR's inhibition. SAXS studies on $VA_I\Delta TS$ and $VA_I\Delta TS$-PKR_{1-169} complex in the presence and absence of Mg^{2+} demonstrated that Mg^{2+} ions do not have significant impact on overall shape of RNA and complex. Finally, SAXS experiments together with activation assays

in the context of the RNA-protein complex points towards possible formation of a pseudoknot, which is thought to be important for stability of the RNA and its function.

The averaged solution conformation of PKR_{1-169}, RNAs and their complexes show an extended shape in solution. PKR_{1-169} adopts an extended structure that appears to orient the individual dsRBMs at opposite ends joined by the interdomain linker. The averaged solution conformation of TAR, VA_I-AS, and $VA_I\Delta TS$ presents an extended shape. TAR and VA_I-AS *ab initio* solution conformations have a slight curvature to their structure with VA_I-AS model showing a more pronounced definition in terms of three distinct bulges. The models for both RNAs lack significant definition in terms of distinct structural features such as the loop or internal bulge. The *ab initio* model of $VA_I\Delta TS$ shows two distinct elongated domains coinciding with apical and central stem-loops consistent with the previously predicted secondary structure. In addition to the solution conformation of $VA_I\Delta TS$, to further visualize the conformations of $VA_I\Delta TS$ RNA, a set of tertiary structure computational models were obtained using the SimRNA program through work with our collaborators. An extended conformation was observed with clearly defined apical and central stems oriented roughly perpendicular to each other. The overall size of the computer-derived model is in good agreement with the overall dimensions of the SAXS *ab initio* model.

The solution conformation of TAR-PKR_{1-169} and VA_I-AS-PKR_{1-169} complexes show a similar solution conformation with overall extended disc-shaped topology. The RNA-protein interface curves along the length of the extended complex structure, with both dsRBMs and the linker region between them are required for the interaction with the RNA. Both the loop and stem region of each RNA are involved in the interaction. In

complex, TAR adopts a significantly more defined conformation as the RNA stem loop is clearly visualized upon complex formation with PKR_{1-169}. The loop region of the VA_I-AS RNA was not pronounced, and no significant conformation change is observed in the RNA molecule upon binding to PKR_{1-169}. *Ab initio* models calculated for the $VA_I\Delta TS$-PKR_{1-169} complex show that PKR_{1-169} and $VA_I\Delta TS$ interact in a side-by-side orientation that involves entire PKR_{1-169} molecule. $VA_I\Delta TS$ undergoes a slight conformational change upon its interaction with PKR_{1-169}. dsRBMs track the length of the apical stem but do not interact extensively with the central stem of VA_I. *In silico* model of $VA_I\Delta TS$-PKR_{1-169} structure supports that both dsRBMs mediate the interaction with the apical stem while making no significant contacts with the central stem. dsRBM1 is interacting with the loop end of the apical stem, whereas dsRBM2 contacts the apical stem at is base near the junction with the central stem.

The complex between PKR_{1-169} and two activator RNAs (TAR and VA_I-AS) show how tandem dsRBMs are capable of tolerating a wide range of sequence and structural motifs (bulges and loops). In addition, positioning of dsRBMs along the length of RNA allows for the argument that two PKR molecules could be potentially accommodated on a single small RNA substrate thus enabling the self-association of PKR. In similar fashion, the orientation of dsRBMs in complex with $VA_I\Delta TS$ positions the central stem of the RNA in close proximity to the interdomain linker and kinase domain which implicates the role of central stem in the inhibition.

Isothermal calorimetry, NMR studies and RNA footprinting have demonstrated that the central stem of $VA_I\Delta TS$ does not make a high affinity interaction with any region of PKR [160, 274, 291, 292]. Based on these findings, the initial working hypothesis was

that the central inhibitory stem-loop domain of $VA_I\Delta TS$ primarily prevents PKR's self-association by serving as steric block preventing two PKR monomers from self-associating. The central stem of $VA_I\Delta TS$ has a complex tertiary structure that contains a flexible loop, a bulge at the base of the stem and a non-canonical base pair. Several studies propose that a pseudoknot plays an important role in stabilizing central stem-loop structure [386, 388]. In addition, the interaction between PKR and $VA_I\Delta TS$ is enhanced in presence of Mg^{2+} ions [386, 388]. To characterize the key structural features to overall tertiary organization and subsequently function of central stem, I have designed truncated versions of $VA_I\Delta TS$ with mutations in central stem-loop.

The *ab initio* models of mutants in the presence of Mg^{2+} ions suggested that they adopt an extended conformation in solution with two extended domains possibly representing apical and central stem-loops, which is consistent with the previously determined structure of $VA_I\Delta TS$. Solution conformations of ΔCD, Δloop and Δbulge mutants show the difference in shape compared to the wt as well as to the rest of the mutants. SAXS models of Δloop and Δbulge demonstrate a large protuberance in the three-way junction region of these mutants that could possibly affect the stability of the central stem. When compared to the previously determined low-resolution structure of $VA_I\Delta TS$, $VA_I\Delta TS + Mg^{2+}$ does not show any significant conformational change in the structure. Activation assays show that mutants lacking central stem (ΔCD), or mutants with large protuberance in the central stem-loop (Δloop and Δbulge) behave as activators of PKR. Similar to the wt, ΔCD2bp and ΔGU mutants did not activate PKR.

A solution structure of $VA_I\Delta TS\text{-}PKR_{1\text{-}169}$ + Mg^{2+} complex was investigated in order to examine the effect of Mg^{2+} on complex formation. SAXS data analysis suggests that the complex of wt-$PKR_{1\text{-}169}$ + Mg^{2+} adopts an extended conformation with side-by-side interaction of RNA and protein where $PKR_{1\text{-}169}$ follows the entire length of an apical stem of RNA. Since the implication of the pseudoknot formation involves the loop of central stem, in addition to obtaining the solution structure of Δloop, an attempt has been made to resolve the solution conformation of Δloop-$PKR_{1\text{-}169}$ complex. The *ab initio* model of Δloop-$PKR_{1\text{-}169}$ + Mg^{2+} complex displays an extended and curved conformation compared to that of wt-$PKR_{1\text{-}169}$ + Mg^{2+}. The DAMAVER processed averaged model of the complex obtained from multiple *ab initio* models suggests Δloop and $PKR_{1\text{-}169}$ complex involves interaction between different regions of RNA and the protein, and it possibly points towards the formation of a pseudoknot in the context of the RNA-protein complex.

Altogether, the low-resolution SAXS models of $VA_I\Delta TS$ suggest that Mg^{2+} ions do not have a significant impact on overall shape of $VA_I\Delta TS\text{-}PKR_{1\text{-}169}$ complex. The individual structures of Δloop together with the Δloop-$PKR_{1\text{-}169}$ complex confirm that the loop of the central stem is crucial for the structural integrity and the function of $VA_I\Delta TS$.

6.2 Future Directions

Innate immunity employs a myriad of PRRs produced through the INF cascade that can recognize conserved structures associated with pathogens called PAMPs [8]. PAMPs include a wide range of molecules such as RNA, lipopolysaccharides, lipoteichoic acid, and peptidoglycans among others [1]. PKR, a key component of innate immunity is an INF-induced PRR that recognizes viral dsRNA. PKR's function is

regulated by tertiary structure of dsRNA that can potentially activate or inhibit PKR. PKR is mostly activated by long stretches of dsRNA while inhibition requires a complex tertiary structure of RNA that contains a PKR binding region and the inhibitory region [151, 160, 234, 235, 258, 290-292].

Ever since PKR has been first observed [393] there has been increased knowledge on PKR-dsRNA interaction. As of now, no high-resolution structure of full length PKR, or the dsRBMs of PKR in complex with either synthetic or natural substrates exists due to the flexible nature and size of both PKR and its dsRNA partners. SAXS is a powerful technique for studying interactions between proteins and their ligands such as dsRNA in solution. SAXS can be used for analyzing protein-ligand complexes, their association states, and their structural characterization in a dynamic equilibrium. Recent advances in SAXS instrumentation and data analysis methods that have become available allowed for analyzing protein-ligand complexes their association states and their structural characterization in a dynamic equilibrium. My work on PKR_{1-169}-TAR complex highlights the effectiveness of small-angle X-ray scattering approaches for systems with highly flexible components. PKR_{1-169}-TAR complex as determined by the software program MONSA demonstrated how upon interaction of two flexible systems (TAR and PKR_{1-169}) a more rigid conformation is adopted. Additionally, modeling with MONSA allowed the ability to visualize both the stem and loop portions of TAR RNA. This was followed by investigation of more complex systems such as adenovirus VA_I RNA and its truncated versions in complex with PKR_{1-169} to elucidate the mechanism of inhibition of PKR by complex tertiary dsRNA structure.

However, the question regarding how initial binding of RNA results in bringing about or preventing of kinase domain self-association still remains to be resolved. Obtaining the structure of full length PKR in complex with a dsRNA substrate would contribute immensely towards understanding the mechanism of PKR self-association. The initial idea was that $VA_I\Delta TS$ would limit PKR's flexibility once bound to each other and this would potentially enable solving complex structure by either a low-resolution or high-resolution methods. However, SAXS modeling of $VA_I\Delta TS$-PKR complex [383] was unsuccessful due to the concentration-dependent increase in r_G and D_{max} values. This could possibly be resolved by finding a more suitable dsRNA substrate and again try a SAXS based or crystallography based approach, or forming the complex at lower concentration. Collection of the data for the low concentration samples is readily performed at a synchrotron source.

As previously stated, a great deal of information has been obtained on PKR's interaction with synthetic and viral dsRNA. Future studies should also involve finding additional cellular RNA ligands of PKR. Several cellular RNA partners of PKR have been reported [238, 394], but the downstream pathways that could possibly be affected due to this interaction are yet to be investigated. In addition, it would be interesting to identify where PKR and its dsRNA substrates are co-localized within the cell, and whether these interactions lead to PKR activation. Specific monoclonal antibodies and confocal microscopy can be implemented to determine the localization of PKR and dsRNAs. PKR phosphorylation state can be determined by specific PKR phospho Thr446 or Thr451 monoclonal antibodies.

The main cellular protein target of PKR is eIF2α [164, 168, 395]; however, it is well established that PKR interacts with a broad spectrum of molecules implicated in myriads of pathways involved in cell growth, cell differentiation, and apoptosis. Some protein targets of PKR have been discussed in Chapter 1. It would be of great interest to characterize additional PKR targets in non-infected cells and whether this requires the kinase function or indicates a role of PKR as an adaptor protein. Several methods including co-immunoprecipitation and mass spectrometry could be implemented to identify cellular targets of PKR. As more PKR targets are discovered, the next question would be how many pathways is PKR involved in under different conditions. Identification of new pathways that PKR is involved can be investigated by microarray analysis by the host response to a given stimulus.

The emergence of new tools and approaches to study PKR's involvement in different signaling pathways will provide further insights into the mode of PKR action, as well as its potential utility as an antiviral and antitumor effector molecule. Overall, PKR is a crucial component of the host defense mechanism against viruses. PKR's role in innate immunity is regulated through tertiary structure of dsRNA that can affect the outcome of viral propagation. The dynamic nature of PKR's structure allows it to interact with viral and many cellular molecules that ultimately affects the function of target molecules and downstream components of their pathways.

REFERENCE:

1. Akira, S., Uematsu, S. and Takeuchi, O. (2006) Pathogen recognition and innate immunity. Cell. **124**, 783-801.

2. Jensen, S. and Thomsen, A. R. (2012) Sensing of RNA viruses: a review of innate immune receptors involved in recognizing RNA virus invasion. J Virol. **86**, 2900-2910.

3. Kasakura, S. (1998) [A role for T-helper type 1 and type 2 cytokines in the pathogenesis of various human diseases]. Rinsho Byori. **46**, 915-921.

4. Kasahara, M. and Sutoh, Y. (2014) Two forms of adaptive immunity in vertebrates: similarities and differences. Adv Immunol. **122**, 59-90.

5. Charles A Janeway, J., Paul Travers, Mark Walport, and Mark J Shlomchik. (2001) Immunobiology. Garland Science, New York. **5th edition**

6. Abbas AK, L. A., Pillai S. (2010) Cellular and Molecular Immunology. Elseviere. **6th edition**

7. Short, J. A. L. (2009) Viral evasion of interferon stimulated genes. Bioscience Horizons. **2**

8. Randall, R. E. and Goodbourn, S. (2008) Interferons and viruses: an interplay between induction, signalling, antiviral responses and virus countermeasures. J Gen Virol. **89**, 1-47.

9. Kumar, H., Kawai, T. and Akira, S. (2011) Pathogen recognition by the innate immune system. Int Rev Immunol. **30**, 16-34.

10. Kumar, H., Kawai, T. and Akira, S. (2009) Pathogen recognition in the innate immune response. Biochem J. **420**, 1-16.

11. Akira, S., Takeda, K. and Kaisho, T. (2001) Toll-like receptors: critical proteins linking innate and acquired immunity. Nat Immunol. **2**, 675-680.

12. Collins, S. E. and Mossman, K. L. (2014) Danger, diversity and priming in innate antiviral immunity. Cytokine Growth Factor Rev. **25**, 525-531.

13. Rassa, J. C., Meyers, J. L., Zhang, Y., Kudaravalli, R. and Ross, S. R. (2002) Murine retroviruses activate B cells via interaction with toll-like receptor 4. Proc Natl Acad Sci U S A. **99**, 2281-2286.

14. Takeda, K. and Akira, S. (2001) Regulation of innate immune responses by Toll-like receptors. Jpn J Infect Dis. **54**, 209-219.

15. Goodbourn, S., Didcock, L. and Randall, R. E. (2000) Interferons: cell signalling, immune modulation, antiviral response and virus countermeasures. J Gen Virol. **81**, 2341-2364.

16. Bieback, K., Lien, E., Klagge, I. M., Avota, E., Schneider-Schaulies, J., Duprex, W. P., Wagner, H., Kirschning, C. J., Ter Meulen, V. and Schneider-Schaulies, S. (2002) Hemagglutinin protein of wild-type measles virus activates toll-like receptor 2 signaling. J Virol. **76**, 8729-8736.

17. Gack, M. U. (2014) Mechanisms of RIG-I-like receptor activation and manipulation by viral pathogens. J Virol. **88**, 5213-5216.

18. Dixit, E. and Kagan, J. C. (2013) Intracellular pathogen detection by RIG-I-like receptors. Adv Immunol. **117**, 99-125.

19. Kawai, T. and Akira, S. (2008) Toll-like receptor and RIG-I-like receptor signaling. Ann N Y Acad Sci. **1143**, 1-20.

20. Lester, S. N. and Li, K. (2014) Toll-like receptors in antiviral innate immunity. J Mol Biol. **426**, 1246-1264.

21. Borden, E. C., Sen, G. C., Uze, G., Silverman, R. H., Ransohoff, R. M., Foster, G. R. and Stark, G. R. (2007) Interferons at age 50: past, current and future impact on biomedicine. Nat Rev Drug Discov. **6**, 975-990.

22. Levraud, J. P., Boudinot, P., Colin, I., Benmansour, A., Peyrieras, N., Herbomel, P. and Lutfalla, G. (2007) Identification of the zebrafish IFN receptor: implications for the origin of the vertebrate IFN system. J Immunol. **178**, 4385-4394.

23. O'Connell, R. M., Saha, S. K., Vaidya, S. A., Bruhn, K. W., Miranda, G. A., Zarnegar, B., Perry, A. K., Nguyen, B. O., Lane, T. F., Taniguchi, T., Miller, J. F. and Cheng, G. (2004) Type I interferon production enhances susceptibility to Listeria monocytogenes infection. J Exp Med. **200**, 437-445.

24. Muller, U., Steinhoff, U., Reis, L. F., Hemmi, S., Pavlovic, J., Zinkernagel, R. M. and Aguet, M. (1994) Functional role of type I and type II interferons in antiviral defense. Science. **264**, 1918-1921.

25. Kadowaki, N., Antonenko, S., Lau, J. Y. and Liu, Y. J. (2000) Natural interferon alpha/beta-producing cells link innate and adaptive immunity. J Exp Med. **192**, 219-226.

26. Le Bon, A. and Tough, D. F. (2002) Links between innate and adaptive immunity via type I interferon. Curr Opin Immunol. **14**, 432-436.

27. Stetson, D. B. and Medzhitov, R. (2006) Type I interferons in host defense. Immunity. **25**, 373-381.

28. Goubau, D., Deddouche, S. and Reis e Sousa, C. (2013) Cytosolic sensing of viruses. Immunity. **38**, 855-869.

29. Satoh, T., Kato, H., Kumagai, Y., Yoneyama, M., Sato, S., Matsushita, K., Tsujimura, T., Fujita, T., Akira, S. and Takeuchi, O. (2010) LGP2 is a positive regulator of RIG-I- and MDA5-mediated antiviral responses. Proc Natl Acad Sci U S A. **107**, 1512-1517.

30. Fitzgerald, M. E., Rawling, D. C., Vela, A. and Pyle, A. M. (2014) An evolving arsenal: viral RNA detection by RIG-I-like receptors. Curr Opin Microbiol. **20**, 76-81.

31. Yoneyama, M., Kikuchi, M., Matsumoto, K., Imaizumi, T., Miyagishi, M., Taira, K., Foy, E., Loo, Y. M., Gale, M., Jr., Akira, S., Yonehara, S., Kato, A. and Fujita, T. (2005) Shared and unique functions of the DExD/H-box helicases RIG-I, MDA5, and LGP2 in antiviral innate immunity. J Immunol. **175**, 2851-2858.

32. Yoneyama, M., Kikuchi, M., Natsukawa, T., Shinobu, N., Imaizumi, T., Miyagishi, M., Taira, K., Akira, S. and Fujita, T. (2004) The RNA helicase RIG-I has an essential function in double-stranded RNA-induced innate antiviral responses. Nat Immunol. **5**, 730-737.

33. Kowalinski, E., Lunardi, T., McCarthy, A. A., Louber, J., Brunel, J., Grigorov, B., Gerlier, D. and Cusack, S. (2011) Structural basis for the activation of innate immune pattern-recognition receptor RIG-I by viral RNA. Cell. **147**, 423-435.

34. Saito, T., Owen, D. M., Jiang, F., Marcotrigiano, J. and Gale, M., Jr. (2008) Innate immunity induced by composition-dependent RIG-I recognition of hepatitis C virus RNA. Nature. **454**, 523-527.

35. Kawai, T., Takahashi, K., Sato, S., Coban, C., Kumar, H., Kato, H., Ishii, K. J., Takeuchi, O. and Akira, S. (2005) IPS-1, an adaptor triggering RIG-I- and Mda5-mediated type I interferon induction. Nat Immunol. **6**, 981-988.

36. Mikkelsen, S. S., Jensen, S. B., Chiliveru, S., Melchjorsen, J., Julkunen, I., Gaestel, M., Arthur, J. S., Flavell, R. A., Ghosh, S. and Paludan, S. R. (2009) RIG-I-mediated activation of p38 MAPK is essential for viral induction of interferon and activation of dendritic cells: dependence on TRAF2 and TAK1. J Biol Chem. **284**, 10774-10782.

37. Meylan, E., Curran, J., Hofmann, K., Moradpour, D., Binder, M., Bartenschlager, R. and Tschopp, J. (2005) Cardif is an adaptor protein in the RIG-I antiviral pathway and is targeted by hepatitis C virus. Nature. **437**, 1167-1172.

38. Alexopoulou, L., Holt, A. C., Medzhitov, R. and Flavell, R. A. (2001) Recognition of double-stranded RNA and activation of NF-kappaB by Toll-like receptor 3. Nature. **413**, 732-738.

39. Medzhitov, R. (2007) Recognition of microorganisms and activation of the immune response. Nature. **449**, 819-826.

40. Malmgaard, L. (2004) Induction and regulation of IFNs during viral infections. J Interferon Cytokine Res. **24**, 439-454.

41. Sato, M., Suemori, H., Hata, N., Asagiri, M., Ogasawara, K., Nakao, K., Nakaya, T., Katsuki, M., Noguchi, S., Tanaka, N. and Taniguchi, T. (2000) Distinct and essential roles of transcription factors IRF-3 and IRF-7 in response to viruses for IFN-alpha/beta gene induction. Immunity. **13**, 539-548.

42. Rawling, D. C. and Pyle, A. M. (2014) Parts, assembly and operation of the RIG-I family of motors. Curr Opin Struct Biol. **25**, 25-33.

43. Saito, T., Hirai, R., Loo, Y. M., Owen, D., Johnson, C. L., Sinha, S. C., Akira, S., Fujita, T. and Gale, M., Jr. (2007) Regulation of innate antiviral defenses through a shared repressor domain in RIG-I and LGP2. Proc Natl Acad Sci U S A. **104**, 582-587.

44. Pichlmair, A., Schulz, O., Tan, C. P., Naslund, T. I., Liljestrom, P., Weber, F. and Reis e Sousa, C. (2006) RIG-I-mediated antiviral responses to single-stranded RNA bearing 5'-phosphates. Science. **314**, 997-1001.

45. Hornung, V., Ellegast, J., Kim, S., Brzozka, K., Jung, A., Kato, H., Poeck, H., Akira, S., Conzelmann, K. K., Schlee, M., Endres, S. and Hartmann, G. (2006) 5'-Triphosphate RNA is the ligand for RIG-I. Science. **314**, 994-997.

46. Vela, A., Fedorova, O., Ding, S. C. and Pyle, A. M. (2012) The thermodynamic basis for viral RNA detection by the RIG-I innate immune sensor. J Biol Chem. **287**, 42564-42573.

47. Luo, D., Kohlway, A., Vela, A. and Pyle, A. M. (2012) Visualizing the determinants of viral RNA recognition by innate immune sensor RIG-I. Structure. **20**, 1983-1988.

48. Schlee, M. and Hartmann, G. (2010) The chase for the RIG-I ligand--recent advances. Mol Ther. **18**, 1254-1262.

49. Schmidt, A., Schwerd, T., Hamm, W., Hellmuth, J. C., Cui, S., Wenzel, M., Hoffmann, F. S., Michallet, M. C., Besch, R., Hopfner, K. P., Endres, S. and Rothenfusser, S. (2009) 5'-triphosphate RNA requires base-paired structures to activate antiviral signaling via RIG-I. Proc Natl Acad Sci U S A. **106**, 12067-12072.

50. Abdullah, Z., Schlee, M., Roth, S., Mraheil, M. A., Barchet, W., Bottcher, J., Hain, T., Geiger, S., Hayakawa, Y., Fritz, J. H., Civril, F., Hopfner, K. P., Kurts, C.,

Ruland, J., Hartmann, G., Chakraborty, T. and Knolle, P. A. (2012) RIG-I detects infection with live Listeria by sensing secreted bacterial nucleic acids. EMBO J. **31**, 4153-4164.

51. Jiang, F., Ramanathan, A., Miller, M. T., Tang, G. Q., Gale, M., Jr., Patel, S. S. and Marcotrigiano, J. (2011) Structural basis of RNA recognition and activation by innate immune receptor RIG-I. Nature. **479**, 423-427.

52. Luo, D., Ding, S. C., Vela, A., Kohlway, A., Lindenbach, B. D. and Pyle, A. M. (2011) Structural insights into RNA recognition by RIG-I. Cell. **147**, 409-422.

53. Peisley, A., Lin, C., Wu, B., Orme-Johnson, M., Liu, M., Walz, T. and Hur, S. (2011) Cooperative assembly and dynamic disassembly of MDA5 filaments for viral dsRNA recognition. Proc Natl Acad Sci U S A. **108**, 21010-21015.

54. Kato, H., Takeuchi, O., Sato, S., Yoneyama, M., Yamamoto, M., Matsui, K., Uematsu, S., Jung, A., Kawai, T., Ishii, K. J., Yamaguchi, O., Otsu, K., Tsujimura, T., Koh, C. S., Reis e Sousa, C., Matsuura, Y., Fujita, T. and Akira, S. (2006) Differential roles of MDA5 and RIG-I helicases in the recognition of RNA viruses. Nature. **441**, 101-105.

55. Wilkins, C. and Gale, M., Jr. (2010) Recognition of viruses by cytoplasmic sensors. Curr Opin Immunol. **22**, 41-47.

56. Zeng, W., Sun, L., Jiang, X., Chen, X., Hou, F., Adhikari, A., Xu, M. and Chen, Z. J. (2010) Reconstitution of the RIG-I pathway reveals a signaling role of unanchored polyubiquitin chains in innate immunity. Cell. **141**, 315-330.

57. Matsumoto, M., Funami, K., Tanabe, M., Oshiumi, H., Shingai, M., Seto, Y., Yamamoto, A. and Seya, T. (2003) Subcellular localization of Toll-like receptor 3 in human dendritic cells. J Immunol. **171**, 3154-3162.

58. Leonard, J. N., Ghirlando, R., Askins, J., Bell, J. K., Margulies, D. H., Davies, D. R. and Segal, D. M. (2008) The TLR3 signaling complex forms by cooperative receptor dimerization. Proc Natl Acad Sci U S A. **105**, 258-263.

59. Matsukura, S., Kokubu, F., Kurokawa, M., Kawaguchi, M., Ieki, K., Kuga, H., Odaka, M., Suzuki, S., Watanabe, S., Takeuchi, H., Kasama, T. and Adachi, M. (2006) Synthetic double-stranded RNA induces multiple genes related to inflammation through Toll-like receptor 3 depending on NF-kappaB and/or IRF-3 in airway epithelial cells. Clin Exp Allergy. **36**, 1049-1062.

60. Tissari, J., Siren, J., Meri, S., Julkunen, I. and Matikainen, S. (2005) IFN-alpha enhances TLR3-mediated antiviral cytokine expression in human endothelial and epithelial cells by up-regulating TLR3 expression. J Immunol. **174**, 4289-4294.

61. Fitzgerald, K. A., McWhirter, S. M., Faia, K. L., Rowe, D. C., Latz, E., Golenbock, D. T., Coyle, A. J., Liao, S. M. and Maniatis, T. (2003) IKKepsilon and TBK1 are essential components of the IRF3 signaling pathway. Nat Immunol. **4**, 491-496.

62. Sharma, S., tenOever, B. R., Grandvaux, N., Zhou, G. P., Lin, R. and Hiscott, J. (2003) Triggering the interferon antiviral response through an IKK-related pathway. Science. **300**, 1148-1151.

63. Guo, B. and Cheng, G. (2007) Modulation of the interferon antiviral response by the TBK1/IKKi adaptor protein TANK. J Biol Chem. **282**, 11817-11826.

64. Diebold, S. S., Kaisho, T., Hemmi, H., Akira, S. and Reis e Sousa, C. (2004) Innate antiviral responses by means of TLR7-mediated recognition of single-stranded RNA. Science. **303**, 1529-1531.

65. Jurk, M., Heil, F., Vollmer, J., Schetter, C., Krieg, A. M., Wagner, H., Lipford, G. and Bauer, S. (2002) Human TLR7 or TLR8 independently confer responsiveness to the antiviral compound R-848. Nat Immunol. **3**, 499.

66. Lund, J. M., Alexopoulou, L., Sato, A., Karow, M., Adams, N. C., Gale, N. W., Iwasaki, A. and Flavell, R. A. (2004) Recognition of single-stranded RNA viruses by Toll-like receptor 7. Proc Natl Acad Sci U S A. **101**, 5598-5603.

67. Heil, F., Hemmi, H., Hochrein, H., Ampenberger, F., Kirschning, C., Akira, S., Lipford, G., Wagner, H. and Bauer, S. (2004) Species-specific recognition of single-stranded RNA via toll-like receptor 7 and 8. Science. **303**, 1526-1529.

68. Diebold, S. S. (2008) Recognition of viral single-stranded RNA by Toll-like receptors. Adv Drug Deliv Rev. **60**, 813-823.

69. Kawai, T., Sato, S., Ishii, K. J., Coban, C., Hemmi, H., Yamamoto, M., Terai, K., Matsuda, M., Inoue, J., Uematsu, S., Takeuchi, O. and Akira, S. (2004) Interferon-alpha induction through Toll-like receptors involves a direct interaction of IRF7 with MyD88 and TRAF6. Nat Immunol. **5**, 1061-1068.

70. Hemmi, H., Kaisho, T., Takeuchi, O., Sato, S., Sanjo, H., Hoshino, K., Horiuchi, T., Tomizawa, H., Takeda, K. and Akira, S. (2002) Small anti-viral compounds activate immune cells via the TLR7 MyD88-dependent signaling pathway. Nat Immunol. **3**, 196-200.

71. Honda, K., Yanai, H., Negishi, H., Asagiri, M., Sato, M., Mizutani, T., Shimada, N., Ohba, Y., Takaoka, A., Yoshida, N. and Taniguchi, T. (2005) IRF-7 is the master regulator of type-I interferon-dependent immune responses. Nature. **434**, 772-777.

72. Gorden, K. B., Gorski, K. S., Gibson, S. J., Kedl, R. M., Kieper, W. C., Qiu, X., Tomai, M. A., Alkan, S. S. and Vasilakos, J. P. (2005) Synthetic TLR agonists reveal functional differences between human TLR7 and TLR8. J Immunol. **174**, 1259-1268.

73. Hornung, V., Rothenfusser, S., Britsch, S., Krug, A., Jahrsdorfer, B., Giese, T., Endres, S. and Hartmann, G. (2002) Quantitative expression of toll-like receptor 1-10 mRNA in cellular subsets of human peripheral blood mononuclear cells and sensitivity to CpG oligodeoxynucleotides. J Immunol. **168**, 4531-4537.

74. Ito, T., Amakawa, R. and Fukuhara, S. (2002) Roles of toll-like receptors in natural interferon-producing cells as sensors in immune surveillance. Hum Immunol. **63**, 1120-1125.

75. Liu, Y. J. (2005) IPC: professional type 1 interferon-producing cells and plasmacytoid dendritic cell precursors. Annu Rev Immunol. **23**, 275-306.

76. Alexopoulou, L., Desnues, B. and Demaria, O. (2012) [Toll-like receptor 8: the awkward TLR]. Med Sci (Paris). **28**, 96-102.

77. Der, S. D., Zhou, A., Williams, B. R. and Silverman, R. H. (1998) Identification of genes differentially regulated by interferon alpha, beta, or gamma using oligonucleotide arrays. Proc Natl Acad Sci U S A. **95**, 15623-15628.

78. Malmgaard, L. (2004) Induction and regulation of IFNs during viral infections. J. Interferon Cytokine Res. **24**, 439-454.

79. Iwasaki, A. (2012) A virological view of innate immune recognition. Annu Rev Microbiol. **66**, 177-196.

80. Trinchieri, G. (2010) Type I interferon: friend or foe? J Exp Med. **207**, 2053-2063.

81. Pestka, S., Krause, C. D. and Walter, M. R. (2004) Interferons, interferon-like cytokines, and their receptors. Immunol Rev. **202**, 8-32.

82. Hertzog, P. J. and Williams, B. R. (2013) Fine tuning type I interferon responses. Cytokine Growth Factor Rev. **24**, 217-225.

83. Ivashkiv, L. B. and Donlin, L. T. (2014) Regulation of type I interferon responses. Nat Rev Immunol. **14**, 36-49.

84. de Weerd, N. A., Samarajiwa, S. A. and Hertzog, P. J. (2007) Type I interferon receptors: biochemistry and biological functions. J Biol Chem. **282**, 20053-20057.

85. Darnell, J. E., Jr., Kerr, I. M. and Stark, G. R. (1994) Jak-STAT pathways and transcriptional activation in response to IFNs and other extracellular signaling proteins. Science. **264**, 1415-1421.

86. Chen, J., Baig, E. and Fish, E. N. (2004) Diversity and relatedness among the type I interferons. J Interferon Cytokine Res. **24**, 687-698.

87. Platanias, L. C. (2003) The p38 mitogen-activated protein kinase pathway and its role in interferon signaling. Pharmacol Ther. **98**, 129-142.

88. Ihle, J. N. (1995) The Janus protein tyrosine kinase family and its role in cytokine signaling. Adv Immunol. **60**, 1-35.

89. Aaronson, D. S. and Horvath, C. M. (2002) A road map for those who don't know JAK-STAT. Science. **296**, 1653-1655.

90. Stark, G. R., Kerr, I. M., Williams, B. R., Silverman, R. H. and Schreiber, R. D. (1998) How cells respond to interferons. Annu Rev Biochem. **67**, 227-264.

91. Parmar, S. and Platanias, L. C. (2003) Interferons: mechanisms of action and clinical applications. Curr Opin Oncol. **15**, 431-439.

92. Platanias, L. C. and Fish, E. N. (1999) Signaling pathways activated by interferons. Exp Hematol. **27**, 1583-1592.

93. Levy, D. E. and Darnell, J. E., Jr. (2002) Stats: transcriptional control and biological impact. Nat Rev Mol Cell Biol. **3**, 651-662.

94. Stark, G. R. and Darnell, J. E., Jr. (2012) The JAK-STAT pathway at twenty. Immunity. **36**, 503-514.

95. Darnell, J. E., Jr. (2007) Interferon research: impact on understanding transcriptional control. Curr Top Microbiol Immunol. **316**, 155-163.

96. MacMicking, J. D. (2012) Interferon-inducible effector mechanisms in cell-autonomous immunity. Nat Rev Immunol. **12**, 367-382.

97. Schoggins, J. W., Wilson, S. J., Panis, M., Murphy, M. Y., Jones, C. T., Bieniasz, P. and Rice, C. M. (2011) A diverse range of gene products are effectors of the type I interferon antiviral response. Nature. **472**, 481-485.

98. Rusinova, I., Forster, S., Yu, S., Kannan, A., Masse, M., Cumming, H., Chapman, R. and Hertzog, P. J. (2013) Interferome v2.0: an updated database of annotated interferon-regulated genes. Nucleic Acids Res. **41**, D1040-1046.

99. George, C. X., John, L. and Samuel, C. E. (2014) An RNA editor, adenosine deaminase acting on double-stranded RNA (ADAR1). J Interferon Cytokine Res. **34**, 437-446.

100. Hartner, J. C., Schmittwolf, C., Kispert, A., Muller, A. M., Higuchi, M. and Seeburg, P. H. (2004) Liver disintegration in the mouse embryo caused by deficiency in the RNA-editing enzyme ADAR1. J Biol Chem. **279**, 4894-4902.

101. Hartner, J. C., Walkley, C. R., Lu, J. and Orkin, S. H. (2009) ADAR1 is essential for the maintenance of hematopoiesis and suppression of interferon signaling. Nat Immunol. **10**, 109-115.

102. Wang, Q., Miyakoda, M., Yang, W., Khillan, J., Stachura, D. L., Weiss, M. J. and Nishikura, K. (2004) Stress-induced apoptosis associated with null mutation of ADAR1 RNA editing deaminase gene. J Biol Chem. **279**, 4952-4961.

103. Toth, A. M., Zhang, P., Das, S., George, C. X. and Samuel, C. E. (2006) Interferon action and the double-stranded RNA-dependent enzymes ADAR1 adenosine deaminase and PKR protein kinase. Prog Nucleic Acid Res Mol Biol. **81**, 369-434.

104. George, C. X., Gan, Z., Liu, Y. and Samuel, C. E. (2011) Adenosine deaminases acting on RNA, RNA editing, and interferon action. J Interferon Cytokine Res. **31**, 99-117.

105. Wulff, B. E., Sakurai, M. and Nishikura, K. (2011) Elucidating the inosinome: global approaches to adenosine-to-inosine RNA editing. Nat Rev Genet. **12**, 81-85.

106. Hogg, M., Paro, S., Keegan, L. P. and O'Connell, M. A. (2011) RNA editing by mammalian ADARs. Adv Genet. **73**, 87-120.

107. Warf, M. B., Shepherd, B. A., Johnson, W. E. and Bass, B. L. (2012) Effects of ADARs on small RNA processing pathways in C. elegans. Genome Res. **22**, 1488-1498.

108. Bass, B. L. (2002) RNA editing by adenosine deaminases that act on RNA. Annu Rev Biochem. **71**, 817-846.

109. Phan, V., Thomas, A., Malasri, K. and Sutter, C. H. (2010) Stability of RNA structural motifs and its influence on editing efficiency by adenosine deaminases. Int J Bioinform Res Appl. **6**, 21-36.

110. Strobel, S. A., Cech, T. R., Usman, N. and Beigelman, L. (1994) The 2,6-diaminopurine riboside.5-methylisocytidine wobble base pair: an isoenergetic substitution for the study of G.U pairs in RNA. Biochemistry. **33**, 13824-13835.

111. Serra, M. J., Smolter, P. E. and Westhof, E. (2004) Pronounced instability of tandem IU base pairs in RNA. Nucleic Acids Res. **32**, 1824-1828.

112. Samuel, C. E. (2011) Adenosine deaminases acting on RNA (ADARs) are both antiviral and proviral. Virology. **411**, 180-193.

113. Nishikura, K. (2010) Functions and regulation of RNA editing by ADAR deaminases. Annu Rev Biochem. **79**, 321-349.

114. Samuel, C. E. (2012) ADARs: viruses and innate immunity. Curr Top Microbiol Immunol. **353**, 163-195.

115. Herbert, A., Alfken, J., Kim, Y. G., Mian, I. S., Nishikura, K. and Rich, A. (1997) A Z-DNA binding domain present in the human editing enzyme, double-stranded RNA adenosine deaminase. Proc Natl Acad Sci U S A. **94**, 8421-8426.

116. Fierro-Monti, I. and Mathews, M. B. (2000) Proteins binding to duplexed RNA: one motif, multiple functions. Trends Biochem Sci. **25**, 241-246.

117. Bass, B. L. and Weintraub, H. (1988) An unwinding activity that covalently modifies its double-stranded RNA substrate. Cell. **55**, 1089-1098.

118. Patterson, J. B. and Samuel, C. E. (1995) Expression and regulation by interferon of a double-stranded-RNA-specific adenosine deaminase from human cells: evidence for two forms of the deaminase. Mol Cell Biol. **15**, 5376-5388.

119. George, C. X. and Samuel, C. E. (1999) Human RNA-specific adenosine deaminase ADAR1 transcripts possess alternative exon 1 structures that initiate from different promoters, one constitutively active and the other interferon inducible. Proc Natl Acad Sci U S A. **96**, 4621-4626.

120. George, C. X., Wagner, M. V. and Samuel, C. E. (2005) Expression of interferon-inducible RNA adenosine deaminase ADAR1 during pathogen infection and mouse embryo development involves tissue-selective promoter utilization and alternative splicing. J Biol Chem. **280**, 15020-15028.

121. Kerr, I. M., Brown, R. E. and Hovanessian, A. G. (1977) Nature of inhibitor of cell-free protein synthesis formed in response to interferon and double-stranded RNA. Nature. **268**, 540-542.

122. Rebouillat, D. and Hovanessian, A. G. (1999) The human 2',5'-oligoadenylate synthetase family: interferon-induced proteins with unique enzymatic properties. J Interferon Cytokine Res. **19**, 295-308.

123. Hovanessian, A. G. and Justesen, J. (2007) The human 2'-5'oligoadenylate synthetase family: unique interferon-inducible enzymes catalyzing 2'-5' instead of 3'-5' phosphodiester bond formation. Biochimie. **89**, 779-788.

124. Clemens, M. J. and Vaquero, C. M. (1978) Inhibition of protein synthesis by double-stranded RNA in reticulocyte lysates: evidence for activation of an endoribonuclease. Biochem Biophys Res Commun. **83**, 59-68.

125. Torralba, S., Sojat, J. and Hartmann, R. (2008) 2'-5' oligoadenylate synthetase shares active site architecture with the archaeal CCA-adding enzyme. Cell Mol Life Sci. **65**, 2613-2620.

126. Ghosh, A., Sarkar, S. N., Guo, W., Bandyopadhyay, S. and Sen, G. C. (1997) Enzymatic activity of 2'-5'-oligoadenylate synthetase is impaired by specific mutations that affect oligomerization of the protein. J Biol Chem. **272**, 33220-33226.

127. Hartmann, R., Justesen, J., Sarkar, S. N., Sen, G. C. and Yee, V. C. (2003) Crystal structure of the 2'-specific and double-stranded RNA-activated interferon-induced antiviral protein 2'-5'-oligoadenylate synthetase. Mol Cell. **12**, 1173-1185.

128. Sarkar, S. N., Pal, S. and Sen, G. C. (2002) Crisscross enzymatic reaction between the two molecules in the active dimeric P69 form of the 2'-5' oligodenylate synthetase. J Biol Chem. **277**, 44760-44764.

129. Meng, H., Deo, S., Xiong, S., Dzananovic, E., Donald, L. J., van Dijk, C. W. and McKenna, S. A. (2012) Regulation of the Interferon−Inducible 2′–5′-Oligoadenylate Synthetases by Adenovirus VAI RNA. J. Mol. Biol. **422**, 635-649.

130. Deo, S., Patel, T. R., Dzananovic, E., Booy, E., Zeid, K., McKenna, S. A., Harding, S. E. and McKenna, S. A. (submitted) Activation of 2'-5'-Oligoadenylate Synthetase by the 5'-Untranslated Region of the West Nile Virus Genome. J. Virol.

131. Hoenen, A., Liu, W., Kochs, G., Khromykh, A. A. and Mackenzie, J. M. (2007) West Nile virus-induced cytoplasmic membrane structures provide partial protection against the interferon-induced antiviral MxA protein. J Gen Virol. **88**, 3013-3017.

132. Rebouillat, D., Hovnanian, A., Marie, I. and Hovanessian, A. G. (1999) The 100-kDa 2',5'-oligoadenylate synthetase catalyzing preferentially the synthesis of dimeric

pppA2'p5'A molecules is composed of three homologous domains. J Biol Chem. **274**, 1557-1565.

133. Donovan, J., Dufner, M. and Korennykh, A. (2013) Structural basis for cytosolic double-stranded RNA surveillance by human oligoadenylate synthetase 1. Proc Natl Acad Sci U S A. **110**, 1652-1657.

134. Castora, F. J., Erickson, C. E., Kovacs, T., Lesiak, K. and Torrence, P. F. (1991) 2',5'-oligoadenylates inhibit relaxation of supercoiled DNA by calf thymus DNA topoisomerase I. J Interferon Res. **11**, 143-149.

135. Nakanishi, M., Goto, Y. and Kitade, Y. (2005) 2-5A induces a conformational change in the ankyrin-repeat domain of RNase L. Proteins. **60**, 131-138.

136. Huang, H., Zeqiraj, E., Dong, B., Jha, B. K., Duffy, N. M., Orlicky, S., Thevakumaran, N., Talukdar, M., Pillon, M. C., Ceccarelli, D. F., Wan, L. C., Juang, Y. C., Mao, D. Y., Gaughan, C., Brinton, M. A., Perelygin, A. A., Kourinov, I., Guarne, A., Silverman, R. H. and Sicheri, F. (2014) Dimeric structure of pseudokinase RNase L bound to 2-5A reveals a basis for interferon-induced antiviral activity. Mol Cell. **53**, 221-234.

137. Floyd-Smith, G., Slattery, E. and Lengyel, P. (1981) Interferon action: RNA cleavage pattern of a (2'-5')oligoadenylate--dependent endonuclease. Science. **212**, 1030-1032.

138. Wreschner, D. H., McCauley, J. W., Skehel, J. J. and Kerr, I. M. (1981) Interferon action--sequence specificity of the ppp(A2'p)nA-dependent ribonuclease. Nature. **289**, 414-417.

139. Malathi, K., Dong, B., Gale, M., Jr. and Silverman, R. H. (2007) Small self-RNA generated by RNase L amplifies antiviral innate immunity. Nature. **448**, 816-819.

140. Zhao, L., Birdwell, L. D., Wu, A., Elliott, R., Rose, K. M., Phillips, J. M., Li, Y., Grinspan, J., Silverman, R. H. and Weiss, S. R. (2013) Cell-type-specific activation of the oligoadenylate synthetase-RNase L pathway by a murine coronavirus. J Virol. **87**, 8408-8418.

141. Silverman, R. H. (2007) Viral encounters with 2',5'-oligoadenylate synthetase and RNase L during the interferon antiviral response. J Virol. **81**, 12720-12729.

142. Hovanessian, A. G. (2007) On the discovery of interferon-inducible, double-stranded RNA activated enzymes: the 2'-5'oligoadenylate synthetases and the protein kinase PKR. Cytokine Growth Factor Rev. **18**, 351-361.

143. Feng, G. S., Chong, K., Kumar, A. and Williams, B. R. (1992) Identification of double-stranded RNA-binding domains in the interferon-induced double-stranded RNA-activated p68 kinase. Proc Natl Acad Sci U S A. **89**, 5447-5451.

144. Barber, G. N., Edelhoff, S., Katze, M. G. and Disteche, C. M. (1993) Chromosomal assignment of the interferon-inducible double-stranded RNA-dependent protein kinase (PRKR) to human chromosome 2p21-p22 and mouse chromosome 17 E2. Genomics. **16**, 765-767.

145. Kuhen, K. L., Shen, X., Carlisle, E. R., Richardson, A. L., Weier, H. U., Tanaka, H. and Samuel, C. E. (1996) Structural organization of the human gene (PKR) encoding an interferon-inducible RNA-dependent protein kinase (PKR) and differences from its mouse homolog. Genomics. **36**, 197-201.

146. Squire, J., Meurs, E. F., Chong, K. L., McMillan, N. A., Hovanessian, A. G. and Williams, B. R. (1993) Localization of the human interferon-induced, ds-RNA activated p68 kinase gene (PRKR) to chromosome 2p21-p22. Genomics. **16**, 768-770.

147. Tanaka, H. and Samuel, C. E. (1994) Mechanism of interferon action: structure of the mouse PKR gene encoding the interferon-inducible RNA-dependent protein kinase. Proc Natl Acad Sci U S A. **91**, 7995-7999.

148. Samuel, C. E. (1993) The eIF-2 alpha protein kinases, regulators of translation in eukaryotes from yeasts to humans. J Biol Chem. **268**, 7603-7606.

149. Wek, R. C., Jiang, H. Y. and Anthony, T. G. (2006) Coping with stress: eIF2 kinases and translational control. Biochem Soc Trans. **34**, 7-11.

150. Haines, G. K., Ghadge, G. D., Becker, S., Kies, M., Pelzer, H., Thimmappaya, B. and Radosevich, J. A. (1993) Correlation of the expression of double-stranded RNA-dependent protein kinase (p68) with differentiation in head and neck squamous cell carcinoma. Virchows Arch B Cell Pathol Incl Mol Pathol. **63**, 289-295.

151. Garcia, M. A., Gil, J., Ventoso, I., Guerra, S., Domingo, E., Rivas, C. and Esteban, M. (2006) Impact of protein kinase PKR in cell biology: from antiviral to antiproliferative action. Microbiol Mol Biol Rev. **70**, 1032-1060.

152. Koromilas, A. E., Roy, S., Barber, G. N., Katze, M. G. and Sonenberg, N. (1992) Malignant transformation by a mutant of the IFN-inducible dsRNA-dependent protein kinase. Science. **257**, 1685-1689.

153. Meurs, E. F., Galabru, J., Barber, G. N., Katze, M. G. and Hovanessian, A. G. (1993) Tumor suppressor function of the interferon-induced double-stranded RNA-activated protein kinase. Proc Natl Acad Sci U S A. **90**, 232-236.

154. Lee, S. B. and Esteban, M. (1994) The interferon-induced double-stranded RNA-activated protein kinase induces apoptosis. Virology. **199**, 491-496.

155. Der, S. D., Yang, Y. L., Weissmann, C. and Williams, B. R. (1997) A double-stranded RNA-activated protein kinase-dependent pathway mediating stress-induced apoptosis. Proc Natl Acad Sci U S A. **94**, 3279-3283.

156. Meurs, E., Chong, K., Galabru, J., Thomas, N. S., Kerr, I. M., Williams, B. R. and Hovanessian, A. G. (1990) Molecular cloning and characterization of the human double-stranded RNA-activated protein kinase induced by interferon. Cell. **62**, 379-390.

157. Nanduri, S., Carpick, B. W., Yang, Y., Williams, B. R. and Qin, J. (1998) Structure of the double-stranded RNA-binding domain of the protein kinase PKR reveals the molecular basis of its dsRNA-mediated activation. Embo J. **17**, 5458-5465.

158. VanOudenhove, J., Anderson, E., Krueger, S. and Cole, J. L. (2009) Analysis of PKR structure by small-angle scattering. J Mol Biol. **387**, 910-920.

159. Lemaire, P. A., Lary, J. and Cole, J. L. (2005) Mechanism of PKR activation: dimerization and kinase activation in the absence of double-stranded RNA. J Mol Biol. **345**, 81-90.

160. McKenna, S. A., Kim, I., Liu, C. W. and Puglisi, J. D. (2006) Uncoupling of RNA binding and PKR kinase activation by viral inhibitor RNAs. J. Mol. Biol. **358**, 1270-1285.

161. Carpick, B. W., Graziano, V., Schneider, D., Maitra, R. K., Lee, X. and Williams, B. R. (1997) Characterization of the solution complex between the interferon-induced, double-stranded RNA-activated protein kinase and HIV-I trans-activating region RNA. J Biol Chem. **272**, 9510-9516.

162. Nanduri, S., Rahman, F., Williams, B. R. and Qin, J. (2000) A dynamically tuned double-stranded RNA binding mechanism for the activation of antiviral kinase PKR. EMBO J. **19**, 5567-5574.

163. Samuel, C. E. (2001) Antiviral actions of interferons. Clin Microbiol Rev. **14**, 778-809, table of contents.

164. Dever, T. E. (2002) Gene-specific regulation by general translation factors. Cell. **108**, 545-556.

165. Dar, A. C., Dever, T. E. and Sicheri, F. (2005) Higher-order substrate recognition of eIF2alpha by the RNA-dependent protein kinase PKR. Cell. **122**, 887-900.

166. Francois, C., Duverlie, G., Rebouillat, D., Khorsi, H., Castelain, S., Blum, H. E., Gatignol, A., Wychowski, C., Moradpour, D. and Meurs, E. F. (2000) Expression of hepatitis C virus proteins interferes with the antiviral action of interferon independently of PKR-mediated control of protein synthesis. J Virol. **74**, 5587-5596.

167. Gale, M., Jr. and Katze, M. G. (1998) Molecular mechanisms of interferon resistance mediated by viral-directed inhibition of PKR, the interferon-induced protein kinase. Pharmacol. Ther. **78**, 29-46.

168. Sudhakar, A., Ramachandran, A., Ghosh, S., Hasnain, S. E., Kaufman, R. J. and Ramaiah, K. V. (2000) Phosphorylation of serine 51 in initiation factor 2 alpha (eIF2 alpha) promotes complex formation between eIF2 alpha(P) and eIF2B and causes inhibition in the guanine nucleotide exchange activity of eIF2B. Biochemistry. **39**, 12929-12938.

169. Bycroft, M., Grunert, S., Murzin, A. G., Proctor, M. and St Johnston, D. (1995) NMR solution structure of a dsRNA binding domain from Drosophila staufen protein

reveals homology to the N-terminal domain of ribosomal protein S5. EMBO J. **14**, 3563-3571.

170. Kharrat, A., Macias, M. J., Gibson, T. J., Nilges, M. and Pastore, A. (1995) Structure of the dsRNA binding domain of E. coli RNase III. Embo J. **14**, 3572-3584.

171. Liao, H. J., Kobayashi, R. and Mathews, M. B. (1998) Activities of adenovirus virus-associated RNAs: purification and characterization of RNA binding proteins. Proc Natl Acad Sci U S A. **95**, 8514-8519.

172. Daher, A., Longuet, M., Dorin, D., Bois, F., Segeral, E., Bannwarth, S., Battisti, P. L., Purcell, D. F., Benarous, R., Vaquero, C., Meurs, E. F. and Gatignol, A. (2001) Two dimerization domains in the trans-activation response RNA-binding protein (TRBP) individually reverse the protein kinase R inhibition of HIV-1 long terminal repeat expression. J Biol Chem. **276**, 33899-33905.

173. Peters, G. A., Hartmann, R., Qin, J. and Sen, G. C. (2001) Modular structure of PACT: distinct domains for binding and activating PKR. Mol Cell Biol. **21**, 1908-1920.

174. St Johnston, D., Brown, N. H., Gall, J. G. and Jantsch, M. (1992) A conserved double-stranded RNA-binding domain. Proc Natl Acad Sci U S A. **89**, 10979-10983.

175. Saunders, L. R. and Barber, G. N. (2003) The dsRNA binding protein family: critical roles, diverse cellular functions. FASEB J. **17**, 961-983.

176. Robertson, H. D. (1982) Escherichia coli ribonuclease III cleavage sites. Cell. **30**, 669-672.

177. Lee, Y., Ahn, C., Han, J., Choi, H., Kim, J., Yim, J., Lee, J., Provost, P., Radmark, O., Kim, S. and Kim, V. N. (2003) The nuclear RNase III Drosha initiates microRNA processing. Nature. **425**, 415-419.

178. St Johnston, D., Beuchle, D. and Nusslein-Volhard, C. (1991) Staufen, a gene required to localize maternal RNAs in the Drosophila egg. Cell. **66**, 51-63.

179. Eckmann, C. R. and Jantsch, M. F. (1997) Xlrbpa, a double-stranded RNA-binding protein associated with ribosomes and heterogeneous nuclear RNPs. J Cell Biol. **138**, 239-253.

180. Stefl, R., Oberstrass, F. C., Hood, J. L., Jourdan, M., Zimmermann, M., Skrisovska, L., Maris, C., Peng, L., Hofr, C., Emeson, R. B. and Allain, F. H. (2010) The solution structure of the ADAR2 dsRBM-RNA complex reveals a sequence-specific readout of the minor groove. Cell. **143**, 225-237.

181. Ramos, A., Grunert, S., Adams, J., Micklem, D. R., Proctor, M. R., Freund, S., Bycroft, M., St Johnston, D. and Varani, G. (2000) RNA recognition by a Staufen double-stranded RNA-binding domain. EMBO J. **19**, 997-1009.

182. Gan, J., Tropea, J. E., Austin, B. P., Court, D. L., Waugh, D. S. and Ji, X. (2006) Structural insight into the mechanism of double-stranded RNA processing by ribonuclease III. Cell. **124**, 355-366.

183. Ryter, J. M. and Schultz, S. C. (1998) Molecular basis of double-stranded RNA-protein interactions: structure of a dsRNA-binding domain complexed with dsRNA. Embo J. **17**, 7505-7513.

184. Launer-Felty, K., Wong, C. J., Wahid, A. M., Conn, G. L. and Cole, J. L. (2010) Magnesium-dependent interaction of PKR with adenovirus VAI. J. Mol. Biol. **402**, 638-644.

185. Tian, B. and Mathews, M. B. (2001) Functional characterization of and cooperation between the double-stranded RNA-binding motifs of the protein kinase PKR. J Biol Chem. **276**, 9936-9944.

186. Dey, M., Cao, C., Dar, A. C., Tamura, T., Ozato, K., Sicheri, F. and Dever, T. E. (2005) Mechanistic link between PKR dimerization, autophosphorylation, and eIF2alpha substrate recognition. Cell. **122**, 901-913.

187. Taylor, S. S., Haste, N. M. and Ghosh, G. (2005) PKR and eIF2alpha: integration of kinase dimerization, activation, and substrate docking. Cell. **122**, 823-825.

188. Hershey, J. W. (1991) Translational control in mammalian cells. Annu Rev Biochem. **60**, 717-755.

189. Majumdar, R. and Maitra, U. (2005) Regulation of GTP hydrolysis prior to ribosomal AUG selection during eukaryotic translation initiation. EMBO J. **24**, 3737-3746.

190. Thomis, D. C. and Samuel, C. E. (1993) Mechanism of interferon action: evidence for intermolecular autophosphorylation and autoactivation of the interferon-induced, RNA-dependent protein kinase PKR. J. Virol. **67**, 7695-7700.

191. Ryter, J. M. and Schultz, S. C. (1998) Molecular basis of double-stranded RNA-protein interactions: structure of a dsRNA-binding domain complexed with dsRNA. EMBO J. **17**, 7505-7513.

192. Zhang, F., Romano, P. R., Nagamura-Inoue, T., Tian, B., Dever, T. E., Mathews, M. B., Ozato, K. and Hinnebusch, A. G. (2001) Binding of double-stranded RNA to protein kinase PKR is required for dimerization and promotes critical autophosphorylation events in the activation loop. J Biol Chem. **276**, 24946-24958.

193. Lemaire, P. A., Lary, J. and Cole, J. L. (2005) Mechanism of PKR activation: dimerization and kinase activation in the absence of double-stranded RNA. J. Mol. Biol. **345**, 81-90.

194. McKenna, S. A., Lindhout, D. A., Kim, I., Liu, C. W., Gelev, V. M., Wagner, G. and Puglisi, J. D. (2007) Molecular framework for the activation of RNA-dependent protein kinase. J. Biol. Chem. **282**, 11474-11486.

195. VanOudenhove, J., Anderson, E., Krueger, S. and Cole, J. L. (2009) Analysis of PKR structure by small-angle scattering. J. Mol. Biol. **387**, 910-920.

196. Lemaire, P. A., Tessmer, I., Craig, R., Erie, D. A. and Cole, J. L. (2006) Unactivated PKR exists in an open conformation capable of binding nucleotides. Biochemistry. **45**, 9074-9084.

197. McKenna, S. A., Lindhout, D. A., Kim, I., Liu, C. W., Gelev, V. M., Wagner, G. and Puglisi, J. D. (2007) Molecular framework for the activation of RNA-dependent protein kinase. J Biol Chem. **282**, 11474-11486.

198. Gabel, F., Wang, D., Madern, D., Sadler, A., Dayie, K., Daryoush, M. Z., Schwahn, D., Zaccai, G., Lee, X. and Williams, B. R. (2006) Dynamic flexibility of double-stranded RNA activated PKR in solution. J Mol Biol. **359**, 610-623.

199. Ruvolo, P. P., Gao, F., Blalock, W. L., Deng, X. and May, W. S. (2001) Ceramide regulates protein synthesis by a novel mechanism involving the cellular PKR activator RAX. J Biol Chem. **276**, 11754-11758.

200. Patel, R. C. and Sen, G. C. (1998) PACT, a protein activator of the interferon-induced protein kinase, PKR. EMBO J. **17**, 4379-4390.

201. Patel, C. V., Handy, I., Goldsmith, T. and Patel, R. C. (2000) PACT, a stress-modulated cellular activator of interferon-induced double-stranded RNA-activated protein kinase, PKR. J Biol Chem. **275**, 37993-37998.

202. Daniels, S. M. and Gatignol, A. (2012) The multiple functions of TRBP, at the hub of cell responses to viruses, stress, and cancer. Microbiol Mol Biol Rev. **76**, 652-666.

203. Huang, X., Hutchins, B. and Patel, R. C. (2002) The C-terminal, third conserved motif of the protein activator PACT plays an essential role in the activation of double-stranded-RNA-dependent protein kinase (PKR). Biochem J. **366**, 175-186.

204. Gatignol, A., Buckler-White, A., Berkhout, B. and Jeang, K. T. (1991) Characterization of a human TAR RNA-binding protein that activates the HIV-1 LTR. Science. **251**, 1597-1600.

205. Gatignol, A., Kumar, A., Rabson, A. and Jeang, K. T. (1989) Identification of cellular proteins that bind to the human immunodeficiency virus type 1 trans-activation-responsive TAR element RNA. Proc Natl Acad Sci U S A. **86**, 7828-7832.

206. Dorin, D., Bonnet, M. C., Bannwarth, S., Gatignol, A., Meurs, E. F. and Vaquero, C. (2003) The TAR RNA-binding protein, TRBP, stimulates the expression of TAR-containing RNAs in vitro and in vivo independently of its ability to inhibit the dsRNA-dependent kinase PKR. J Biol Chem. **278**, 4440-4448.

207. Park, H., Davies, M. V., Langland, J. O., Chang, H. W., Nam, Y. S., Tartaglia, J., Paoletti, E., Jacobs, B. L., Kaufman, R. J. and Venkatesan, S. (1994) TAR RNA-binding protein is an inhibitor of the interferon-induced protein kinase PKR. Proc Natl Acad Sci U S A. **91**, 4713-4717.

208. Laraki, G., Clerzius, G., Daher, A., Melendez-Pena, C., Daniels, S. and Gatignol, A. (2008) Interactions between the double-stranded RNA-binding proteins TRBP and PACT define the Medipal domain that mediates protein-protein interactions. RNA Biol. **5**, 92-103.

209. Singh, M., Castillo, D., Patel, C. V. and Patel, R. C. (2011) Stress-induced phosphorylation of PACT reduces its interaction with TRBP and leads to PKR activation. Biochemistry. **50**, 4550-4560.

210. Daher, A., Laraki, G., Singh, M., Melendez-Pena, C. E., Bannwarth, S., Peters, A. H., Meurs, E. F., Braun, R. E., Patel, R. C. and Gatignol, A. (2009) TRBP control of PACT-induced phosphorylation of protein kinase R is reversed by stress. Mol Cell Biol. **29**, 254-265.

211. Ito, T., Yang, M. and May, W. S. (1999) RAX, a cellular activator for double-stranded RNA-dependent protein kinase during stress signaling. J Biol Chem. **274**, 15427-15432.

212. Bennett, R. L., Blalock, W. L., Abtahi, D. M., Pan, Y., Moyer, S. A. and May, W. S. (2006) RAX, the PKR activator, sensitizes cells to inflammatory cytokines, serum withdrawal, chemotherapy, and viral infection. Blood. **108**, 821-829.

213. Yeung, M. C., Liu, J. and Lau, A. S. (1996) An essential role for the interferon-inducible, double-stranded RNA-activated protein kinase PKR in the tumor necrosis factor-induced apoptosis in U937 cells. Proc Natl Acad Sci U S A. **93**, 12451-12455.

214. Cuddihy, A. R., Wong, A. H., Tam, N. W., Li, S. and Koromilas, A. E. (1999) The double-stranded RNA activated protein kinase PKR physically associates with the

tumor suppressor p53 protein and phosphorylates human p53 on serine 392 in vitro. Oncogene. **18**, 2690-2702.

215. Ghosh, S., May, M. J. and Kopp, E. B. (1998) NF-kappa B and Rel proteins: evolutionarily conserved mediators of immune responses. Annu Rev Immunol. **16**, 225-260.

216. Ghosh, S. and Karin, M. (2002) Missing pieces in the NF-kappaB puzzle. Cell. **109 Suppl**, S81-96.

217. Gil, J., Alcami, J. and Esteban, M. (2000) Activation of NF-kappa B by the dsRNA-dependent protein kinase, PKR involves the I kappa B kinase complex. Oncogene. **19**, 1369-1378.

218. Gil, J., Alcami, J. and Esteban, M. (1999) Induction of apoptosis by double-stranded-RNA-dependent protein kinase (PKR) involves the alpha subunit of eukaryotic translation initiation factor 2 and NF-kappaB. Mol Cell Biol. **19**, 4653-4663.

219. Maran, A., Maitra, R. K., Kumar, A., Dong, B., Xiao, W., Li, G., Williams, B. R., Torrence, P. F. and Silverman, R. H. (1994) Blockage of NF-kappa B signaling by selective ablation of an mRNA target by 2-5A antisense chimeras. Science. **265**, 789-792.

220. Yang, Y. L., Reis, L. F., Pavlovic, J., Aguzzi, A., Schafer, R., Kumar, A., Williams, B. R., Aguet, M. and Weissmann, C. (1995) Deficient signaling in mice devoid of double-stranded RNA-dependent protein kinase. EMBO J. **14**, 6095-6106.

221. Bonnet, M. C., Weil, R., Dam, E., Hovanessian, A. G. and Meurs, E. F. (2000) PKR stimulates NF-kappaB irrespective of its kinase function by interacting with the IkappaB kinase complex. Mol Cell Biol. **20**, 4532-4542.

222. Zamanian-Daryoush, M., Mogensen, T. H., DiDonato, J. A. and Williams, B. R. (2000) NF-kappaB activation by double-stranded-RNA-activated protein kinase (PKR) is mediated through NF-kappaB-inducing kinase and IkappaB kinase. Mol Cell Biol. **20**, 1278-1290.

223. Gil, J., Rullas, J., Garcia, M. A., Alcami, J. and Esteban, M. (2001) The catalytic activity of dsRNA-dependent protein kinase, PKR, is required for NF-kappaB activation. Oncogene. **20**, 385-394.

224. Chu, W. M., Ostertag, D., Li, Z. W., Chang, L., Chen, Y., Hu, Y., Williams, B., Perrault, J. and Karin, M. (1999) JNK2 and IKKbeta are required for activating the innate response to viral infection. Immunity. **11**, 721-731.

225. Weber, F., Wagner, V., Rasmussen, S. B., Hartmann, R. and Paludan, S. R. (2006) Double-stranded RNA is produced by positive-strand RNA viruses and DNA viruses but not in detectable amounts by negative-strand RNA viruses. J Virol. **80**, 5059-5064.

226. Kim, I., Liu, C. W. and Puglisi, J. D. (2006) Specific recognition of HIV TAR RNA by the dsRNA binding domains (dsRBD1-dsRBD2) of PKR. J Mol Biol. **358**, 430-442.

227. McKenna, S. A., Kim, I., Liu, C. W. and Puglisi, J. D. (2006) Uncoupling of RNA binding and PKR kinase activation by viral inhibitor RNAs. J Mol Biol. **358**, 1270-1285.

228. Bevilacqua, P. C. and Cech, T. R. (1996) Minor-groove recognition of double-stranded RNA by the double-stranded RNA-binding domain from the RNA-activated protein kinase PKR. Biochemistry. **35**, 9983-9994.

229. Puthenveetil, S., Whitby, L., Ren, J., Kelnar, K., Krebs, J. F. and Beal, P. A. (2006) Controlling activation of the RNA-dependent protein kinase by siRNAs using site-specific chemical modification. Nucleic Acids Res. **34**, 4900-4911.

230. Nallagatla, S. R., Hwang, J., Toroney, R., Zheng, X., Cameron, C. E. and Bevilacqua, P. C. (2007) 5'-triphosphate-dependent activation of PKR by RNAs with short stem-loops. Science. **318**, 1455-1458.

231. Nallagatla, S. R. and Bevilacqua, P. C. (2008) Nucleoside modifications modulate activation of the protein kinase PKR in an RNA structure-specific manner. Rna. **14**, 1201-1213.

232. Thomis, D. C. and Samuel, C. E. (1993) Mechanism of interferon action: evidence for intermolecular autophosphorylation and autoactivation of the interferon-induced, RNA-dependent protein kinase PKR. J Virol. **67**, 7695-7700.

233. Berkhout, B., Silverman, R. H. and Jeang, K. T. (1989) Tat trans-activates the human immunodeficiency virus through a nascent RNA target. Cell. **59**, 273-282.

234. Kitajewski, J., Schneider, R. J., Safer, B., Munemitsu, S. M., Samuel, C. E., Thimmappaya, B. and Shenk, T. (1986) Adenovirus VAI RNA antagonizes the antiviral action of interferon by preventing activation of the interferon-induced eIF-2 alpha kinase. Cell. **45**, 195-200.

235. Katze, M. G., DeCorato, D., Safer, B., Galabru, J. and Hovanessian, A. G. (1987) Adenovirus VAI RNA complexes with the 68 000 Mr protein kinase to regulate its autophosphorylation and activity. EMBO J. **6**, 689-697.

236. Clarke, P. A., Schwemmle, M., Schickinger, J., Hilse, K. and Clemens, M. J. (1991) Binding of Epstein-Barr virus small RNA EBER-1 to the double-stranded RNA-activated protein kinase DAI. Nucleic Acids Res. **19**, 243-248.

237. Shimoike, T., McKenna, S. A., Lindhout, D. A. and Puglisi, J. D. (2009) Translational insensitivity to potent activation of PKR by HCV IRES RNA. Antiviral Res. **83**, 228-237.

238. Ben-Asouli, Y., Banai, Y., Pel-Or, Y., Shir, A. and Kaempfer, R. (2002) Human interferon-gamma mRNA autoregulates its translation through a pseudoknot that activates the interferon-inducible protein kinase PKR. Cell. **108**, 221-232.

239. Aboul-ela, F., Karn, J. and Varani, G. (1996) Structure of HIV-1 TAR RNA in the absence of ligands reveals a novel conformation of the trinucleotide bulge. Nucleic Acids Res. **24**, 3974-3981.

240. Puglisi, J. D., Tan, R., Calnan, B. J., Frankel, A. D. and Williamson, J. R. (1992) Conformation of the TAR RNA-arginine complex by NMR spectroscopy. Science. **257**, 76-80.

241. Bannwarth, S. and Gatignol, A. (2005) HIV-1 TAR RNA: the target of molecular interactions between the virus and its host. Curr HIV Res. **3**, 61-71.

242. Chang, Y. N., Kenan, D. J., Keene, J. D., Gatignol, A. and Jeang, K. T. (1994) Direct interactions between autoantigen La and human immunodeficiency virus leader RNA. J Virol. **68**, 7008-7020.

243. Dugre-Brisson, S., Elvira, G., Boulay, K., Chatel-Chaix, L., Mouland, A. J. and DesGroseillers, L. (2005) Interaction of Staufen1 with the 5' end of mRNA facilitates translation of these RNAs. Nucleic Acids Res. **33**, 4797-4812.

244. Soto-Rifo, R., Rubilar, P. S., Limousin, T., de Breyne, S., Decimo, D. and Ohlmann, T. (2012) DEAD-box protein DDX3 associates with eIF4F to promote translation of selected mRNAs. EMBO J. **31**, 3745-3756.

245. Mancebo, H. S., Lee, G., Flygare, J., Tomassini, J., Luu, P., Zhu, Y., Peng, J., Blau, C., Hazuda, D., Price, D. and Flores, O. (1997) P-TEFb kinase is required for HIV Tat transcriptional activation in vivo and in vitro. Genes Dev. **11**, 2633-2644.

246. Wei, P., Garber, M. E., Fang, S. M., Fischer, W. H. and Jones, K. A. (1998) A novel CDK9-associated C-type cyclin interacts directly with HIV-1 Tat and mediates its high-affinity, loop-specific binding to TAR RNA. Cell. **92**, 451-462.

247. Zhu, Y., Pe'ery, T., Peng, J., Ramanathan, Y., Marshall, N., Marshall, T., Amendt, B., Mathews, M. B. and Price, D. H. (1997) Transcription elongation factor P-TEFb is required for HIV-1 tat transactivation in vitro. Genes Dev. **11**, 2622-2632.

248. Peterlin, B. M. and Price, D. H. (2006) Controlling the elongation phase of transcription with P-TEFb. Mol Cell. **23**, 297-305.

249. Benkirane, M., Neuveut, C., Chun, R. F., Smith, S. M., Samuel, C. E., Gatignol, A. and Jeang, K. T. (1997) Oncogenic potential of TAR RNA binding protein TRBP and its regulatory interaction with RNA-dependent protein kinase PKR. Embo J. **16**, 611-624.

250. Dimitrova, D. I., Yang, X., Reichenbach, N. L., Karakasidis, S., Sutton, R. E., Henderson, E. E., Rogers, T. J. and Suhadolnik, R. J. (2005) Lentivirus-mediated transduction of PKR into CD34(+) hematopoietic stem cells inhibits HIV-1 replication in differentiated T cell progeny. J Interferon Cytokine Res. **25**, 345-360.

251. SenGupta, D. N. and Silverman, R. H. (1989) Activation of interferon-regulated, dsRNA-dependent enzymes by human immunodeficiency virus-1 leader RNA. Nucleic Acids Res. **17**, 969-978.

252. Maitra, R. K., McMillan, N. A., Desai, S., McSwiggen, J., Hovanessian, A. G., Sen, G., Williams, B. R. and Silverman, R. H. (1994) HIV-1 TAR RNA has an intrinsic ability to activate interferon-inducible enzymes. Virology. **204**, 823-827.

253. Endo-Munoz, L., Warby, T., Harrich, D. and McMillan, N. A. (2005) Phosphorylation of HIV Tat by PKR increases interaction with TAR RNA and enhances transcription. Virol J. **2**, 17.

254. Heinicke, L. A., Wong, C. J., Lary, J., Nallagatla, S. R., Diegelman-Parente, A., Zheng, X., Cole, J. L. and Bevilacqua, P. C. (2009) RNA dimerization promotes PKR dimerization and activation. J Mol Biol. **390**, 319-338.

255. Langland, J. O., Cameron, J. M., Heck, M. C., Jancovich, J. K. and Jacobs, B. L. (2006) Inhibition of PKR by RNA and DNA viruses. Virus Res. **119**, 100-110.

256. Kumar, K. U., Srivastava, S. P. and Kaufman, R. J. (1999) Double-stranded RNA-activated protein kinase (PKR) is negatively regulated by 60S ribosomal subunit protein L18. Mol Cell Biol. **19**, 1116-1125.

257. Sharp, T. V., Schwemmle, M., Jeffrey, I., Laing, K., Mellor, H., Proud, C. G., Hilse, K. and Clemens, M. J. (1993) Comparative analysis of the regulation of the interferon-inducible protein kinase PKR by Epstein-Barr virus RNAs EBER-1 and EBER-2 and adenovirus VAI RNA. Nucleic Acids Res. **21**, 4483-4490.

258. Ghadge, G. D., Malhotra, P., Furtado, M. R., Dhar, R. and Thimmapaya, B. (1994) In vitro analysis of virus-associated RNA I (VAI RNA): inhibition of the double-

stranded RNA-activated protein kinase PKR by VAI RNA mutants correlates with the in vivo phenotype and the structural integrity of the central domain. J Virol. **68**, 4137-4151.

259. Laing, K. G., Matys, V. and Clemens, M. J. (2001) Analysis of the expression and function of the EBV-encoded small RNAs, the EBERs, in heterologous cells. Methods Mol Biol. **174**, 45-66.

260. Young, L. S. and Rickinson, A. B. (2004) Epstein-Barr virus: 40 years on. Nat Rev Cancer. **4**, 757-768.

261. Busson, P., Keryer, C., Ooka, T. and Corbex, M. (2004) EBV-associated nasopharyngeal carcinomas: from epidemiology to virus-targeting strategies. Trends Microbiol. **12**, 356-360.

262. Gandhi, M. K., Tellam, J. T. and Khanna, R. (2004) Epstein-Barr virus-associated Hodgkin's lymphoma. Br J Haematol. **125**, 267-281.

263. Thompson, M. P. and Kurzrock, R. (2004) Epstein-Barr virus and cancer. Clin Cancer Res. **10**, 803-821.

264. Amon, W. and Farrell, P. J. (2005) Reactivation of Epstein-Barr virus from latency. Rev Med Virol. **15**, 149-156.

265. Hammerschmidt, W. and Sugden, B. (2004) Epstein-Barr virus sustains Burkitt's lymphomas and Hodgkin's disease. Trends Mol Med. **10**, 331-336.

266. Sugimoto, M., Tahara, H., Ide, T. and Furuichi, Y. (2004) Steps involved in immortalization and tumorigenesis in human B-lymphoblastoid cell lines transformed by Epstein-Barr virus. Cancer Res. **64**, 3361-3364.

267. Young, L. S. and Murray, P. G. (2003) Epstein-Barr virus and oncogenesis: from latent genes to tumours. Oncogene. **22**, 5108-5121.

268. Saridakis, V., Sheng, Y., Sarkari, F., Holowaty, M. N., Shire, K., Nguyen, T., Zhang, R. G., Liao, J., Lee, W., Edwards, A. M., Arrowsmith, C. H. and Frappier, L. (2005) Structure of the p53 binding domain of HAUSP/USP7 bound to Epstein-Barr nuclear antigen 1 implications for EBV-mediated immortalization. Mol Cell. **18**, 25-36.

269. Izumi, K. M. (2004) Epstein-Barr virus signal transduction and B-lymphocyte growth transformation. Prog Mol Subcell Biol. **36**, 269-288.

270. Morrison, J. A., Gulley, M. L., Pathmanathan, R. and Raab-Traub, N. (2004) Differential signaling pathways are activated in the Epstein-Barr virus-associated malignancies nasopharyngeal carcinoma and Hodgkin lymphoma. Cancer Res. **64**, 5251-5260.

271. Glickman, J. N., Howe, J. G. and Steitz, J. A. (1988) Structural analyses of EBER1 and EBER2 ribonucleoprotein particles present in Epstein-Barr virus-infected cells. J Virol. **62**, 902-911.

272. Vuyisich, M., Spanggord, R. J. and Beal, P. A. (2002) The binding site of the RNA-dependent protein kinase (PKR) on EBER1 RNA from Epstein-Barr virus. EMBO Rep. **3**, 622-627.

273. Nanbo, A., Inoue, K., Adachi-Takasawa, K. and Takada, K. (2002) Epstein-Barr virus RNA confers resistance to interferon-alpha-induced apoptosis in Burkitt's lymphoma. EMBO J. **21**, 954-965.

274. McKenna, S. A., Lindhout, D. A., Shimoike, T., Aitken, C. E. and Puglisi, J. D. (2007) Viral dsRNA inhibitors prevent self-association and autophosphorylation of PKR. J. Mol. Biol. **372**, 103-113.

275. Tsukiyama-Kohara, K., Iizuka, N., Kohara, M. and Nomoto, A. (1992) Internal ribosome entry site within hepatitis C virus RNA. J Virol. **66**, 1476-1483.

276. Wang, C., Sarnow, P. and Siddiqui, A. (1993) Translation of human hepatitis C virus RNA in cultured cells is mediated by an internal ribosome-binding mechanism. J Virol. **67**, 3338-3344.

277. Guidotti, L. G. and Chisari, F. V. (2006) Immunobiology and pathogenesis of viral hepatitis. Annu Rev Pathol. **1**, 23-61.

278. Pestova, T. V., Shatsky, I. N., Fletcher, S. P., Jackson, R. J. and Hellen, C. U. (1998) A prokaryotic-like mode of cytoplasmic eukaryotic ribosome binding to the initiation codon during internal translation initiation of hepatitis C and classical swine fever virus RNAs. Genes Dev. **12**, 67-83.

279. Otto, G. A. and Puglisi, J. D. (2004) The pathway of HCV IRES-mediated translation initiation. Cell. **119**, 369-380.

280. Ji, H., Fraser, C. S., Yu, Y., Leary, J. and Doudna, J. A. (2004) Coordinated assembly of human translation initiation complexes by the hepatitis C virus internal ribosome entry site RNA. Proc Natl Acad Sci U S A. **101**, 16990-16995.

281. Kieft, J. S., Zhou, K., Grech, A., Jubin, R. and Doudna, J. A. (2002) Crystal structure of an RNA tertiary domain essential to HCV IRES-mediated translation initiation. Nat Struct Biol. **9**, 370-374.

282. Kim, I., Lukavsky, P. J. and Puglisi, J. D. (2002) NMR study of 100 kDa HCV IRES RNA using segmental isotope labeling. J Am Chem Soc. **124**, 9338-9339.

283. Lukavsky, P. J., Otto, G. A., Lancaster, A. M., Sarnow, P. and Puglisi, J. D. (2000) Structures of two RNA domains essential for hepatitis C virus internal ribosome entry site function. Nat Struct Biol. **7**, 1105-1110.

284. Lukavsky, P. J., Kim, I., Otto, G. A. and Puglisi, J. D. (2003) Structure of HCV IRES domain II determined by NMR. Nat Struct Biol. **10**, 1033-1038.

285. Kieft, J. S., Zhou, K., Jubin, R. and Doudna, J. A. (2001) Mechanism of ribosome recruitment by hepatitis C IRES RNA. RNA. **7**, 194-206.

286. Kolupaeva, V. G., Pestova, T. V. and Hellen, C. U. (2000) An enzymatic footprinting analysis of the interaction of 40S ribosomal subunits with the internal ribosomal entry site of hepatitis C virus. J Virol. **74**, 6242-6250.

287. Lytle, J. R., Wu, L. and Robertson, H. D. (2001) The ribosome binding site of hepatitis C virus mRNA. J Virol. **75**, 7629-7636.

288. Otto, G. A., Lukavsky, P. J., Lancaster, A. M., Sarnow, P. and Puglisi, J. D. (2002) Ribosomal proteins mediate the hepatitis C virus IRES-HeLa 40S interaction. RNA. **8**, 913-923.

289. Pestova, T. V., de Breyne, S., Pisarev, A. V., Abaeva, I. S. and Hellen, C. U. (2008) eIF2-dependent and eIF2-independent modes of initiation on the CSFV IRES: a common role of domain II. EMBO J. **27**, 1060-1072.

290. O'Malley, R. P., Mariano, T. M., Siekierka, J. and Mathews, M. B. (1986) A mechanism for the control of protein synthesis by adenovirus VA RNAI. Cell. **44**, 391-400.

291. Wahid, A. M., Coventry, V. K. and Conn, G. L. (2008) Systematic deletion of the adenovirus-associated RNAI terminal stem reveals a surprisingly active RNA inhibitor of double-stranded RNA-activated protein kinase. J. Biol. Chem. **283**, 17485-17493.

292. Wahid, A. M., Coventry, V. K. and Conn, G. L. (2009) The PKR-binding domain of adenovirus VA RNAI exists as a mixture of two functionally non-equivalent structures. Nucleic Acids Res. **37**, 5830-5837.

293. Rowe, W. P., Huebner, R. J., Gilmore, L. K., Parrott, R. H. and Ward, T. G. (1953) Isolation of a cytopathogenic agent from human adenoids undergoing spontaneous degeneration in tissue culture. Proc Soc Exp Biol Med. **84**, 570-573.

294. Carnero, E., Sutherland, J. D. and Fortes, P. (2011) Adenovirus and miRNAs. Biochim Biophys Acta. **1809**, 660-667.

295. Rohde, J. E. and Northrup, R. S. (1976) Taking science where the diarrhoea is. Ciba Found Symp, 339-366.

296. Gray, G. C. (2006) Adenovirus transmission--worthy of our attention. J Infect Dis. **194**, 871-873.

297. Gray, G. C., Goswami, P. R., Malasig, M. D., Hawksworth, A. W., Trump, D. H., Ryan, M. A. and Schnurr, D. P. (2000) Adult adenovirus infections: loss of orphaned vaccines precipitates military respiratory disease epidemics. For the Adenovirus Surveillance Group. Clin Infect Dis. **31**, 663-670.

298. Kopecky-Bromberg, S. A. and Palese, P. (2009) Recombinant vectors as influenza vaccines. Curr Top Microbiol Immunol. **333**, 243-267.

299. Harvey, A. R., Hellstrom, M. and Rodger, J. (2009) Gene therapy and transplantation in the retinofugal pathway. Prog Brain Res. **175**, 151-161.

300. Limbach, K. J. and Richie, T. L. (2009) Viral vectors in malaria vaccine development. Parasite Immunol. **31**, 501-519.

301. Ginsberg, H. S. (1999) The life and times of adenoviruses. Adv Virus Res. **54**, 1-13.

302. Mathews, M. B. (1995) Structure, function, and evolution of adenovirus virus-associated RNAs. Curr Top Microbiol Immunol. **199 (Pt 2)**, 173-187.

303. Reichel, P. A., Merrick, W. C., Siekierka, J. and Mathews, M. B. (1985) Regulation of a protein synthesis initiation factor by adenovirus virus-associated RNA. Nature. **313**, 196-200.

304. Shenk, T. (1996) Adenoviridae: The viruses and their replication. Raven publishers editor

305. Kondo, S., Yoshida, K., Suzuki, M., Saito, I. and Kanegae, Y. (2014) Adenovirus-encoding virus-associated RNAs suppress HDGF gene expression to support efficient viral replication. PLoS One. **9**, e108627.

306. Bruton, R. K., Pelka, P., Mapp, K. L., Fonseca, G. J., Torchia, J., Turnell, A. S., Mymryk, J. S. and Grand, R. J. (2008) Identification of a second CtBP binding site in adenovirus type 5 E1A conserved region 3. J Virol. **82**, 8476-8486.

307. Dery, C. V., Herrmann, C. H. and Mathews, M. B. (1987) Response of individual adenovirus promoters to the products of the E1A gene. Oncogene. **2**, 15-23.

308. Pelka, P., Ablack, J. N., Torchia, J., Turnell, A. S., Grand, R. J. and Mymryk, J. S. (2009) Transcriptional control by adenovirus E1A conserved region 3 via p300/CBP. Nucleic Acids Res. **37**, 1095-1106.

309. Liu, F. and Green, M. R. (1990) A specific member of the ATF transcription factor family can mediate transcription activation by the adenovirus E1a protein. Cell. **61**, 1217-1224.

310. Liu, F. and Green, M. R. (1994) Promoter targeting by adenovirus E1a through interaction with different cellular DNA-binding domains. Nature. **368**, 520-525.

311. Pelka, P., Miller, M. S., Cecchini, M., Yousef, A. F., Bowdish, D. M., Dick, F., Whyte, P. and Mymryk, J. S. (2011) Adenovirus E1A directly targets the E2F/DP-1 complex. J Virol. **85**, 8841-8851.

312. Blais, A. and Dynlacht, B. D. (2004) Hitting their targets: an emerging picture of E2F and cell cycle control. Curr Opin Genet Dev. **14**, 527-532.

313. Chen, C. and Wells, A. D. (2007) Comparative analysis of E2F family member oncogenic activity. PLoS One. **2**, e912.

314. Dimova, D. K. and Dyson, N. J. (2005) The E2F transcriptional network: old acquaintances with new faces. Oncogene. **24**, 2810-2826.

315. McClellan, K. A. and Slack, R. S. (2007) Specific in vivo roles for E2Fs in differentiation and development. Cell Cycle. **6**, 2917-2927.

316. Whyte, P., Buchkovich, K. J., Horowitz, J. M., Friend, S. H., Raybuck, M., Weinberg, R. A. and Harlow, E. (1988) Association between an oncogene and an anti-oncogene: the adenovirus E1A proteins bind to the retinoblastoma gene product. Nature. **334**, 124-129.

317. Bayley, S. T. and Mymryk, J. S. (1994) Adenovirus e1a proteins and transformation (review). Int J Oncol. **5**, 425-444.

318. Sha, J., Ghosh, M. K., Zhang, K. and Harter, M. L. (2010) E1A interacts with two opposing transcriptional pathways to induce quiescent cells into S phase. J Virol. **84**, 4050-4059.

319. Shen, Y. and Shenk, T. E. (1995) Viruses and apoptosis. Curr Opin Genet Dev. **5**, 105-111.

320. Ghadge, G. D., Swaminathan, S., Katze, M. G. and Thimmapaya, B. (1991) Binding of the adenovirus VAI RNA to the interferon-induced 68-kDa protein kinase correlates with function. Proc Natl Acad Sci U S A. **88**, 7140-7144.

321. Bhat, R. A., Domer, P. H. and Thimmappaya, B. (1985) Structural requirements of adenovirus VAI RNA for its translation enhancement function. Mol. Cell. Biol. **5**, 187-196.

322. Thimmappaya, B., Weinberger, C., Schneider, R. J. and Shenk, T. (1982) Adenovirus VAI RNA is required for efficient translation of viral mRNAs at late times after infection. Cell. **31**, 543-551.

323. Pe'ery, T., Mellits, K. H. and Mathews, M. B. (1993) Mutational analysis of the central domain of adenovirus virus-associated RNA mandates a revision of the proposed secondary structure. J. Virol. **67**, 3534-3543.

324. Furtado, M. R., Subramanian, S., Bhat, R. A., Fowlkes, D. M., Safer, B. and Thimmappaya, B. (1989) Functional dissection of adenovirus VAI RNA. J. Virol. **63**, 3423-3434.

325. Gwizdek, C., Ossareh-Nazari, B., Brownawell, A. M., Doglio, A., Bertrand, E., Macara, I. G. and Dargemont, C. (2003) Exportin-5 mediates nuclear export of minihelix-containing RNAs. J Biol Chem. **278**, 5505-5508.

326. Andersson, M. G., Haasnoot, P. C., Xu, N., Berenjian, S., Berkhout, B. and Akusjarvi, G. (2005) Suppression of RNA interference by adenovirus virus-associated RNA. J Virol. **79**, 9556-9565.

327. Lu, S. and Cullen, B. R. (2004) Adenovirus VA1 noncoding RNA can inhibit small interfering RNA and MicroRNA biogenesis. J Virol. **78**, 12868-12876.

328. Andersson, M. G., Haasnoot, P. C., Xu, N., Berenjian, S., Berkhout, B. and Akusjarvi, G. (2005) Suppression of RNA interference by adenovirus virus-associated RNA. J. Virol. **79**, 9556-9565.

329. Kim, V. N., Han, J. and Siomi, M. C. (2009) Biogenesis of small RNAs in animals. Nat. Rev. Mol. Cell. Biol. **10**, 126-139.

330. Aparicio, O., Carnero, E., Abad, X., Razquin, N., Guruceaga, E., Segura, V. and Fortes, P. (2010) Adenovirus VA RNA-derived miRNAs target cellular genes involved in cell growth, gene expression and DNA repair. Nucleic Acids Res. **38**, 750-763.

331. Aparicio, O., Razquin, N., Zaratiegui, M., Narvaiza, I. and Fortes, P. (2006) Adenovirus virus-associated RNA is processed to functional interfering RNAs involved in virus production. J Virol. **80**, 1376-1384.

332. Wong, C. J., Launer-Felty, K. and Cole, J. L. (2011) Analysis of PKR-RNA interactions by sedimentation velocity. Methods Enzymol. **488**, 59-79.

333. Friedman, R. M., Metz, D. H., Esteban, R. M., Tovell, D. R., Ball, L. A. and Kerr, I. M. (1972) Mechanism of interferon action: inhibition of viral messenger ribonucleic acid translation in L-cell extracts. J Virol. **10**, 1184-1198.

334. McKenna, S. A., Lindhout, D. A., Shimoike, T. and Puglisi, J. D. (2007) Biophysical and biochemical investigations of dsRNA-activated kinase PKR. Methods Enzymol. **430**, 373-396.

335. Patel, T. R., Morris, G. A., de la Torre, J. G., Ortega, A., Mischnick, P. and Harding, S. E. (2008) Molecular flexibility of methylcelluloses of differing degree of substitution by combined sedimentation and viscosity analysis. Macromol Biosci. **8**, 1108-1115.

336. Dam, J. and Schuck, P. (2004) Calculating sedimentation coefficient distributions by direct modeling of sedimentation velocity concentration profiles. Numerical Computer Methods, Pt E. **384**, 185-212.

337. Schuck, P. (1998) Sedimentation analysis of noninteracting and self-associating solutes using numerical solutions to the Lamm equation. Biophysical Journal. **75**, 1503-1512.

338. Laue, T. M., Shah, B. D., Ridgeway, T. M. and Pelletier, S. L. (1992) Computer-aided interpretation of analytical sedimentation data for proteins. In Analytical Ultracentrifugation in Biochemistry and Polymer Science (Harding, S. E., Rowe, A. J. and Horton, J. C., eds.). pp. 90-125, Royal Society of Chemistry, Cambridge, United Kingdom.

339. Meng, H., Deo, S., Xiong, S., Dzananovic, E., Donald, L. J., van Dijk, C. W. and McKenna, S. A. (2012) Regulation of the interferon-inducible 2'-5'-oligoadenylate synthetases by adenovirus VA(I) RNA. J Mol Biol. **422**, 635-649.

340. Hura, G. L., Menon, A. L., Hammel, M., Rambo, R. P., Poole, F. L., 2nd, Tsutakawa, S. E., Jenney, F. E., Jr., Classen, S., Frankel, K. A., Hopkins, R. C., Yang, S.

J., Scott, J. W., Dillard, B. D., Adams, M. W. and Tainer, J. A. (2009) Robust, high-throughput solution structural analyses by small angle X-ray scattering (SAXS). Nat Methods. **6**, 606-612.

341. Glatter, O. K., O. (1982) Small Angle X-ray scattering. Academic Press Inc. (London) LTD., 14.

342. Putnam, C. D., Hammel, M., Hura, G. L. and Tainer, J. A. (2007) X-ray solution scattering (SAXS) combined with crystallography and computation: defining accurate macromolecular structures, conformations and assemblies in solution. Q Rev Biophys. **40**, 191-285.

343. Pauw, B. R. (2014) Everything SAXS:small-angle scattering pattern collection and correction. J Phys Condens Matter. **26**, 239501.

344. Konarev, P. V., Volkov, V. V., Sokolova, A. V., Koch, M. H. J. and Svergun, D. I. (2003) PRIMUS: a Windows PC-based system for small-angle scattering data analysis. Journal of Applied Crystallography. **36**, 1277-1282.

345. Vachette, P., Koch, M. H. and Svergun, D. I. (2003) Looking behind the beamstop: X-ray solution scattering studies of structure and conformational changes of biological macromolecules. Methods Enzymol. **374**, 584-615.

346. Svergun, D. I. a. S. H. B. (1991) New developments in direct shape determination from small-angle scattering. 1. Theory and model calculations. Acta Crystallogr., Sect. D. **A47**, 736–744.

347. Svergun, D. I. (1993) A direct indirect method of small-angle scattering data treatment. J. Appl. Crystallogr. **26**, 258–267.

348. Pilz, I., Glatter, O. and Kratky, O. (1979) Small-angle X-ray scattering. Methods Enzymol. **61**, 148-249.

349. Svergun, D. I. (1999) Restoring low resolution structure of biological macromolecules from solution scattering using simulated annealing (vol 76, pg 2879, 1999). Biophysical Journal. **77**, 2896-2896.

350. Koch, M. H., Vachette, P. and Svergun, D. I. (2003) Small-angle scattering: a view on the properties, structures and structural changes of biological macromolecules in solution. Q Rev Biophys. **36**, 147-227.

351. Svergun, D. I. (1992) Determination of the Regularization Parameter in Indirect-Transform Methods Using Perceptual Criteria. Journal of Applied Crystallography. **25**, 495-503.

352. Franke, D. and Svergun, D. I. (2009) DAMMIF, a program for rapid ab-initio shape determination in small-angle scattering. Journal of Applied Crystallography. **42**, 342-346.

353. Kirkpatrick, S., Gelatt, C. D., Jr. and Vecchi, M. P. (1983) Optimization by simulated annealing. Science. **220**, 671-680.

354. Svergun D, B. C., Koch MHJ. (1995) CRYSOL - A program to evaluate x-ray solution scattering of biological macromolecules from atomic coordinates. Journal of Applied Crystallography. **28**, 768–773.

355. Schneidman-Duhovny, D., Hammel, M. and Sali, A. (2010) FoXS: a web server for rapid computation and fitting of SAXS profiles. Nucleic Acids Res. **38**, W540-544.

356. DI, K. M. a. S. (2001) Automated matching of high- and low resolution structural models. J. Appl. Crystallogr. **34**, 33-41.

357. Dzananovic, E., Patel, T. R., Deo, S., McEleney, K., Stetefeld, J. and McKenna, S. A. (2013) Recognition of viral RNA stem-loops by the tandem double-stranded RNA binding domains of PKR. RNA. **19**, 333-344.

358. Svergun, D. I. (1992) Determination of the regularization parameter in indirect-transform methods using perceptual criteria. J Appl Crystallogr. **25**, 495-503.

359. Svergun, D. I. (1999) Restoring low resolution structure of biological macromolecules from solution scattering using simulated annealing. Biophys. J. **76**, 2879-2886.

360. Volkov, V. V. and Svergun, D. I. (2003) Uniqueness of ab initio shape determination in small-angle scattering. J. Appl. Crystallogr. **36**, 860-864.

361. GarcÌa de la Torre, J., Huertas, M. L. and Carrasco, B. (2000) Calculation of Hydrodynamic Properties of Globular Proteins from Their Atomic-Level Structure. Biophys. J. **78**, 719-730.

362. Voss, N. R. and Gerstein, M. (2005) Calculation of standard atomic volumes for RNA and comparison with proteins: RNA is packed more tightly. J. Mol. Biol. **346**, 477-492.

363. Rother, K., Rother, M., Boniecki, M., Puton, T., Tomala, K., Łukasz, P. and Bujnicki, J. (2012) Template-Based and Template-Free Modeling of RNA 3D Structure: Inspirations from Protein Structure Modeling. In RNA 3D Structure Analysis and Prediction (Leontis, N. and Westhof, E., eds.). pp. 67-90, Springer Berlin Heidelberg

364. Clarke, P. A., Pe'ery, T., Ma, Y. and Mathews, M. B. (1994) Structural features of adenovirus 2 virus-associated RNA required for binding to the protein kinase DAI. Nucleic Acids Res. **22**, 4364-4374.

365. Adams, P. D., Afonine, P. V., Bunkoczi, G., Chen, V. B., Davis, I. W., Echols, N., Headd, J. J., Hung, L.-W., Kapral, G. J., Grosse-Kunstleve, R. W., McCoy, A. J., Moriarty, N. W., Oeffner, R., Read, R. J., Richardson, D. C., Richardson, J. S., Terwilliger, T. C. and Zwart, P. H. (2010) PHENIX: a comprehensive Python-based system for macromolecular structure solution. Acta Crystallogr., Sect. D. **66**, 213-221.

366. Winn, M. D., Ballard, C. C., Cowtan, K. D., Dodson, E. J., Emsley, P., Evans, P. R., Keegan, R. M., Krissinel, E. B., Leslie, A. G. W., McCoy, A., McNicholas, S. J., Murshudov, G. N., Pannu, N. S., Potterton, E. A., Powell, H. R., Read, R. J., Vagin, A. and Wilson, K. S. (2011) Overview of the CCP4 suite and current developments. Acta Crystallogr., Sect. D. **67**, 235-242.

367. Nanduri, S., Carpick, B. W., Yang, Y., Williams, B. R. and Qin, J. (1998) Structure of the double-stranded RNA-binding domain of the protein kinase PKR reveals the molecular basis of its dsRNA-mediated activation. EMBO J. **17**, 5458-5465.

368. Volkov, V. V. and Svergun, D. I. (2003) Uniqueness of ab initio shape determination in small-angle scattering. Journal of Applied Crystallography. **36**, 860-864.

369. de la Torre, J. G., Huertas, M. L. and Carrasco, B. (2000) Calculation of hydrodynamic properties of globular proteins from their atomic-level structure. Biophysical Journal. **78**, 719-730.

370. Petoukhov, M. V. and Svergun, D. I. (2005) Global rigid body modeling of macromolecular complexes against small-angle scattering data. Biophys J. **89**, 1237-1250.

371. Jaeger, J. A. and Tinoco, I., Jr. (1993) An NMR study of the HIV-1 TAR element hairpin. Biochemistry. **32**, 12522-12530.

372. Fulle, S., Christ, N. A., Kestner, E. and Gohlke, H. (2010) HIV-1 TAR RNA spontaneously undergoes relevant apo-to-holo conformational transitions in molecular dynamics and constrained geometrical simulations. J Chem Inf Model. **50**, 1489-1501.

373. Bardaro, M. F., Jr., Shajani, Z., Patora-Komisarska, K., Robinson, J. A. and Varani, G. (2009) How binding of small molecule and peptide ligands to HIV-1 TAR alters the RNA motional landscape. Nucleic Acids Res. **37**, 1529-1540.

374. Al-Hashimi, H. M., Gosser, Y., Gorin, A., Hu, W., Majumdar, A. and Patel, D. J. (2002) Concerted motions in HIV-1 TAR RNA may allow access to bound state conformations: RNA dynamics from NMR residual dipolar couplings. J Mol Biol. **315**, 95-102.

375. Raghunathan, D., Sanchez-Pedregal, V. M., Junker, J., Schwiegk, C., Kalesse, M., Kirschning, A. and Carlomagno, T. (2006) TAR-RNA recognition by a novel cyclic aminoglycoside analogue. Nucleic Acids Res. **34**, 3599-3608.

376. Wu, H., Henras, A., Chanfreau, G. and Feigon, J. (2004) Structural basis for recognition of the AGNN tetraloop RNA fold by the double-stranded RNA-binding domain of Rnt1p RNase III. Proc Natl Acad Sci U S A. **101**, 8307-8312.

377. Reich, P. R., Forget, B. G. and Weissman, S. M. (1966) RNA of low molecular weight in KB cells infected with adenovirus type 2. J. Mol. Biol. **17**, 428-439.

378. Soderlund, H., Pettersson, U., Vennstrom, B., Philipson, L. and Mathews, M. B. (1976) A new species of virus-coded low molecular weight RNA from cells infected with adenovirus type 2. Cell. **7**, 585-593.

379. Schneider, R. J., Weinberger, C. and Shenk, T. (1984) Adenovirus VAI RNA facilitates the initiation of translation in virus-infected cells. Cell. **37**, 291-298.

380. Dzananovic, E., Patel, T. R., Deo, S., McEleney, K., Stetefeld, J. and McKenna, S. A. (2013) Recognition of viral RNA stem-loops by the tandem double-stranded RNA binding domains of PKR. RNA. **19**, 333-344.

381. Guinier, A. and Fourner, G. (1955) Small angle scattering of X-rays. Wiley, New York.

382. Masliah, G., Barraud, P. and Allain, F. H. (2013) RNA recognition by double-stranded RNA binding domains: a matter of shape and sequence. Cell Mol Life Sci. **70**, 1875-1895.

383. Dzananovic, E., Patel, T. R., Chojnowski, G., Boniecki, M. J., Deo, S., McEleney, K., Harding, S. E., Bujnicki, J. M. and McKenna, S. A. (2014) Solution conformation of adenovirus virus associated RNA-I and its interaction with PKR. J Struct Biol. **185**, 48-57.

384. Ma, Y. and Mathews, M. B. (1996) Secondary and tertiary structure in the central domain of adenovirus type 2 VA RNA I. RNA. **2**, 937-951.

385. Launer-Felty, K. and Cole, J. L. (2014) Domain interactions in adenovirus VAI RNA mediate high-affinity PKR binding. J Mol Biol. **426**, 1285-1295.

386. Wilson, J. L., Vachon, V. K., Sunita, S., Schwartz, S. L. and Conn, G. L. (2014) Dissection of the adenoviral VA RNAI central domain structure reveals minimum requirements for RNA-mediated inhibition of PKR. J Biol Chem. **289**, 23233-23245.

387. Launer-Felty, K., Wong, C. J., Wahid, A. M., Conn, G. L. and Cole, J. L. (2010) Magnesium-dependent interaction of PKR with adenovirus VAI. J Mol Biol. **402**, 638-644.

388. Launer-Felty, K., Wong, C. J. and Cole, J. L. (2015) Structural analysis of adenovirus VAI RNA defines the mechanism of inhibition of PKR. Biophys J. **108**, 748-757.

389. Husain, B., Mukerji, I. and Cole, J. L. (2012) Analysis of high-affinity binding of protein kinase R to double-stranded RNA. Biochemistry. **51**, 8764-8770.

390. Hovanessian, A. G. and Galabru, J. (1987) The double-stranded RNA-dependent protein kinase is also activated by heparin. Eur J Biochem. **167**, 467-473.

391. Clarke, P. A. and Mathews, M. B. (1995) Interactions between the double-stranded RNA binding motif and RNA: definition of the binding site for the interferon-induced protein kinase DAI (PKR) on adenovirus VA RNA. RNA. **1**, 7-20.

392. Tuukkanen, A. T. and Svergun, D. I. (2014) Weak protein-ligand interactions studied by small-angle X-ray scattering. FEBS J. **281**, 1974-1987.

393. Metz, D. H. and Esteban, M. (1972) Interferon inhibits viral protein synthesis in L cells infected with vaccinia virus. Nature. **238**, 385-388.

394. Chu, W. M., Ballard, R., Carpick, B. W., Williams, B. R. and Schmid, C. W. (1998) Potential Alu function: regulation of the activity of double-stranded RNA-activated kinase PKR. Mol Cell Biol. **18**, 58-68.

395. Gale, M., Jr. and Katze, M. G. (1998) Molecular mechanisms of interferon resistance mediated by viral-directed inhibition of PKR, the interferon-induced protein kinase. Pharmacol Ther. **78**, 29-46.